Scale size-dependent characteristics of the magnetosphere-ionosphere system using auroral imaging

Beate Krøvel Humberset

Thesis for the degree of philosophiae doctor (PhD)
at the University of Bergen

2017

Date of defence: October 6th

Abstract

The spectacular and breathtaking aurora dancing around on the night sky visualizes the fundamental behavior of complex processes in the near Earth space. The plethora of papers published over the last five decades have laid the foundation of our understanding of how the Earth's magnetosphere solves the problem of stored energy and momentum provided by the solar wind. A dominant energy sink in this system is the ionosphere around 100 km above the Earth's surface where energy and momentum is dissipated with significant implications to the neutral atmosphere. While the magnetosphere-ionosphere system has been shown to be highly dynamic and structured, as visualized by the aurora, most of the observations in space cannot separate between the changes in space and time. Our current understanding of electrodynamic parameters of the magnetosphere-ionosphere system is largely based on simplistic empirical models. The purpose of this thesis is to get beyond the large-scale static picture and advance our understanding of the dynamic magnetosphere-ionosphere system by performing an analysis that allows a separation of spatial gradients and temporal variability and thereby provide new insight into the fascinating Earth-space interactions.

To overcome the time-space ambiguity of space observations, we utilize ground-based observations of auroral emissions since they provide extended periods of continuous observations at a fixed position in the ionosphere with high spatial and temporal resolution. The observations are made with an all-sky imager which allows for an analysis of a wide range of auroral scale sizes from microscale to mesoscale auroral scale sizes of a few km to around 250 km. We first utilize these powerful observations to study the often occurring phenomenon of persistent pulsating auroral patches and, secondly, we separate the aurora into different scale sizes and quantify their lifetimes.

In Papers I and II [*Humberset et al.*, 2016, 2017a] we provide objective and quantitative characteristics of pulsating auroral patches in order to give better observational constraints on the suggested mechanisms and address some of the questions about fundamental aspects of pulsating aurora. In Paper I we address the underlying mechanism(s) that controls the on-off fluctuations, while Paper II addresses what controls the

shape and coherency of pulsating auroral patches. We find that the fluctuating auroral patches display a striking and puzzling variability. The patches do not fluctuate in a coherent fashion, the energy deposition is highly variable from one fluctuation to the next, the on-time varies wildly and does not show any correlation to the preceding off-time, nor the peak intensity. The only parameter which appears to be consistent for pulsating auroral patches, is their shape. The name pulsating aurora is therefore a misnomer, and fluctuating aurora is a more appropriate description of the phenomenon. There are no clear winning candidates of the suggested mechanisms to explain the observational constraints set by the fluctuating auroral patches in a satisfactory manner. Our interpretation of the findings is that the mechanism is located at lower altitudes and not in the plasma sheet.

In Paper III [*Humberset et al.*, 2017b] we developed an innovative image analysis combining spatial frequency filtering to separate the images into 2D scale sizes, and a temporal correlation to reveal the time scales of change in the different scale sizes. The analysis was tested on an event of a pre-midnight auroral display during a period of fairly constant moderate geomagnetic disturbances. The resulting characteristics showed a scale size dependent variability where the largest scale sizes are stable on time scales of minutes while the small scale sizes are more variable. The average spatiotemporal characteristics of the auroral emissions are in remarkable agreement with the spatiotemporal characteristics of the nightside Birkeland currents during moderately disturbed times. Thus, two different electrodynamical parameters of the M-I coupling show similar behavior. This result is interpreted as an indication of a system that uses repeatable solutions to transfer energy and momentum from the magnetosphere to the ionosphere.

Δ

“All our science, measured against reality, is primitive and childlike, and yet it is the most precious thing we have"
Albert Einstein

Acknowledgements

I am proud and forever grateful for the opportunity to pursue a doctor's degree. It has been an unique experience where my job has been to be curious, ask question, and to get confused. The more I have learned about a topic the more I realize how little we actually know. It is slightly frustrating, but it is foremost great fun! Especially when I finally connect the dots.

First and foremost I would like to thank my supervisor, Jesper Gjerloev. You are truly an inspiration in the way you re-think fundamental questions and assumptions in the field of space physics. You once said, the trick is to make it look so easy that others are left with the thought: "Why didn't I think of that?!". Thank you for constantly reminding me to structure my programming routines, talks, presentations, projects, articles and paragraphs, for your big words, for introducing me to your colleagues and friends, and teaching me how to be a scientist.

I would like to thank my co-supervisor Kjellmar Oksavik for your enthusiasm, eagerness to help, and prompt feedback (46 pages of thesis in one night!). Further I would like to thank Thomas Gjesteland for encouraging me to do a PhD, Nikolai Østgaard who always explain things from scratch by drawing, Paul Tenfjord for explaining everything with MHD equations, Karl Magnus Laundal for keeping me updated on his many findings, Johan Stadsnes for taking the time to answering my every question in writing, Hulda Seterås Fadnes and Tonje Vedde Fiskarstrand for our interesting group discussions, Jone Reistad and Brage Førland for being the go-to persons on IDL programming and many other things, Hilde Nesse Tyssøy for acknowledging my work and encouraging collaboration, Stein Haaland for combining physics with hiking, Kjartan Olafsson for your catching enthusiasm for space and and for giving me the opportunity to encourage kids to experiment with physics at the Research days, and Norah Kaggwa Kwagala and Christine Smith-Johnsen for keeping me company during late nights of working. I would have liked to mention you all, both previous and current members of the Birkeland Centre for Space Science, but I would have filled a whole page. I privileged to have worked with people that are not only highly skilled, but also open and

including. You have all been the best company either we met by the coffee machine, at a party or a workshop. Thank you to Group 2 and the Ground-based instrumentation group for the discussions we have had, and to the Birkeland Centre for creating a community where the threshold to share knowledge and ideas is low, and also for the funding that have made it possible for me to present my work and to meet other scientists at international conferences in Japan, USA, Austria and Germany. Finally, I would like to thank my co-authors Ian Mann, Robert Michell and Marilia Samara for fruitful discussions, and Jesper, Kjellmar, Karl Magnus, Norah, Hilde, and Guro for proof-reading my thesis.

The years as a PhD candidate have been filled with experiences. I have presented our scientific results on the International Conference on Substorm and the Andøya Rocket Range 50th Anniversary, and received the Dr. Frank McDonald Student Travel Grant Award and the Outstanding Student Poster Award at the European Geosciences Union. I was later trusted the role as Early-Career Scientist representative for the Solar-Terrestrial Division at EGU, and have had the privilege to work with committed colleagues to arrange short courses and scientific sessions at EGU, AOGS and AGU. The biggest experience of them all was to be awarded the Fulbright Scholarship that made it possible to spend one academic year at the Johns Hopkins University Applied Physics Laboratory in USA and be a part of Fulbright events, such as the Enrichment Seminar in Austin. A special thank you to Abigail Rymer, Lars Dyrud, Jonathan Fentzke, and of course Jesper Gjerloev for welcoming me, and amongst many other things, made sure I experienced Halloween the American way. I would also like to thank my fellow PhD-student or physics girls Guro Sandnes, Hege Erdal, Sabrina Eder, Jenny Luneng, and Sigrid Meyer for all the memorable times we have shared at the university and beyond.

Last, but definitely not least, I would like to thank my family, my wonderful daughter Aria for her never-ending distractions from work and everything else, and my beloved Erik Staurset Andresen for the memorable and everyday moments we have shared the last years, and especially for taking such good care of me, our family and home for the last few months.

Bergen, June 2017
Beate Krøvel Humberset

Contents

Abbreviations

AACGM	Altitude Adjusted Corrected Geomagnetic coordinate system, p. 54
ASI	All-Sky Imager, p. 43
ECH	Electron Cyclotron Harmonic wave, p. 23
EMCCD	Electron Multiplying Charge Coupled Device, p. 49
EMIC	ElectroMagnetic Ion Cyclotron wave, p. 23
FAC	Field-Aligned Current, also known as Birkeland current, p. 12
FAST	Fast Auroral Snapshot Explorer satellite, p. 23
FFT	Fast Fourier Transform, p. 62
FOV	Field-Of-View, p. 43
IMF	Interplanetary Magnetic Field, p. 9
IRI	International Reference Ionosphere model, p. 13
M-I	Magnetosphere-Ionosphere, p. 3
MLat	Magnetic Latitude, p. 24
MLT	Magnetic local time, p. 23
MOOSE	Multi-Spectral Observatory Of Sensitive EMCCDs experiment, p. 48
MSIS	Mass Spectrometer and Incoherent Scatter model of the atmosphere, p. 13
PA	Pulsating Aurora, also called fluctuating aurora [*Humberset et al.*, 2016], p. 25
R_E	Earth radii, on average 6371 km, p. 10
R1/R2	Region-1 and Region-2 Birkeland currents, p. 17

SNOE	Student Nitric Oxide Explorer, p. 13
SOC	Self-Organized Criticality, p. 72
SuperDARN	Super Dual Auroral Radar Network, p. 16
THEMIS	Time History of Events and Macroscale Interactions during Substorms mission, p. 27
UCAR	University Corporation for Atmospheric Research, p. 45
UV	UltraViolet, p. 12
VIS	Visible Imaging System, p. 43

Chapter 1

Introduction

The overarching thesis objective is to provide new insight into the characteristics of the dynamic magnetosphere-ionosphere system as visually manifested by the aurora. This was motivated by a need to advance our understanding of how the magnetosphere-ionosphere system responds to the solar wind driver and how it internally transports and dissipates energy and momentum. This understanding does not only stem from scientific curiosity but also from humanity's ever increasing dependence on the conditions in our near space environment.

The magnetic field of the Earth shields our living environment and technology from a continuous stream of energy and particles from the Sun, called the solar wind. A fraction of the solar wind energy enters the magnetosphere through a process that includes complex interactions between the magnetic field embedded in the solar wind and the magnetic field of the magnetosphere. The energy is stored in the magnetosphere until it is unloaded. Typically, this unloading occurs in a very abrupt fashion and a large fraction of the energy is dissipated in the ionosphere, where it leads to the spectacular auroral display. The magnetosphere-ionosphere (M-I) system is thus highly dynamic and structured, as illustrated in Figure 1.1. This brief snapshot of an auroral arc is truly intriguing as it reveals a change in the arc that after 2 s and 10 s comprises increasingly larger auroral features, and after only 60 s the large-scale auroral arc is profoundly different. This indicates a wide range of auroral scale sizes with completely different lifetimes.

Our current understanding of the electrodynamic parameters of the magnetosphere-ionosphere system is largely based on simplistic empirical models [e.g. *Iijima and Potemra*, 1978; *Weimer*, 1995]. A common assumption is that the electrodynamic parameter is variable in space only, and the temporal variations are ignored. This is of course a valid assumption if the aim is to study the large-scale phenomenon inte-

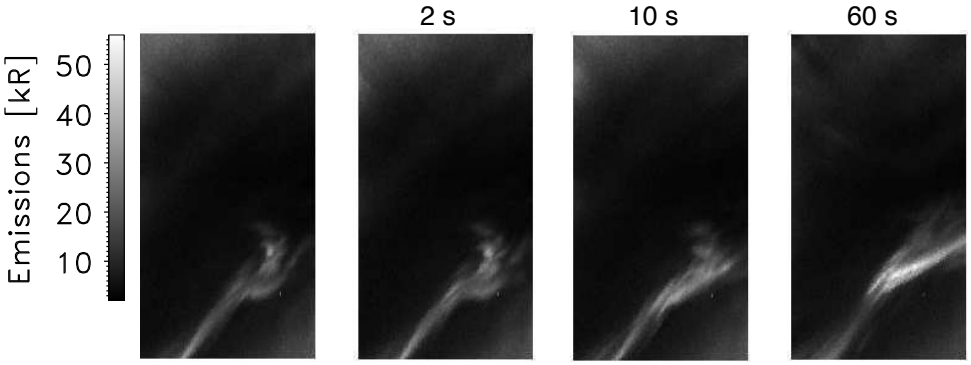

Figure 1.1: Snapshots of an auroral arc to illustrate the highly dynamic and structured magnetosphere-ionosphere system. The figure is adapted from Paper III.

grated over long time scales, but can in some contexts be an oversimplification. The main reason for this shortcoming is the observational challenges. Observations must be made at a fixed point in the space over an extended period of time. This is not possible with a single satellite or rocket for which measurements are separated in both time and space. The parameter measured can have changed considerably between measurement, as illustrated in Figure 1.2. This typical example leaves us with two options: 1) assume the system is static and all variations are due to spatial gradients; or, 2) assume the system is uniform and all variations are due to the dynamics of the system. Virtually all papers ever published chose the first assumption. Ideally, for a satellite moving at near infinite speed we can assume that all variations are due to spatial gradients, while on the other hand, a satellite fixed in space provides measurements of the dynamics. One example is the pulsating aurora, for which a few to hundreds of kilometers wide nearby forms vary in intensity on time scales ranging from less than 1 s to several tens of seconds. A satellite in low-Earth orbit could then cross a pulsating auroral form in less than an on-off cycle, while a slower moving rocket could cross the form within a few on-off cycles. Within that time, the observed variations are due to both temporal and spatial variations.

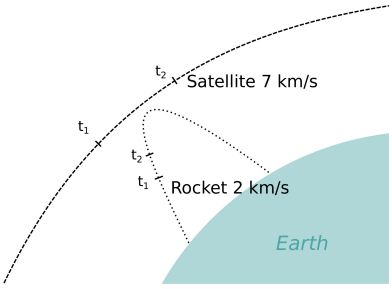

Figure 1.2: Illustration of observational challenges in space. The M-I system parameter measured by single satellites and rockets can have changed considerably between a measurement at time t_1 and time t_2.

Another complexity is relating ionospheric observations made at low altitudes and magnetospheric observations made at high altitudes. These distantly separated regions are connected by the magnetic field, but the mapping is complex and every changing. Thus, for high altitude satellites (e.g. geostationary orbits) the magnetic field line mapping between the satellite and the ionosphere is very challenging, and thus we must question the relationship between the auroral form and the satellite observations.

Only a few studies have attempted to address the spatiotemporal behavior of any electrodynamic parameter of the magnetosphere-ionosphere system [e.g. *Boudouridis and Spence*, 2007; *Gjerloev et al.*, 2011; *Karlsson et al.*, 2004; *Le et al.*, 2009; *Lynch et al.*, 2012]. In stark contrast to the massive amount of single satellite and rocket data, only a very limited number of multi-point observations exist [e.g. Auroral Turbulence II sounding rocket mission *Lynch et al.* [1999]; Enstrophy sounding rocket mission *Zheng et al.* [2003]; Science and Technology 5 *Slavin et al.* [2008]; Cluster II mission *Escoubet et al.* [2001]; Swarm satellite constellation *Olsen et al.* [2013]]. This calls for analyses that can separate between changes in time and in space and to evaluate the importance of the different scale sizes. Such analyses are needed both to complement the few existing multipoint missions, and to provide quantitative estimates to the validity of assumptions applied to measurements obtained from single satellite and sounding rocket missions.

The purpose of this thesis is to provide scale size-dependent characteristics of the dynamic magnetosphere-ionosphere system as visually manifested by the nightside aurora. The auroral display visualizes the behavior of processes in the M-I system. The presence of small to mesoscale features suggests that they play a role in the M-I system. However, both their role and scale-size dependent variability are to a large degree unclear. By investigating the range of different scale sizes and their lifetimes in the auroral display, we get information of how energy is deposited in the ionosphere and thus insight into how the magnetosphere solves the problem of stored energy and momentum provided by the solar wind. We thus address one of the fundamental problems in the physics of the ionosphere-magnetosphere system. One way to separate changes in time and space, is to use 2D auroral images to characterize auroral phenomena over some time, such as arc distortions in the form of for example curls, or pulsating aurora. Pulsating aurora is an excellent example of an often occurring auroral phenomenon that likely constitutes an important process within the magnetosphere-ionosphere system. However, fundamental aspects of pulsating aurora are not yet solved [*Hosokawa et al.*, 2015; *Lessard*, 2012], and we do not know its role in the large-scale transport

of energy and momentum. A different approach is to apply mathematical techniques to separate the aurora into different scale sizes and quantify their lifetimes. The more specific science objectives of this thesis are therefore:

1. Provide objective and quantitative characteristics of pulsating auroral patches in order to give better observational constraints on the suggested mechanisms.

2. Describe the scale size dependent variability of the magnetosphere-ionosphere system as observed by the auroral emissions.

To address the thesis objectives we utilize ground-based observations of auroral emissions since they provide extended periods of continuous observations at a fixed position in the ionosphere. To capture a large range of auroral scale sizes (small to mesoscale) with high spatial and temporal resolution, we use an all-sky imager, which covers almost the width of the auroral oval as it rotates with the Earth along the auroral oval from evening to morning.

In the next chapters I will give an overall perspective of some of the basic concept and processes that we refer to in the papers. I start by introducing basic concepts of Earth's magnetosphere-ionosphere system in Chapter 2, and provide a description of the diffuse aurora, the pulsating aurora, and the discrete aurora and a brief introduction to their proposed mechanisms in Chapter 3. In Chapter 4 I introduce the auroral spectrum and a selection of emissions that are important for auroral studies, including the green 557.7 nm auroral emissions utilized in Papers I-III. Then I describe the all-sky imager and how we process the images to answer the science objectives. A summary of the individual papers is given in Chapter 5, before I highlight the connection between the individual papers by discussing the overarching thesis objective and future prospects in Chapter 6, and conclusions in Chapter 7.

The central part of this thesis is the three scientific papers that are published or submitted for publication in an international peer reviewed journal:

Paper I B. K. Humberset, J. W. Gjerloev, M. Samara, R. G. Michell, and I. R. Mann, Temporal characteristics and energy deposition of pulsating auroral patches, *Journal of Geophysical Research: Space Physics*, Vol. 121, doi:10.1002/2016JA022921, 2016

Paper II B. K. Humberset, J. W. Gjerloev, I. R. Mann, R. G. Michell, and M. Samara, Do pulsating auroral patches vary in a coherent fashion?, Submitted to *Journal of Geophysical Research: Space Physics*, 2017

Paper III B. K. Humberset, J. W. Gjerloev, M. Samara, and R. G. Michell, Scale size-dependent characteristics of the nightside aurora, *Journal of Geophysical Research: Space Physics*, Vol. 122, doi:10.1002/2016JA023695, 2017

In Papers I and II we provide objective and quantitative characteristics of pulsating auroral patches in order to give better observational constraints on the suggested mechanisms and address some of the questions about fundamental aspects of pulsating aurora. In Paper I we address the underlying mechanism(s) that controls their on-off fluctuation, while Paper II addresses what controls the shape and coherency of fluctuating auroral patches. Paper III describes the scale size dependent variability of one event of nightside aurora during a period of fairly constant moderate geomagnetic disturbances. We developed an innovative two-dimensional analysis of all-sky images to reveal the characteristics of the magnetosphere-ionosphere system and thereby provide a glimpse of its scale-size dependent variability.

Chapter 2

Basic concepts of the Earth's magnetosphere-ionosphere system

This thesis investigates the spatiotemporal characteristics of the magnetosphere-ionosphere system as manifested in auroral emissions. First I introduce some basic concepts and processes that we will later refer to in the papers. For more details on the physics I refer to text books, such as *Baumjohann and Treumann* [1997a, b]; *Brekke* [2013]; *Kivelson and Russell* [1995]. An extended introduction of the aurora follows next in Chapter 3.

2.1 Transport of energy and momentum from the Sun to the Earth

The sun emits electromagnetic radiation and a continuous dynamic outflow of plasma (solar wind) and magnetic field radially into space. Some of the electromagnetic radiation can be seen in the form of visible light, while the solar wind and interplanetary magnetic field (IMF) must be observed through in-situ instruments on satellites. The distance from the Sun to the mean radius of Earth's orbit is around $150 \cdot 10^6$ km (1 astronomical unit). The solar wind with an average speed of around 400-500 km/s will therefore on average take four days to reach the Earth.

The solar wind interacts with the Earth's magnetic field and directs the charged particles around the magnetosphere. At the front of the magnetosphere we typically have pressure balance such that the dynamic pressure of the solar wind equals the magnetic pressure of the magnetosphere. The layer separating these two regions is known as the magnetopause which on the front side is located some Earth radii ($R_E = 6371$ km)

up-stream from the Earth. On the nightside, the magnetic field becomes stretched into a tail-like configuration that extends far downstream.

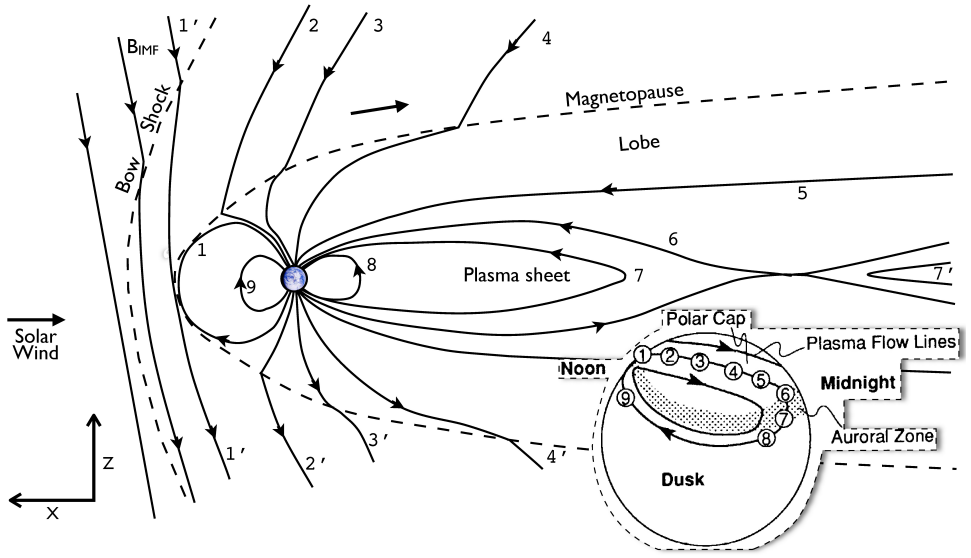

Figure 2.1: Schematic illustration of the large-scale circulation process of the open magnetosphere during southward IMF. We follow the circulation of one magnetic field line as denoted by the numbers. The ionospheric footpoints are illustrated in the inset. The Figure is adapted from *Hughes* [1995], page 243.

The solar wind and the magnetospheric plasmas are mainly collision-less, thus diffusion is negligible and electrical conductivity along the magnetic field line can be considered infinite. As a result the plasma and the magnetic field lines moves together which is referred to at the so-called frozen-in condition [*Alfvén*, 1942]. As the solar wind approaches the magnetospheric magnetic field their interactions are highly complex and for a thorough description I refer to the rich literature on the topic. For the purpose of this introduction we can view the magnetospheric magnetic field as expelling the solar wind and thereby creating a region in space where the Earth's magnetic field dominates. The interactions between the solar wind and the magnetosphere can be simplistically split into two situations: When the IMF has a northward component, and when the IMF has a southward component. For the former situation the charged particles of the solar wind exit the solar wind and enter the magnetosphere in the cusp regions where they spiral down into the ionosphere following the magnetic field lines. For the latter situation the IMF merges with the oppositely directed magnetospheric magnetic field and solar wind charged particles can spiral down into the ionosphere. These so-called open field lines are connected to the solar wind and follow

the solar wind drift. As the merging process continues more and more open field lines are moved from the front of the magnetosphere to the tail where they accumulate. The morphology of the magnetosphere changes, and the tail becomes more stretched. The solar wind particles have low energies, so their associated auroral emissions is limited compared to, for example the auroral ovals. The ionospheric region of low emissions expands, and moves the auroral oval equatorward. This period is known as the loading phase or the growth phase. Naturally, there is a limit to the loading as the morphology of the magnetosphere gets more and more stretched. Eventually, instabilities that are still under debate lead to an abrupt unloading of the magnetospheric energy and an associated reconfiguration of the magnetospheric morphology. The energy is transported along the field lines to the northern and southern ionosphere where it leads to the spectacular auroral display. This large-scale circulation process of the open magnetosphere, was first described by *Dungey* [1961], and is schematically illustrated in Figure 2.1, where we follow the convection circulation of one magnetic field line.

2.2 Magnetosphere

The magnetosphere is the part of space that is controlled by the Earth's magnetic field. Figure 2.2 shows a schematic diagram of Earth's magnetosphere. The magnetosphere is a complex and dynamic system that responds to both internal and external influences to produce a myriad of physical behavior. The sketch is therefore at best an average picture, but it illustrates the major distinct regions of different plasma populations and electric currents. The magnetopause is the outermost region controlled by the magnetic field of the Earth. Outside is the solar wind and interplanetary magnetic field that to a large degree is responsible for most of the large-scale dynamics observed within Earth's magnetosphere, ionosphere, and thermosphere. In the inner magnetosphere the magnetic field is nearly dipolar. The *ionosphere* (pale blue) is a thin layer of partially ionized and relatively cold plasma surrounding the Earth. The *plasmasphere* (dark blue) consists of a cold plasma that co-rotates with Earth mapping to low latitudes. Further out (orange) is the *outer van Allen radiation belt* and the *ring current*, whose bulk of energy is carried by energetic ($\sim$10–200 keV) protons that encircles the Earth in the vicinity of the geosynchronous orbit (at 6.6 R_E) and the inner plasma sheet on the nightside. Here the magnetic field starts to deviate considerably from the magnetic dipole and stretches into a long tail away from the sun (nightside). The lobes of the magnetotail, where the magnetic field lines are open, are encircled by the magnetopause currents that are closed by the dawn-dusk directed cross-tail current in the equatorial magnetotail. This cross-tail current region, called the *plasma sheet* (yellow) is the

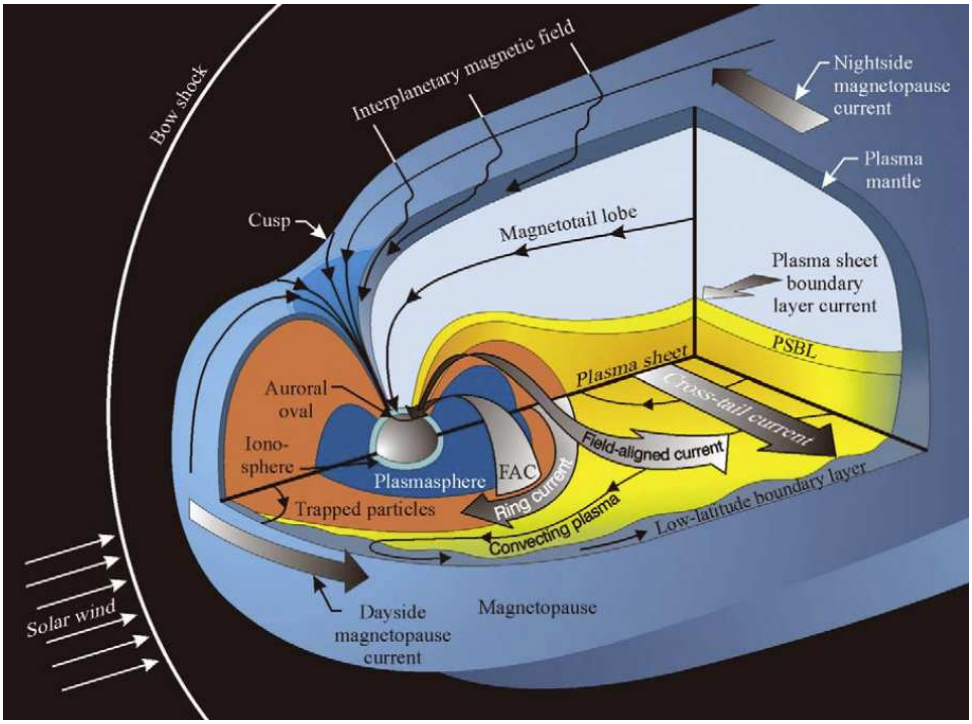

Figure 2.2: Schematic diagram of Earth's magnetosphere. It illustrates the major distinct regions of different plasma populations and electric current systems. The Figure is from *Pollock et al.* [2003], p. 156.

region of closed field lines in the equatorial magnetotail which is important for auroral physics, since it maps to the nighttime auroral oval. The *Birkeland currents* or *field-aligned currents* (FAC) are electric currents that flow along geomagnetic field lines connecting the magnetosphere to the high latitude ionosphere.

2.3 Ionosphere

The ionosphere is the upper part of the atmosphere, but unlike the neutral atmosphere at lower altitudes it has free charges allowing electrical currents to flow. It was probably inferred in the early 1800 by a demonstration that radio waves could propagate large distanced as if they were guided between the ground and a conducting layer, but it was not until 1924 that its existence was fully proven [*Brekke*, 2013].

The free charges in the ionosphere are produced from ionization of the neutral atmospheric atoms and molecules. The main causes are ultraviolet (UV) and X-ray radi-

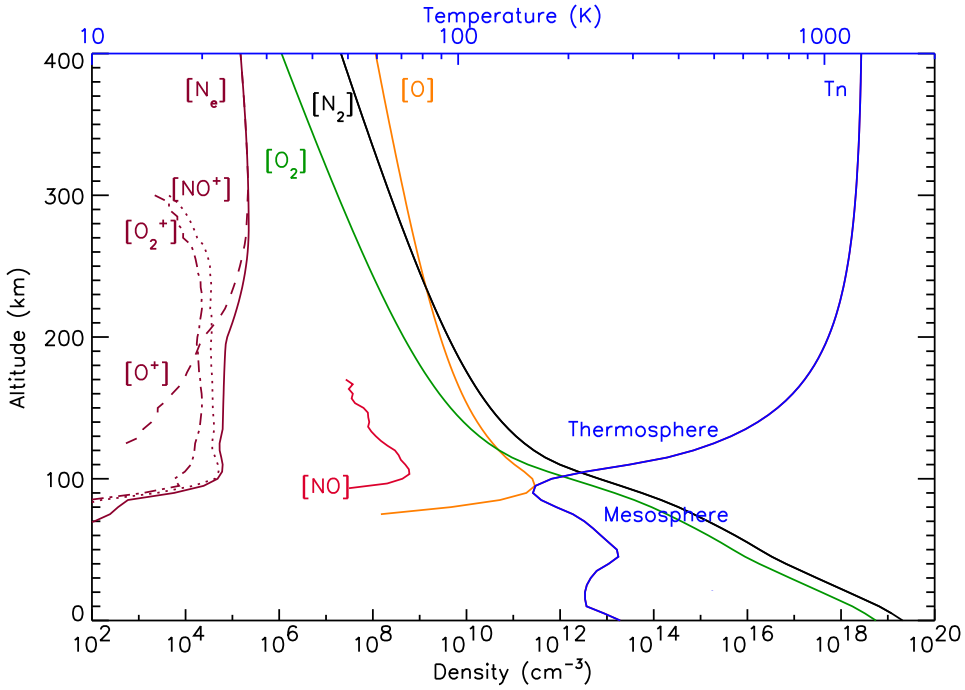

Figure 2.3: Overview of the main constituents and regions of the nightside ionosphere and upper atmosphere. The figure is after *Sætre* [2007], who got the distributions from the empirical models Mass Spectrometer and Incoherent Scatter radar (MSIS) of the atmosphere, and International Reference Ionosphere (IRI) in addition to measurements by the Student Nitric Oxide Explorer (SNOE) satellite.

ation from the Sun on the dayside, particle precipitation on the nightside, and cosmic rays. Figure 2.3 shows the regions of the nightside ionosphere and upper atmosphere along with their main constituents. The upper atmosphere above 100 km altitude has rather strong variations during a solar cycle, while the ionosphere also varies between sunlit and darkness as well as with geomagnetic activity. The main neutrals are molecular nitrogen (N_2) and molecular and atomic oxygen (O_2, O), while the neutral temperature (T_n) defines the mesospheric (∼50 to 85-100 km) and thermospheric regions (>85-100 km) of the atmosphere that overlaps with the ionosphere. The main ions of the ionosphere are O_2^+, O^+, nitric oxide NO^+, and electrons. The ionosphere stretches from around 65 km to 1000 km altitude. The electron density (N_e) historically defines different regions of the ionosphere. At night these are the E-layer (∼90–120 km), named due to its ability to reflect electric fields, and the F-layer above that followed alphabetically [*Brekke*, 2013]. Today it is more common to talk about regions as the distinction between the layers is not clear, and the nomenclature has turned out to be useful since

the regions are physically different because of their different chemistry. The F-region contains the maximum electron density around 300 km (varies between 200–600 km), and below there often appears bumps in the profile, sometimes distinct enough to form secondary peaks such as during auroral events when they can form rather sharp layers.

2.3.1 Ionization and excitation by precipitation

When precipitating electrons and protons enter the atmosphere they ionize, dissociate, and excite the neutral gas atoms and molecules which result in the optical emissions that we see as the aurora. Both the primary particle and the secondary (sometimes also higher order) electrons contribute to the excitation.

Ionization

The energy loss per ion-electron pair formation for impact ionization of N_2, O_2, and O has experimentally been found to be on average $\Delta\varepsilon_{ion} = 35$ eV. The ionization rate q in the ionosphere can therefore be estimated by the energy deposition ε divided by the energy loss:

$$q(z, E_p) = \varepsilon(z, E_p)/\Delta\varepsilon_{ion}$$

where the energy deposition ε (eV/cm^{3}s) is a function of altitude z and initial energy of the precipitating electron E_p [*Rees*, 1989]. Figure 2.4 shows the ionization profiles from unidirectional electron fluxes of 10^8 erg/cm^{2}s of different energies.

The ionization in the ionosphere above around 100 km altitude is balanced by recombination, where the ionospheric electrons and ions are lost through reactions like:

$X^+ + e \rightarrow X + h\nu$ Radiative recombination

$XY^+ + e \rightarrow X + Y$ Dissociative recombination

Dissociative recombination is faster than radiative recombination and is the main recombination process in the aurora [*Chamberlain*, 1961].

Excitation

The different processes of auroral excitations are:

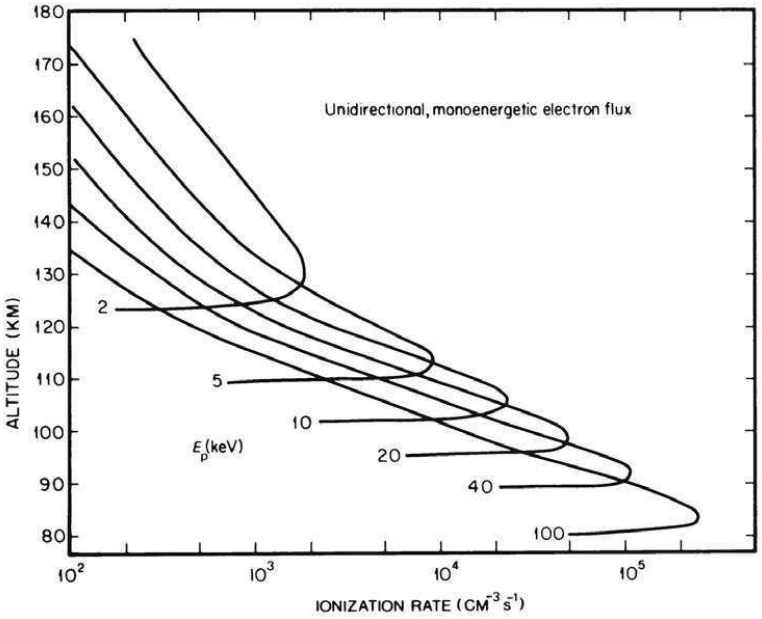

Figure 2.4: Ionization profiles in the Earth's atmosphere caused by precipitating electrons of different energies (E_p given in keV) with a flux of 10^8 erg/cm^{2}s. The figure is from *Rees* [1989].

$$e_p + Z \rightarrow Z^{+*} + e_s \qquad \text{Ionization excitation}$$

$$e_p + XY \rightarrow e_p + X^{+*} + Y^{+*} + e_s \qquad \text{Dissociative ionization excitation}$$

$$e_p + XY \rightarrow e_p + X^{*} + Y^{*} \qquad \text{Dissociative excitation}$$

$$e_s + Z \rightarrow e_s + Z^{*} \qquad \text{Excitation}$$

where X/Y is an atmospheric atom, XY is an atmospheric molecule, Z can be either an atmospheric atom or molecule, e_p and e_s are the primary and secondary electrons, and the asterisk denotes the formation of excited states [*Rees*, 1989]. In addition, indirect processes like dissociative recombination, charge/atom exchange and thermal excitation of electrons can also contribute to the excitation [*Brekke*, 2013].

The excited states spontaneously (without any outside influence) decays by a process where the electron jumps from a higher energy level to a lower one. An electron in state 2 with energy E_2 will decay spontaneously to state 1 with energy E_1, emitting a photon with an energy $E_2 - E_1 = h\nu$. The resulting auroral spectrum includes a

number of emission bands from neutral or ionized atmospheric constituents molecular nitrogen, atomic oxygen, molecular oxygen, and maybe also a small contribution from nitric oxide.

2.3.2 Convection

The motion of the plasma due to the global magnetospheric convection introduced in Section 2.1, maps down to the ionosphere. At lower altitudes it is referenced to as ionospheric convection or $\mathbf{E} \times \mathbf{B}$-velocity. An observer on the Earth will measure an electric field $\mathbf{E} = -\mathbf{v_c} \times \mathbf{B}$ due to the motion $\mathbf{v_c}$ of the plasma. The global ionospheric convection pattern forms two large cells at dawn and dusk. Flow from the dayside cross the polar cap to the nightside and returns toward the dayside at lower latitudes corresponding roughly to the auroral oval. Global ionospheric convection patterns from observations by a collection of coherent scattering radars, the Super Dual Auroral Radar Network (SuperDARN), can be found at the website vt.superdarn.org. An example of a SuperDARN convection map is shown in Figure 2.5 for the event in Paper II. There are, however, large deviations from the simplistic two cell pattern. This is in in both magnitude and direction of the flow. The reason for this structure and dynamics is still under debate, where the complex solar-wind-magnetosphere interactions as well as internal magnetosphere-ionosphere processes play a role.

2.3.3 Conductivity

In the high altitude part of the F-region, collisions between ions, electrons and neutral are rare so the electrons and ions $\mathbf{E} \times \mathbf{B}$ drift at the same speed and in the same direction producing no net current. In the D- and E-region and the low altitude F-region the electrons can still be assumed collision free while the ion-neutral collision frequency is larger than or comparable to the gyro-frequency. This leads to two different types of currents:

1. The Pedersen current flowing in the direction of the electric field has a broad maximum near the E- and F-region boundary. The effect of the ion-neutral collisions is an ion-drift in the electric field direction while the electrons drift in the $\mathbf{E} \times \mathbf{B}$ direction, thereby resulting in a current in the direction of the electric field. The current is dissipative since $\mathbf{j} \cdot \mathbf{E} \neq 0$, and usually $\mathbf{j} \cdot \mathbf{E} > 0$, evident of a downward Poynting flux.

2. The Hall current flows in the $-\mathbf{E} \times \mathbf{B}$ direction with a narrow peak within the E-region at $\sim$105 km altitude. It is a result of the electrons drifting in the $\mathbf{E} \times \mathbf{B}$

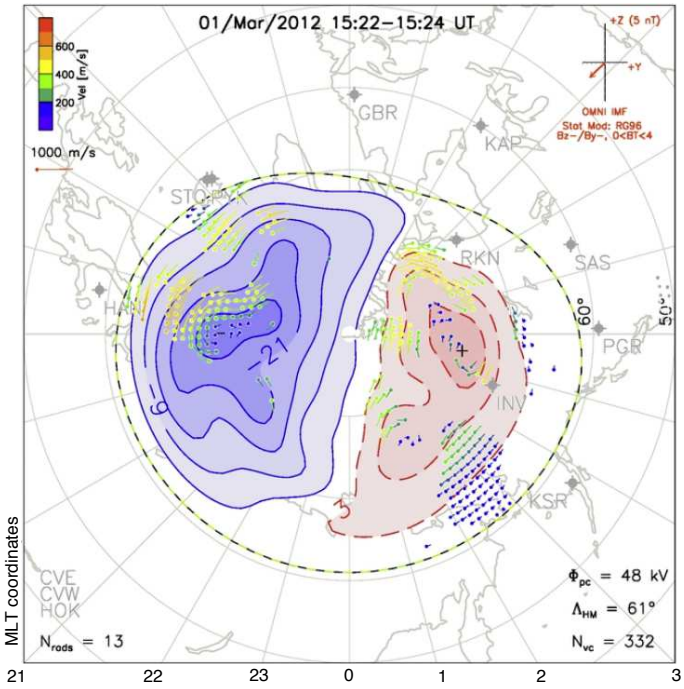

Figure 2.5: Preview of a SuperDARN convection map for the event in Paper II. The figure is from the convection map browser on the website vt.superdarn.org.

direction, while the ions do not drift at all since the ion-neutral collision frequency is much larger than the ion gyro-frequency. In contrast to the Pedersen current the Hall current is non-dissipative, $\mathbf{j} \cdot \mathbf{E} = 0$.

2.4 Birkeland currents

The Birkeland currents are electric currents that flow along the magnetic field lines between the magnetosphere and the high-latitude ionosphere at all times. *Birkeland* [1908] was the first to propose that electric currents flow between the Earth and space. We now know that these currents are the main mechanism for transport of energy and momentum in the magnetosphere-ionosphere system. Almost 50 years later, *Zmuda et al.* [1966, 1967] published the first in-situ measurements and thus provided direct evidence of Birkeland currents. Later, *Iijima and Potemra* [1976, 1978] followed with a ground breaking study of the large-scale empirical description of the currents. They found that the upward and downward field aligned current system consists of two approximately concentric circles with an overlap in the pre-midnight region as shown in Figure 2.6a. The inner ring is termed region-1 (R1) current, and the outer ring is the

region-2 (R2). In the ionosphere the Birkeland currents are largely closed by Pedersen currents [*Hoffman et al.*, 1994] along the electric field, thus northward in the dusk sector and southward in the dawn sector. The closures of the currents in the ionosphere are not fully understood, and the generators in the magnetosphere are also under debate. R1 currents are associated to the currents on the outer magnetospheric boundaries, and R2 to the partial ring current in the inner magnetosphere. The mechanism for the large-scale Birkeland current is magnetic pressure gradients and magnetic tension forces associated with the magnetospheric convection. However, field-aligned currents can also arise due to for example conductivity gradients in the ionosphere. Recent studies have focused on the dynamic behavior of the Birkeland currents, for example how the large-scale Birkeland current pattern varies with the solar wind, IMF and ionospheric conductivity, and the role of the range of current filaments of different scale sizes much smaller than the large-scale region 1 and 2 current sheets. Figure 2.6b shows an example of satellite observations used to derive the statistical pattern. The observations do not show a simple two sheets current system, but rather a vast range of Birkeland current filaments of different scale sizes. These are supported by the multitude of auroral features in auroral image in Figure 2.6c. However, the single satellite observations do not allow us to determine if the observed structure is due to temporal or spatial variations.

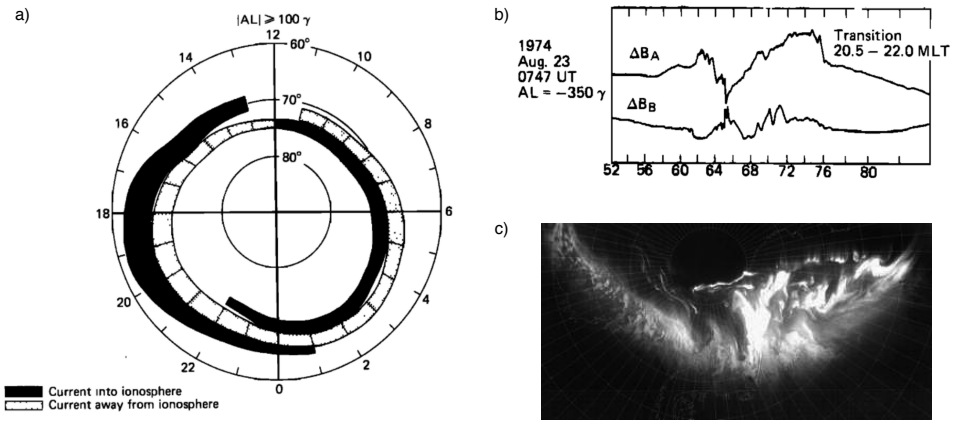

Figure 2.6: (a) The large-scale empirical description of the Birkeland currents and (b) an example of satellite observations used to derive the statistical pattern [*Iijima and Potemra*, 1978]. The observations do not show a simple two sheets current system, but rather a range of current filaments. (c) These are supported by the multitude of auroral features in the auroral image (unknown origin) from the very high resolution scanning ultraviolet imager on the Freja satellite [*Murphree et al.*, 1994].

2.5 Pitch-angle scattering

Pitch angle scattering is needed to put trapped particles into the loss cone. Without it even the brightest aurora would stop within a few seconds. The pitch angle of a particle is the angle between the magnetic field line and the velocity of the particle. As the magnetic field strength increases towards the poles, so does the pitch angle of the particle, until it reaches 90° and is mirrored to bounce back. These are trapped magnetospheric particles. Alternatively, if the mirror point is located deep within the atmosphere, the chances for collisions with neutral atoms and molecules increase, and the particle may loose its energy, and if it has a sufficiently high initial energy it can contribute to the aurora. The equatorial loss cone defines the pitch angles of the precipitating particles at the magnetic equator, which in the plasma sheet usually is a small solid angle on the order of only a few degrees. Thus, only a tiny fraction of plasma sheet particles would precipitate without any influence to their motion, and auroral particle precipitation proceeds primarily because plasma waves change the pitch angle of the particles. This happens when the charged particle and the wave is in resonance, where the energy can be transferred either way. When a wave grows at the expense of the energy of the particle, it can for example effectively decrease the perpendicular energy of the particle, and thus decrease the pitch angle of the particle. *Kennel and Petschek* [1966] provided the theoretical ground-work for how plasma waves and stably trapped charged particles interact. In simple terms, the charged particle must see fluctuations near its own gyro-frequency, suggesting that high-frequency fluctuations in the whistler and ion cyclotron mode plasma waves interact with electrons and ions, respectively. Since then there have been a plethora of studies on the relation between particle precipitation, plasma waves and their origin. One example are the studies of pulsating aurora, where a time-variation in the pitch-angle scattering is suggested to be a mechanism for the pulsations.

2.6 Substorm

Substorms are the most common occurring large-scale auroral phenomenon and energy transfer process in the M-I system. It was first proposed by *Akasofu* [1964], who found a systematic behavior in the evolution of the auroral display from a vast amount of all-sky camera observations. He found that in the order of a few hours the quiet auroral arcs suddenly exploded and became intensely active and bright (onset) and expanding rapidly poleward, westward and eastward (substorm auroral bulge) before the brightness and extensiveness decreased. The substorm evolution was therefore divided into two phases named expansion (10–30 min) and recovery (∼2 h). To make a distinction

to the geomagnetic storms, which is used for a longer period (days) of strong geomagnetic activity, the sequence was called a substorm. Later, *McPherron* [1970] added the growth phase to the substorm from the principle that in order to have a release of energy, there must be a period of loading, which he observed through the commencement or gradual enhancement in the ionospheric currents before the onset of the expansion phase. In the aurora, the growth phase can often be seen as a series of equatorward moving arcs following the magnetospheric convective motion (stretching of the magnetotail).

In general, the substorm manifested as aurora is called the auroral substorm, while the underlying magnetospheric processes are called the magnetospheric substorm. From a magnetospheric point of view, a substorm is the rapid release of energy stored in the magnetotail, associated with dipolarization of the magnetic field, as well as a host of processes covering many scale-sizes and bursty bulk flow events. In an auroral substorm the phases and the related ionospheric phenomena are fairly well understood. There is a general idea of how it will evolve, but the individual substorms are often very different from each other. The corresponding processes and accurate time sequence of events in the magnetospheric substorms, however, are still debated. In Paper I and II we discuss the characteristics of fluctuating/pulsating aurora that is believed to be related to the high-energy tail of the plasma sheet electron distribution that quickly starts drifting towards the morning local times due to magnetic drift. In Paper III we discuss the scale-size dependent characteristics of nightside aurora during continuous substorm activity.

Chapter 3

Aurora

The aurora is the visible manifestation the magnetosphere-ionosphere coupling, where parallel electric fields and plasma waves accelerates and scatter particles in order to transfer energy and momentum within the magnetosphere-ionosphere system. The aurora can be classified in different ways depending on the focus of the study; whether it is dayside or nightside, open or closed magnetic field-lines, characteristics of the magnetospheric source, the type of particle precipitation, or the emissions themselves [e.g. *Paschmann et al.*, 2003; *Sandholt et al.*, 2002]. In this thesis I focus on the nightside aurora within the auroral oval. Figure 3.1 shows a photograph of the aurora australis (south of Australia) captured by the crew onboard the International Space Station at an altitude of around 350 km. The bright green curtains are the discrete aurora, while the more chaotic dim structured region of green light is the diffuse and pulsating aurora. Papers I and II determine the characteristics of the pulsating aurora, while Paper III establishes the scale size dependent characteristics of the nightside aurora during. To set the stage for the papers, I here provide a description of the diffuse aurora, the pulsating aurora, and the discrete aurora and a brief introduction to their proposed mechanisms. For a description of the auroral spectrum and a selection of emissions that are important for auroral studies I refer to Chapter 4.

3.1 Diffuse aurora

The diffuse aurora is characterized by a lack of structure and can from ground be seen as a fairly uniform background. It is the result of electron precipitation originating from the central plasma sheet and can, at times, be a significant source of energy input into the nightside upper atmosphere. At times, the largest fraction of the total precipitating energy ($\sim$60 %) can be carried by the diffuse (including the pulsating aurora) electron precipitation [*Newell et al.*, 2009]. *Lui and Anger* [1973] did the first space observations

Figure 3.1: Photograph of the aurora australis (south of Australia) captured by the crew onboard the International Space Station at an altitude of around 350 km. The bright green curtains are the discrete aurora, while the more chaotic dim structured region of green light is the diffuse and pulsating aurora. The red aurora at higher altitudes can be seen on top of the green rayed aurora near the limb of the Earth. Image courtesy of the Earth Science and Remote Sensing Unit, NASA Johnson Space Center, The Gateway to Astronaut Photography of Earth (eol.jsc.nasa.gov).

and described a striking and persistent fairly uniform belt of diffuse auroral emission extending along the auroral oval. The equatorward edge is easily identified, while the poleward edge, where discrete aurorae (arcs and bands) often are located, is not as easily defined. They found that the representative intensities in the 557.7 nm line are 1-2 kR at quiet times and may reach 5 kR during an auroral substorm. However, the diffuse aurora can be of very low intensity or sub-visual. Virtually anywhere within the auroral oval, wave-particle interactions produce a weak “drizzle" of particles into the loss cone, which cause a quasi-permanent aurora of intensity > 5 R in 427.8 nm [*Eather and Mende*, 1971].

3.1.1 Source and mechanism

The diffuse aurora was defined as central plasma sheet type precipitation by *Winningham et al.* [1975]. The origins of the diffuse auroral precipitation was recently reviewed by *Ni et al.* [2016]. While resonant wave-particle interactions have been long proposed as a fundamental process contributing to the formation of diffuse aurora, understanding the relative importance of various magnetospheric waves, has been intensively ad-

vanced in recent years [*Ni et al.*, 2016]. The diffuse aurora is in general most intense from premidnight to dawn owing to a combination of the plasma convection ($\mathbf{E} \times \mathbf{B}$-drift) and gradient drift that transport the electrons predominantly eastward and the ions predominantly westward around the Earth. The weaker dayside electron diffuse auroral precipitation can be accounted for, in part, by dayside chorus pitch angle scattering [*Li et al.*, 2009; *Shi et al.*, 2012]. The most intense inner magnetospheric electron diffuse auroral precipitation on the nightside results from a combined scattering by upper- and lower-band chorus. However, electrostatic electron cyclotron harmonic (ECH) waves are an important or even dominant scattering mechanism for the nightside electron diffuse auroral precipitation beyond $\sim$8 R_E [*Zhang et al.*, 2015]. Using the Fast Auroral Snapshot Explorer (FAST) satellite and airborne imagers, *Peticolas et al.* [2002] suggested that ECH waves are generally responsible for scattering less than 2 keV plasma sheet electrons, and that upper band whistler mode chorus is responsible for scattering the higher energy ($\geq$2 keV) plasma sheet electrons into the loss cone, while *Sergienko et al.* [2008] found that ECH waves were responsible for scattering the lower energy electrons (3–4 keV) that produce the structureless background auroral luminosity, while whistler mode chorus was responsible for scattering higher-energy ($\geq$4 keV) electrons that cause the more intense diffuse aurora with fine structures.

The ion precipitation also contributes to the diffuse aurora. The ion precipitation is thought to mainly result from field line curvature scattering when the radius of the curvature of the field lines in the stretched magnetotail becomes comparable to the gyro-radius of protons in the central plasma sheet [e.g. *Sergeev et al.*, 1983]. However, theoretical and observational results have positioned scattering by electromagnetic ion cyclotron (EMIC) waves as the leading candidate responsible for the ion precipitation in certain regions of the inner central plasma sheet and ring current [e.g. *Liang et al.*, 2014; *Lundblad and Søraas*, 1978; *Ni et al.*, 2016; *Søraas et al.*, 1999]. The average integral number flux and energy flux of the precipitating ions is typically one to two orders of magnitude less than that of the precipitating electrons at all latitudes, magnetic local times (MLT), and activities [*Hardy et al.*, 1989], but can exceed that of electron precipitation, such as in the pre-midnight local times at sub-auroral latitudes during substorms. The ion precipitation is therefore an indivisible part of the global-scale diffuse auroral precipitation, but the electron precipitation is the dominant source of the diffuse aurora.

3.1.2 Internal structure

The term “diffuse" implies that there is no internal structure. The diffuse aurorae have generally been regarded as pretty much uniform. However, fine scale structures have been reported equatorward of the diffuse auroral oval, for example diffuse forms which exceed 200 km in width, which frequently show fine-scale (∼50 km) structure [*Wallis et al.*, 1979] and subvisual (100 R in the green line) diffuse regions of precipitation that break up into small irregular swirls and spots [*Pedersen et al.*, 2007]. *Sergienko et al.* [2008] reported on fine structures in the equatorward diffuse aurora that took form as significantly brighter regular parallel auroral stripes (∼5 km wide) that extended along the magnetic latitude (MLat), moving southward with a velocity of around 100 m/s. It is implied that they can be explained by spatial (and temporal) modulation of the efficiency of whistler mode wave-particle interaction, but the detailed mechanism(s) behind the fine structures are not known. Also the black aurora is found within diffuse aurora. In association with diffuse aurora, the term *black aurora* is used for relatively small, well defined regions with a distinct reduction of luminosity within large-scale regions of otherwise homogeneous, diffuse aurora [*Davis*, 1978]. A more broad definition is the lack of particle precipitation and emissions, either it is within the diffuse aurora or discrete aurora. *Peticolas et al.* [2002] found signatures of depletion in the precipitating high energy electrons and suggested that the black aurora was caused by a localized suppression of the chorus waves, while *Fritz et al.* [2015] suggested that the orientation and morphology of black aurora in conjunction with pulsating aurora fit the possibility of an ionospheric feedback system generating fine-scale structure through small-scale intense electric fields and currents. It is clear that the diffuse aurora despite its name indeed can have a plethora of internal structures.

The pulsating aurora, or fluctuating aurora [*Humberset et al.*, 2016], is the dynamic auroral structures embedded in the diffuse aurora. They can, however, be separated from the diffuse aurora by their higher-energy electron precipitation reaching lower altitudes. Figure 3.2 shows a sketch of the difference in altitude for the diffuse and pulsating aurora along with the discrete aurora for reference [*Brown et al.*, 1976]. The old questions about fundamental aspects of the relationship between the pulsating aurora and the diffuse aurora persist, for example if they are linked via some parent process or by a process internal to the ionosphere [*Lessard*, 2012].

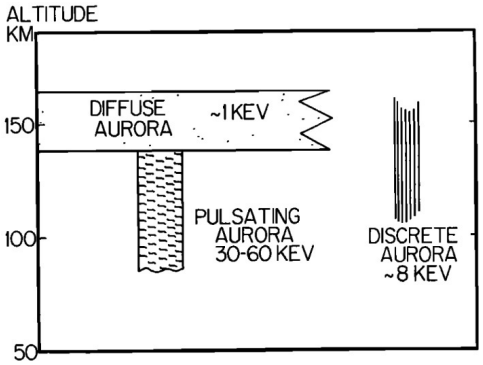

Figure 3.2: Sketch of the difference in altitude for the diffuse and pulsating aurora along with the discrete aurora for reference. The diffuse background is created by electron precipitations of energies $\geq$3–4 keV at higher altitudes. The pulsating auroral emissions are created by time-varying electron precipitation of energies up to tens of keV reaching lower altitudes. The Figure is from *Brown et al.* [1976].

3.2 Pulsating aurora

The pulsating aurora (PA) can be an impressive display (although not as bright or colorful as the discrete aurora) covering the entire sky with faint aurora of intermixed large- and small-scale spatial and temporal variations. As a curiosity, it was first identified based on observations in Bergen, Norway, in 1879 [*Störmer*, 1955]. Clearly, the pulsating aurora is a highly dynamic type of aurora. However, in the shape of persistent patches, it is also a phenomenon that we relatively easy can trace in its frame of reference. Thus we are to a large degree able to separate between how it varies in time and in space. The scale size and dynamics of pulsating aurora, however, present a considerable observational challenge. PA is part of substorms and has recently been shown to be both widespread and persistent. This implies that the pulsating aurora indeed corresponds to a considerable transfer of energy from the magnetosphere to the ionosphere in the form of auroral precipitation, which also can affect the thermospheric neutral wind [*Oyama et al.*, 2010] and other dynamics of the neutral atmosphere. Papers I and II therefore find objective characteristics of the dynamics of pulsating auroral patches.

3.2.1 Broad definition

The broad definition of pulsating aurora covers low-intensity aurora that undergoes repetitive, quasi-periodic, or occasionally periodic fluctuations of alternating increases and decreases in luminosity on time scales ranging from less than 1 s to several tens of seconds [*Royrvik and Davis*, 1977].

3.2.2 Large-scale morphology

Oguti and Watanabe [1976] related the drift of the pulsating aurora region to the electrons drifting eastward around the Earth owing to a combination of the plasma convection ($\mathbf{E} \times \mathbf{B}$-drift) and gradient drift. This was followed up by *Akasofu* [1977] who suggested the mechanism to be pitch angle scattering of high-energy electrons injected into the plasma sheet by magnetospheric substorms.

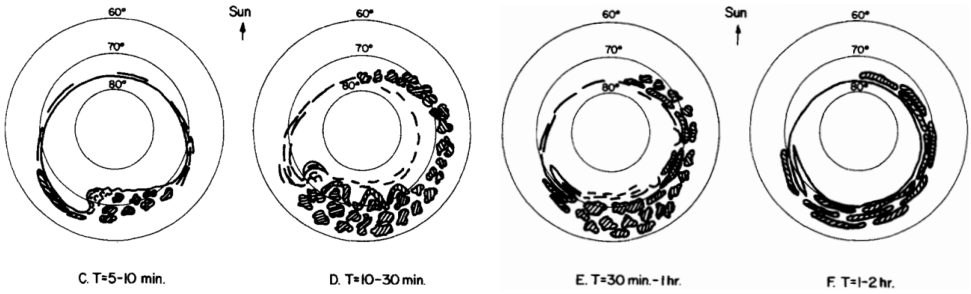

Figure 3.3: Schematic diagram illustrating the development and location of pulsating aurorae in an auroral substorm. The pulsating aurorae are indicated by hatched regions. I show the frames (C-F) where the pulsating aurorae are pronounced, starting at 5-10 minutes after the substorm onset. The figure is adapted from *Royrvik and Davis* [1977].

Figure 3.3 shows a schematic diagram illustrating the development and location of pulsating aurorae in an auroral substorm. The pulsating aurorae are indicated by hatched regions. I show the frames (C-F) where the pulsating aurorae are pronounced, starting at 5-10 minutes after the substorm onset. The sketch is from *Royrvik and Davis* [1977] describing the pulsating aurora in the context of an auroral substorm. The pulsating aurorae appear around midnight a few minutes after substorm onset, before they expand equatorward and eastward into the morning sector in the form of patches and irregular arc segments superposed on a diffuse background. Any discrete aurorae are always located poleward of the diffuse region containing the pulsating forms. In the evening sector, pulsating aurorae were observed also prior to an isolated substorm. The pulsating aurorae around midnight were in general more complex, brighter and extensive in latitude than those in the morning sector. *Royrvik and Davis* [1977] concluded that they were unable to find any significant relationship between PA behavior and the type of activity, the level of activity, or for that matter relative time or location.

More recent studies suggest that pulsating aurora is a persistent, long-lived phenomenon that is not strictly a substorm phenomenon, but may be temporarily disrupted by auroral substorms. *Jones et al.* [2011] found that pulsating aurora is quite common

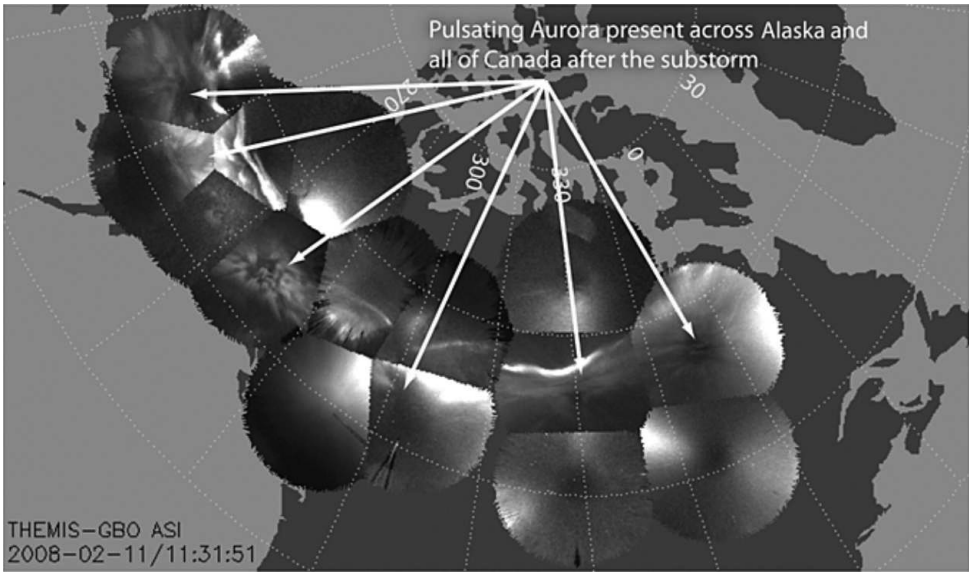

Figure 3.4: An event of pulsating aurora observed by the entire THEMIS ASI array across North America. This event lasted more than 15 hours, covering a region corresponding to more than 10 hours in MLT. The figure is from *Jones et al.* [2013].

with the occurrence rate increasing towards morning hours to around 60 %, with 69 % of pulsating aurora onsets occurring after substorm breakup. Later, *Jones et al.* [2013] investigated one of the very long-lived events lasting for more than 15 hours. A snapshot of the event is shown in Figure 3.4, where pulsating aurora is observed by the entire Time History of Events and Macroscale Interactions during Substorms (THEMIS) mission ASI array. They found that the optical pulsations at times are locally interrupted or drowned out by auroral substorm activity but are observed in the same location once the discrete aurora recedes. Moreover, the pulsations following the auroral breakup appear to be brighter and have a larger patch size than before breakup. The high occurrence rate, the sometimes missing substorm precursor and the finding of many events lasting significantly longer than the typical 2–3 hours substorm recovery phase, suggest that pulsating aurora is not strictly a substorm recovery phase phenomenon and indeed is an important part of the magnetosphere-ionosphere coupling.

3.2.3 Characteristics

The pulsating aurorae have joint characteristics other than their intensity fluctuations. However, as will be described in this section, there are large variations within typical characteristics, and there are still several unclarified issues regarding the fundamental characteristics, such as what mechanism determines the on-off intensity variation

[*Hosokawa et al.*, 2015].

Luminosity

The PA is a faint or even subvisual aurora that sometimes can be confused with clouds. It has a brightness in the range from a few hundred Rayleighs to a maximum intensity of $\sim$10 kR in the 427.8 nm line [*Royrvik and Davis*, 1977].

The typical luminosity variation is often described as having periods from 2 to 20 s, with an average period of 8 ± 2 s [*Royrvik and Davis*, 1977]. Also, the term “pulsating" is by definition a regular periodic behavior. However, the luminosity is repetitive in a periodic, quasi-periodic or variable way, and there is a tremendous variety in a train of pulsations. Abrupt changes are often observed, where the shape, duration and spacing of the pulsations from a single form immediately are followed by pulsations of different character. This luminosity behavior were pointed out by the same authors that presented the average period, and are confirmed by the objective temporal characteristics that we present in Paper I. In Paper I we further suggest that the terms “on-time" and “off-time" serve as a more accurate description of the luminosity variations.

Faster fluctuations are frequently observed superposed on slower on-off fluctuation. When the pulsating aurora is viewed with narrow field of view imagers at high frame rates, pulsations of 10 Hz to 15 Hz [*Samara and Michell*, 2010] and as high as $\sim$50 Hz [*Kataoka et al.*, 2012] have been observed superposed on top of slower fluctuations. From recent advances it seems like these high-frequency fluctuations can be split into two categories: the $\sim$3 Hz modulation that has been observed many times in the past (common, but not universal) and the higher frequency fluctuations (>10 Hz) whose occurrence rate is unknown.

Shape and persistency

The pulsating aurora occurs in very different shapes such as east-west aligned bands and arc segments, and irregularly shaped patches, having horizontal sizes of a few km to hundreds of km. To further complicate the decision of shape, they can exhibit very different spatiotemporal characteristics. The standing/pure mode is a synchronous intensity fluctuation over the entire form, while a streaming/expansion mode usually involves outward growth followed by contraction or disappearance as the pulse decays. There are also propagating/moving modes where a patch brightens quickly and sweeps away from its original position as the intensity starts to drop, or forms that propagate laterally across the sky continuously or sequentially [*Yamamoto and Oguti*, 1982].

Scourfield et al. [1972] found that the pulsating forms were coherent within dimensions of around 30–50 km, and that separate patches pulsate independently of each other. It is not clear why the pulsating aurora occurs in the mentioned shapes, and neither why the shapes are sometimes streaming and sometimes not.

While some pulsating aurorae only repeat for a few times [e.g. *Scourfield and Parsons*, 1971], a common characteristic for pulsating patches is their persistence, where the same shape can disappear and appear repeatedly over several minutes. However, how the underlying reason for this persistence is possible remains unclear [*Lessard*, 2012], and the persistence is to our knowledge not quantified in a systematic manner. It is suggested that the shape of fluctuating patches is governed by the wave resonance/cold plasma region at the magnetospheric equator, and that cold plasma of ionospheric origin acts to keep the region stable [e.g. *Li et al.*, 2012; *Liang et al.*, 2015; *Oguti*, 1976]. Alternatively, it is suggested that conductivity gradients in the ionosphere due to the energetic electron precipitation can modify the shapes of fluctuating auroral patches [*Hosokawa et al.*, 2010]. There are however no detailed predictions of patch evolution from these processes. In Paper II we therefore provide objective and quantitative measurements of the extent to which pulsating auroral patches maintain their morphology.

Precipitation, altitude and vertical extent

The earliest observations of fluctuating energetic electron precipitation was made by sounding rockets above pulsating aurora. The electron energies are found within the range of a of a few keV to several tens of keV [*Bryant et al.*, 1975, 1967; *McEwen et al.*, 1981; *Saito et al.*, 1992; *Sandahl et al.*, 1980; *Smith et al.*, 1980; *Yau et al.*, 1981]. However, there are also reports of energies up to 140 keV [*Sandahl et al.*, 1980] and cases of surprisingly low energies (1–2 keV) [*McEwen et al.*, 1981]. *Evans et al.* [1987] observed fluctuating energetic electron precipitation by satellite above morningside pulsating aurora, and found that the maximum amplitude of the pulsating precipitation generally occurred somewhere in the range of 5 to 25 keV, though the percentage modulation increased continuously with energy. More recently, *Jaynes et al.* [2013] reported energies ranging from 30 keV to 50 keV near the equatorial magnetosphere, and *Samara et al.* [2015] found a range of electron energies mostly from 3 keV to 20 keV, but also up to 30 keV for different types of aurora. The $\sim$3 Hz fluctuations have been found in the electron precipitation, in particular *Sato et al.* [2004] found $\sim$3 Hz fluctuations in the down-going high-energy electron flux (>7 keV) that also were apparent in the pulsating aurora at the footpoint of the satellite. Electron energies at which the

fluctuations occur seem to vary from one event to the next. This is also apparent in the altitude of pulsating aurora which is found to vary from event to event and within a train of fluctuations/pulsations from 80 km to around 110 km altitude [*Hosokawa and Ogawa*, 2015; *Jones et al.*, 2009; *Störmer*, 1948], while [*Miyoshi et al.*, 2015] found electron density enhancements at altitudes down to 68 km suggesting that electrons with a wide energy range ($\sim$10 keV up to at least 200 keV) simultaneously precipitate into the ionosphere in association with the pulsating aurora.

Stenbaek-Nielsen and Hallinan [1979] observed pulsating aurora with a vertical thickness ($\leq$2 km), which is less than the scale height of the atmosphere and therefore could not be produced by the traditional collisional process by precipitating particles. The vertical extent has later been supported by EISCAT observations of enhanced ionospheric electron densities with a thickness of 8 km and 4.5 km or less [*Kaila et al.*, 1989; *Wahlund et al.*, 1989]. *Hallinan et al.* [1985] however, followed up on the study by *Stenbaek-Nielsen and Hallinan* [1979] and found that the thinness occurs irregularly in pulsating aurora. Recently, *Jones et al.* [2009] examined four events of electron density profiles associated with the pulsating patches using an incoherent scatter radar and found that they all had a vertical thickness of $\sim$15–25 km, a result in support of vertically thinness being a subclass of pulsating aurora.

Drift

It has been proposed that imaging of pulsating auroral patches can be used to remote sense magnetospheric convection [e.g. *Nakamura and Oguti*, 1987; *Yang et al.*, 2015, 2017]. The assumption here is that all PA patches move with the plasma convection $\mathbf{E} \times \mathbf{B}$ velocity. The drift speed has been consistently measured to be on the order of 1 km/s in the morning sector, presumably at the $\mathbf{E} \times \mathbf{B}$ velocity [*Davis*, 1978; *Scourfield et al.*, 1983], but there have been studies which suggests that the PA drift can be different from the plasma convection. As an example, the magnetospheric electric field above a pulsating aurora were found to be larger than what was expected from the auroral drift [*Swift and Gurnett*, 1973], and a barium ion cloud was observed to drift in the same eastward direction, but at a higher speed than the widespread display of pulsating aurorae below [*Wescott et al.*, 1976]. In the detailed investigation on the coherency of four PA patches in Paper II we therefore compare their drift to the $\mathbf{E} \times \mathbf{B}$ velocity, in order to test if all patches are drifting solely with the plasma convection.

Poor conjugacy

Conjugacy of PA is investigated by cameras on airplanes along conjugate paths in the southern and northern hemisphere, or on conjugate ground stations. Conjugacy means occurring at the two opposite ends of the same magnetic field line. Due to the complexity of a pulsating auroral display, we can distinguish two types of non-conjugacy: 1) PA appears in both hemispheres with similar shapes, but the pulsation periods are almost always different. 2) PA appears only in one hemisphere (e.g. in form of an isolated large patch).

From a few events of pulsating aurorae from aircrafts in magnetically conjugate paths, clearly identifiable simultaneous pulsation were observed [*Belon et al.*, 1968, 1969; *Davis*, 1978], while *Stenbaek-Nielsen et al.* [1972, 1973] reported that the general conjugacy was not obvious as some had identifiable phase-shift or no recognizable hemispherical relation, suggesting that there must be different classes of pulsating aurora. From conjugate ground observations, *Fujii et al.* [1987] reported that pulsating aurora appeared synchronously in both hemispheres, except from the streaming that occurred out of phase or asynchronously. Other ground-based studies showed a distinct lack of correlation where no pulsating aurora appeared synchronously and most individual pulsating patches did not have clear counterparts in the opposite hemisphere [*Minatoya et al.*, 1995; *Sato et al.*, 1998, 2004; *Watanabe et al.*, 2007]. An example of the two types of non-conjugacy is shown in Figure 3.5.

As evident from above and also stated in the review by *Sato et al.* [2012], the mounting evidence from different studies suggests that the conjugacy of PA is generally poor, and as far as they can check, there are only two good conjugacy events (both in shape and phase). It is also possible that early studies were biased for good conjugacy because good conjugacy is easier to identify than poor conjugacy. The pulsating aurora is therefore occasionally conjugate, but mostly poor or non-conjugate. The pulsating aurora is therefore mostly poor or non-conjugate, and occasionally conjugate.

3.2.4 Source and mechanisms

There is an agreement that the high-energy precipitating electrons result from pitch angle scattering. The source particles are therefore likely the same as for the dominant part of the diffuse aurora but of higher-energy, namely substorm injected plasma sheet electrons that drift to the morning sector [*Nemzek et al.*, 1995]. However, exactly how the bright/on-dim/off pulsation occurs is still up for discussion. Historically the mechanism has been suggested to be located at magnetic equator, a region much further

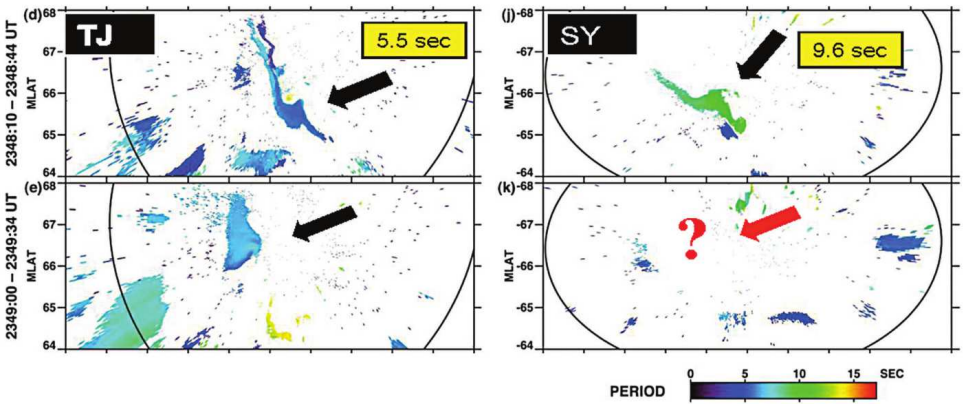

Figure 3.5: This is an example of non-conjugacy in pulsating aurora during recovery after an auroral breakup found by *Watanabe et al.* [2007]. It also shows the two types of non-conjugacy. One is the case in which the pulsating aurora appears in both hemispheres, and the shapes are similar but the pulsation periods are almost always different in the two hemispheres (d and j). The other is the case in which the pulsating aurora appears only in one hemisphere (e and k). The black arrows indicate pulsating aurora patches and the pulsation periods are determined from an autocorrelation analysis. This also an example an event where there is no uncertainty in identifying the conjugate regions because the aurorae during the auroral breakup showed remarkable conjugacy. The figure is from *Sato et al.* [2012] that adapted it from from *Watanabe et al.* [2007] .

earthward, or a source in the ionosphere, as will be outlined below.

Time varying pitch-angle scattering

Most studies point towards a time varying pitch-angle scattering close to the magnetic equator. In-situ studies have observed lower-band chorus [*Nishimura et al.*, 2010, 2011] (Figure 3.6), and continuous measurements of fluctuations in the electron flux [*Jaynes et al.*, 2013] correlated with the luminosity fluctuation of a pixel within a pulsating patch using the best-fit within the ASI FOV containing the mapped footpoint. However, *Nakajima et al.* [2012] observed fluctuating precipitation without the presence of whistler (and ECH) waves with sufficient amplitude. Instead they suggested that the electrons were already accelerated by earthward flows (Fermi-type acceleration) so that even small pitch angle modulation around the loss cone angle by weak waves possibly could produce fluctuations of aurorae. A correlation in the fluctuation of all three parameters (waves, precipitation and auroral luminosity) is yet to be published.

Before these studies, velocity dispersion (or time dispersion) gave indirect evidence of a mechanism close to the magnetic equator. In a beam of energetic electron precipitation the highest-energy electrons reach the atmosphere first and will at ionospheric

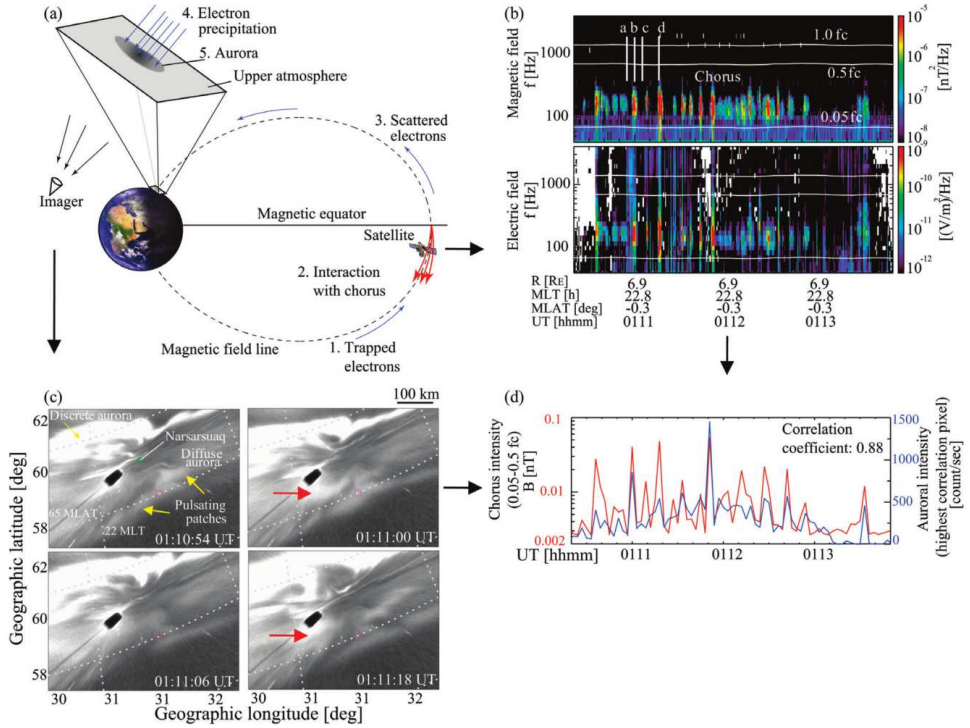

Figure 3.6: Correlated observations of pulsating aurora and lower-band chorus by *Nishimura et al.* [2010]. (a) Schematic diagram showing the geometry of chorus wave propagation (red arrows), electron precipitation (blue arrows), and PA. (b) THEMIS A spacecraft observations of lower-band chorus bursts (electromagnetic field spectra). The local electron cyclotron frequencies (fc) are calculated from the measured magnetic field and marked with white horizontal lines. (c) Snapshots of ASI data projected onto geographic coordinates at 110 km altitude. The pulsating patch that is correlated with chorus is indicated by the red arrows. The snapshot times are also marked in panel b by white vertical lines. The pink square shows the magnetic footprint of the spacecraft that is located close to the center of the imager field of view (green square on top right image). Dashed lines represent magnetic coordinates every 3° in latitude and 1 h in local time. (d) Correlation of lower-band chorus wave amplitude integrated over a frequency range of 0.05 to 0.5 fc (red) and auroral intensity (blue) at the highest cross-correlation pixel. The figure and results are from [*Nishimura et al.*, 2010].

altitudes result in time delays in fluctuations between the low-energy and high-energy electron populations. This has been used to estimate the travel distance assuming that the fluctuations are generated at one altitude. The first studies [e.g. *Bryant et al.*, 1971; *Yau et al.*, 1981] had large error bars and found sources distributed almost continuously from magnetic latitudes of 50° to −20°. Later studies found the sources confined to the equatorial region up to around 15° when accounting for the details of the suggested pitch angle scattering mechanism, for which the waves propagate toward higher latitudes and scatter electrons with increasingly higher energy electrons traveling in the

opposite direction [*Miyoshi et al.*, 2010; *Nishiyama et al.*, 2011]. In Paper I we discuss time dispersion in more detail, and we find that the characteristics of the energy deposition of the pulsating auroral patches are due to the generation mechanism and not a dispersion effect.

The most frequently mentioned theoretical candidates for a time varying pitch-angle scattering are summarized in Paper I (Table 2), where we also list the corresponding auroral observational consequences. One of the first theories outlined was that ultra-low frequency (ULF) waves changes the velocity distribution of the resonant electrons and thus the whistler mode wave growth rate [*Coroniti and Kennel*, 1970a, b]. However, as we also discuss in Paper I, the in-situ ULF waves (also called micropulsations or magnetic pulsations in the Earth's magnetic field) are not found to correlate with chorus waves on the typical time scales [*Tsurutani and Smith*, 1974]. Recently, *Jaynes et al.* [2015] suggested that substorm-driven Pc4–5 magnetospheric ULF pulsations (field line resonance as a result of a substorm injection) modulates chorus waves, and link observations of chorus with $\sim$45 s to 1 min periods to ULF waves having periods closer to 2 min, thus occurring with twice the periodicity. On the other hand *Li et al.* [2011b] found a one-to-one variation in the ULF and chorus modulations, but they also focused on the modulation of whistler mode waves by long period compressional pulsations in the Pc4-5 range and did not investigate individual chorus elements, but rather a group of chorus elements showing intensification over a timescale of tens of seconds to a few minutes. The first proposed theory on time varying pitch-angle scattering by ULF waves [*Coroniti and Kennel*, 1970a, b] have therefore largely been discarded.

Other frequently mentioned theories are the nonlinear relaxation oscillator [*Davidson*, 1979, 1986a, b] and the flow cyclotron maser [*Demekhov and Trakhtengerts*, 1994]. The nonlinear relaxation oscillator is based on solving three non-linear differential equations that jointly describe the time variations of waves and of particles (trapped particle flux, pitch-angle diffusion coefficient, and anisotropy). The control of wave growth is attributed to changes in the anisotropy as the loss cone is filled and emptied, where the particles that are lost need to be replenished for the cycle to start again. The flow cyclotron maser is a theory similar to the nonlinear relaxation oscillator, but explicitly deals with the details of the wave particle interaction, which has the distinct advantage of providing quantitative testable predictions. It can thus be compared with observations. The flow cyclotron maser starts with a continuous stream of energetic electrons that enters a flux tube with enhanced cold plasma density, which serves as a resonance cavity. Low-frequency waves start to scatter the high-energy electrons into the loss-cone. The scattering moves towards higher wave-frequencies

and lower-energy electrons and thus includes more particles. This continues until a maximum of the electrons participate and the waves are damped. A new injection of an anisotropic high-energy electron distribution is needed for the cycle to start again. Also the loss of electrons within the loss cone will cause anisotropy, but only sufficient to cause a small part of the electron distribution to diffuse. The wave growth and thus pulsation periods are very sensitive to the density of the cold plasma (the less dense, the shorter periods), which must be over a certain threshold (10 cm^{-3} and 1000 times denser that the injected electrons). The model also includes the wave reflection coefficient, R, in the ionosphere and a dependence on L-shell. The total injected energy must be over a certain threshold, and higher L-shells give larger injections of higher-energy electrons. However, large injections will dampen the pulsations, meaning that the most pronounced fluctuations should be seen at lower latitudes. From measurements of energetic electrons and plasma density at geosynchronous orbit, *Nemzek et al.* [1995] found support for the minimum energetic electron density, but likely not the plasma density conditions predicted by the nonlinear relaxation oscillator, while the minimum change in plasma density and electron flux predicted by the flow cyclotron maser seem to be supported. Further, *Nishiyama et al.* [2014] points out that the flux of the active high-energy electrons in the flow cyclotron maser has not been found to change drastically between the on and off stages. This was based on the observation that the Reimei satellite usually measures trapped energetic electrons in the pitch angle range from 60° to 120° at ∼650 km altitude regardless of on and off stages of PAs, and the observation by *Jaynes et al.* [2013] where the 30–50 keV precipitating electrons were found to fluctuate, while the trapped electrons of the same energy range did not show similar fluctuations. The in-situ parameters seem to not give a clear support to these theories. In Paper I we discuss how the temporal characteristics and energy deposition of a detailed analysis of six pulsating patches from ground fit within the observational constraints of these theories.

There is also debate around the time-variation of ∼3 Hz commonly found to be superposed on the main emission fluctuation. *Nishiyama et al.* [2016] suggest that the movement of ∼3 Hz substructures embedded within a pulsating patch compares to the propagation whistler mode chorus elements in support of a time-varying pitch-angle scattering near the magnetic equator, while *Fukuda et al.* [2016] suggests, based on rapid quasi-periodic expansions of the edge of pulsating features, that the ∼3 Hz variation is rather caused by Alfvén waves modulating the electron precipitation.

In the last few years, an increasing number of in-situ observations at the magnetic equator have made it possible to compare local plasma parameters (chorus waves, elec-

tron cyclotron harmonic waves, plasma densities and ULF waves etc.) and thereby understand the time-varying pitch-angle scattering. There are for example an ongoing research on the role of the cold background plasma as driver of the chorus emissions. *Li et al.* [2011a] reported that depletions in the total electron density were correlated with increases in chorus wave amplitude and demonstrated that they could lead to an intensification of chorus waves by calculating the linear growth rates of chorus waves using the observed plasma parameters. Further, *Nishimura et al.* [2015] found fluctuations of low-energy ion fluxes that correlated with chorus intensity, and *Liang et al.* [2015] observed low-energy ion precipitation by low-Earth-orbit satellites above pulsating auroral patches suggesting that the changes in the cold plasma might be associated with ion outflows from the ionosphere.

Processes closer to Earth

The pulsating aurorae also have well known characteristics, such as thin vertical extents and conjugate points in each hemisphere that is either poorly correlated or not correlated at all, which is difficult to explain with a single mechanism located at the magnetic equator.

The vertical extent of PA can be either very thin <4.5 km or ∼15–25 km (see Section 3.2.3). The very thin pulsating aurora cannot be produced by the traditional collisional process by precipitating particles, not even a monoenergetic beam, therefore ionospheric effects must contribute to the process [*Stenbaek-Nielsen and Hallinan*, 1979] . One likely process [*Stenbaek-Nielsen and Hallinan*, 1979; *Wahlund et al.*, 1989] is the so called enhanced aurora [*Hallinan et al.*, 1985]. It supposedly occurs when precipitating electrons cause growth of ionospheric plasma waves in the electron plasma frequency range, which then accelerate the ambient ionospheric electrons to reach the ionization threshold. However, as *Hallinan et al.* [1985] points out, enhanced aurora can be observed in all types of aurora below around 130 km altitude and it "*partakes the motions and luminosity fluctuations characteristic of the aurora in which it is observed*" (page 8472). If the subset of very thin PA is indeed enhanced aurora, it seems likely that it is not the ionosphere that creates the fluctuations in luminosity.

A rather direct evidence of the contribution of ionospheric processes is that fluctuations in luminosity and particle precipitation can be artificially induced by chemical releases in the ionosphere [*Deehr and Romick*, 1977; *Holmgren et al.*, 1980]. To my knowledge there is no accepted theory for the process, but *Holmgren et al.* [1980] suggested that the artificially induced low-energy part of the acceleration could be due to

parallel electric fields, created by field-aligned currents that were set up by the plasma injection, and further that pitch angle scattering in the magnetosphere may account for particle precipitation continuing for as long as $\sim$2 min after their release.

Observations and time-of-flight calculations from velocity dispersion of the precipitating electron have given unambiguous results to where the mechanism is located. As I explained earlier, time-of-flight calculations have been used as indirect evidence of a mechanism close to the magnetic equator. However, *Sato et al.* [2004] demonstrated that the source region of the pulsating aurorae that they observed was located earthward, far from the equatorial plane. Further, in his review of pulsating aurora *Lessard* [2012] mentions that *Williams* [2002] found no evidence of velocity dispersion in the pulsating electron data obtained from the PARX sounding rocket in the region over a pulsating aurora event. Thus, the different results can point toward both a near earth mechanism and maybe even a mechanism within the ionosphere.

The characteristic of poor or non-conjugacy is hard to explain with a time-varying pitch angle scattering mechanism at the magnetic equator. *Sato et al.* [2004, 2002] showed observations of velocity dispersed high-energy electron precipitation in correlation with non-conjugate pulsating aurora and anti-correlated with the proton flux. These are instead suggested to have a near Earth mechanisms which set up time-varying field-aligned potential drops [*Fedorov et al.*, 2004; *Pilipenko et al.*, 1999; *Sato et al.*, 2004]. In particular, *Fedorov et al.* [2004] found that Alfvén wave structures can penetrate into the auroral acceleration region (1-2 R_E altitude) and produce oscillatory variations of the already existing field-aligned potential drop, and thus acceleration and resulting fluctuations in the electron precipitation in the range around fractions of one Hz.

There seems to be a concensus that the ionosphere and neutral atmosphere are not entirely passive, but exactly what role they play remains largely unclear [*Lessard*, 2012; *Stenbaek-Nielsen*, 1980]. There are not many suggestions of a source local to the ionosphere and atmosphere. One idea is that the neutral atmosphere can drive fluctuations in the auroral luminosity. Steady particle precipitation can get enhanced and reduced repeatedly by atmospheric oscillations that increase and decrease the loss altitude (effectively a variation in the size of the loss cone) that can be provided by acoustic-gravity waves [*Luhmann*, 1979]. The pulse shape and the magnitude of the pulsations depend on both the energy spectrum and the pitch angle distribution of the particles and the amplitude and altitude distribution of the atmospheric waves. However, *Davidson* [1990] claimed that the mechanism would impose a spatial regularity that is not observed. Maybe it is more likely that the lower ionosphere and atmosphere have an alternating

component, such as an ionospheric feed-back mechanism based on the flow cyclotron maser theory suggested by *Tagirov et al.* [1999]. However, as pointed out by *Watanabe et al.* [2007], it is unlikely that the participation of the ionosphere suggested by *Tagirov et al.* [1999] can alter the fluctuation characteristics as drastically as they see in the pulsating aurora at conjugate locations in the southern and northern hemispheres.

It is likely that the ionosphere is not passive. Other indications that it can be active or modifying are fine-scale structures embedded in pulsating aurora and the persistence in the shape of pulsating auroral patches. Earlier, I mentioned that ion outflows from the ionosphere can cause changes in the cold plasma suggested to drive a time-varying pitch-angle scattering. Further, *Fritz et al.* [2015] observed a black aurora curl structure in conjunction with pulsating aurora and suggested that they could be generated by a mechanism similar to the ionospheric feedback mechanism that is suggested to cause fine-scale structures in an auroral arc through small-scale intense electric fields and currents. They could, however, not rule out magnetospheric processes. What causes the persistence in patch shape can be of ionospheric influence, but it is largely an open question that we discuss further in Paper II.

In summary, even if the pulsating aurorae have similar characteristics, these characteristics are also highly variable. It is a mystery whether pulsating aurorae can have different mechanisms as suggested by *Sato et al.* [2004], or whether the large variation can be explained by one mechanism. To understand the latter we also need to solve some fundamental questions on pulsating aurora, such as what underlying mechanism(s) controls their on-off fluctuation, shape and coherency. This illustrates the need for better characterization. We therefore do a careful study of the shape, coherency and drift of pulsating aurora in the form of patches.

In summary, most of the research now focus on the magnetospheric region for a source and mechanism for the pulsating aurora. However, it remains to figure out if the large variation within the different characteristics points towards several types of pulsating aurorae (with different mechanisms) that falls into the same broad category of pulsating aurora, or whether they can all be explained by time-varying pitch-angle scattering alone.

3.2.5 Open questions

A burst of interest drove a concentrated research effort on pulsating aurora in the 1970s, but later it did not receive the same attention as many other types of auroral phe-

nomenon. Recent results, however, imply that the pulsating aurora may be a more important part of the magnetosphere-ionosphere coupling, and spacecraft observations at geosynchronous orbit have made new observations allowing us to advance our understanding of the processes behind pulsating aurora. While this recent research has answered some of the most fundamental questions about pulsating aurora, it has also led to other, more comprehensive questions [*Lessard*, 2012]. However, even as these new questions emerge, older questions about fundamental aspects of pulsating aurora remain. In the most recent review, monograph and introduction to a special section on pulsating aurora *Lessard* [2012], *Li et al.* [2012], and *Hosokawa et al.* [2015] (respectively) list or highlight the open questions that remains to be resolved. Here I highlight a few of the open questions that I find the most intriguing.

What mechanism(s) governs the on-off fluctuations?

Chorus wave intensity as measured by single satellites at the magnetic equator are found to be correlated to the best-fit pixel of auroral luminosity in the ASI containing the mapped footprint of the satellite. So, if chorus waves are responsible for the fluctuations, why is the chorus wave intensity fluctuating? Furthermore, can time-varying field-aligned potentials far from the magnetic equator play a role in the pulsating aurora? In Paper I we therefore determine the characteristics of pulsating auroral patches in order to provide better observational constraints on the suggested mechanisms.

What governs the shape and persistency of pulsating auroral patches?

As discussed in Section 3.2.3, the underlying reason for the persistent shape of pulsating auroral patches as they disappear and reappear repeatedly over several minutes is not fully understood. Also, exactly how persistent the patches are is often loosely described and there are no quantitative measures to how the shape of a patch evolves. In Paper II we therefore provide objective and quantitative measurements of the extent to which pulsating auroral patches maintain their morphology.

What are the causes of the spatiotemporal variations within the pulsating auroral patch?

It is not known to what extent the pulsating auroral shapes fluctuate coherently. Three fundamentally different modes, described in Section 3.2.3, have been proposed. However, why the shapes sometimes pulsate coherently and sometimes not, and the underlying cause(s) of the spatiotemporal variations remains to be determined. In Paper II we therefore estimate the extent to which each of the patches fluctuate in a coherent

fashion.

3.3 Discrete aurora

The most known form of the discrete aurorae are the bright auroral arcs within the auroral oval. They can be both relatively quiet or highly dynamic with rapidly changing structures depending on geomagnetic activity. By observing the discrete aurora alone, it is difficult to distinguish the exact processes causing the display [e.g. *Paschmann et al.*, 2003]. The discrete aurorae are therefore often divided into the characteristics of the precipitation (a few to tens of keV), as they can result from mono-energetic/inverted-V or broadband/Alfvénic electron precipitation. In Paper III we describe the dynamics of the aurora during moderately disturbed conditions leading up the a substorm onset. We find that the scale size dependent characteristics differ for two smaller time intervals of the event. It seems reasonable that the characteristics of the emissions is also the characteristics of the precipitating electrons, but we have no objective way to separate the different emissions and their characteristics. We are therefore careful in discussing how the characteristics vary in response to the types of electron precipitation that produce the discrete aurora. However, for context I here give a brief description of the two types of discrete aurorae, acknowledging that its underlying processes, scale sizes and lifetimes is still an active area of research.

3.3.1 Monoenergetic aurora

The monoenergetic aurora comes from plasma sheet electrons that are accelerated in relation to quasi-static potential drops parallel to the geomagnetic field at an altitude from 1000 km up to a few R_E. Auroral arcs are produced by thin sheets of precipitating electrons that also carries a considerable upward directed Birkeland current. In simple terms, the auroral acceleration by potential drops is associated with the need to maintain ionospheric current continuity which require an enhancement of the ionospheric conductivity. Although the precise generation mechanism of these structures has been thoroughly examined over the last several decades, it remains an open topic of research [*Colpitts*, 2015, and references therein]. The precipitating electron energy spectrum has a distinct “mono energetic" peak, meaning that a small range of energies dominate completely over other energies. This characteristic is consistent with electrons that are accelerated by a potential drop somewhere along the field line [*Evans*, 1974]. The potential drop typically decrease as a function of distance from its maximum. The spectrogram measured along a satellites' trajectory will then look like an inverted-V, which is the reason that the monoenergetic aurora is often referred to as

inverted-V aurora. Inverted-V structures are found stable over the time it takes a low earth orbit satellite to traverse them (up to tens of seconds). However, *Thieman and Hoffman* [1985] observed precipitating particles made by the two Dynamics Explorer spacecraft and found that a few minutes could result in significant differences in the maximum energy of inverted-V events.

3.3.2 Broadband aurora

Discrete aurora can also result from very high fluxes of electron precipitation with a broadband energy distribution. They are likely accelerated by dispersive Alfvén waves at altitudes between 1 and 2 R_E as they propagate from the magnetosphere along the geomagnetic field [*Andersson et al.*, 2002; *Chaston et al.*, 2000, 2003a; *Mende*, 2016]. The Alfvénic/broadband precipitation is often viewed as a transition between two states and for example found associated with the poleward boundary of the auroral oval in the premidnight sector [*Chaston et al.*, 2003a] and in substorm aurora [*Mende et al.*, 2003]. *Newell et al.* [2009] found that the total energy carried by broadband aurora is more sensitive to solar wind driving than other types of aurora and responsible for as much as 28 % of the particle number flux to the ionosphere during active times.

Alfvénic aurora is the most challenging type to investigate since it covers scale sizes up to a few tens of km with lifetimes less than the Alfvén transit time between the magnetosphere and the ionosphere, which is on the orders of minutes. It is in general difficult to distinguish between the mono-energetic and broadband precipitation by observing the discrete aurora alone. For example *Colpitts et al.* [2013] observed Alfvénic aurora intermittently and perhaps simultaneously with inverted-V aurora during an event of continuous substorm activity. They described the aurora as extremely dynamic changing on timescales of seconds with bright spots and arcs that were not as elongated in the east-west direction as during typical inverted-V events. Further, *Mende et al.* [2003] found that in substorm aurora outside of the surge, the Alfvénic electrons were less clearly separated from the inverted-Vs.

Chapter 4

Ground-based auroral imaging

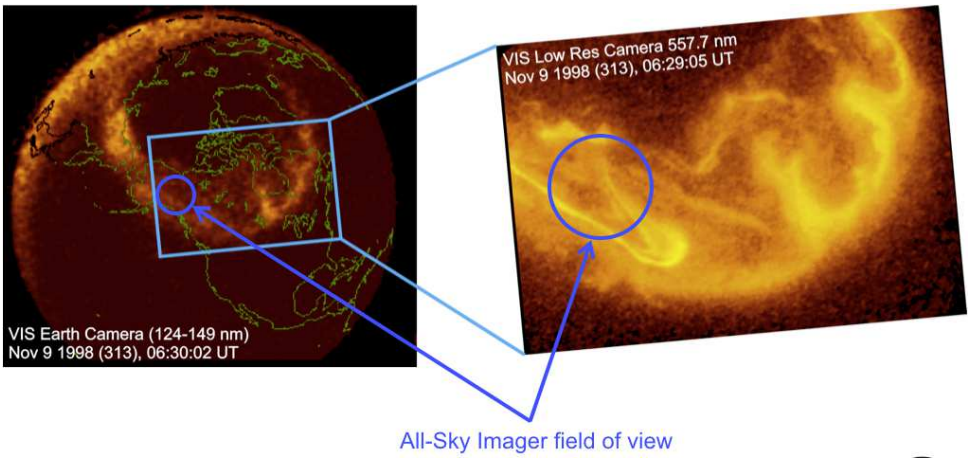

Figure 4.1: The FOV of an ASI imager superposed on the auroral oval as captured by the Visible Imaging System (VIS) [*Frank et al.*, 1995] onboard the Polar spacecraft. The sunlight on the dayside and the UV-auroral oval on the nightside is imaged by the VIS Earth camera, while the VIS Low Resolution Camera captures the aurora (green-line) in more details.

The aurora was originally studied from ground as a broad band emission covering the entire visible spectrum. Then filters and photo multipliers made it possible to study narrow band emissions. We utilize ground-based observations of auroral emissions since they provide extended periods of continuous observations at a fixed position in the ionosphere. To capture a large range of scale sizes we use an all-sky imager (ASI). As can be seen in Figure 4.1, an ASI field-of-view (FOV) can almost cover the width of the auroral oval, and rotates with the Earth along the auroral from evening to morning. At the same time this effectively means that we neglect the fine scale-sizes ($<$ 1-2 km), which can be captured with narrow-field of view imager with high time resolutions. This inherent limitation is further discussed in Chapter 6.1. In this chapter I introduce

the auroral spectrum and a selection of emissions that are important for auroral studies, including green line (557.7 nm) auroral emissions utilized in Papers I-III. Then I describe the all-sky imager and how we process the images to answer the science objectives.

4.1 Auroral spectrum

Figure 4.2 shows a typical spectrum of bright aurora. The spectrum is covering the aurora that is visible to the human eye (around 390 to 700 nm), but also a some of the ultraviolet aurora (<400 nm) and infrared aurora (>700 nm). The ultraviolet and X-ray aurorae are best observed from space, because atmospheric scattering (attenuation and absorption) of the emissions increase with the frequency of the photons. In general, the visible aurora can be divided into three colors: red, green and blue. Other colors, like yellow or pink in the aurora, are due to a composition of different emissions. The aurora can at times appear white or grey in color, yet it is usually green aurora that is too dim to meet the color threshold of the human eye. For example the pulsating aurora is typically very dim, and can be mistaken for clouds.

The aurora is due to de-excitation by spontaneous radiation of the excited atoms and molecules. The probability for this happening has an exponential decay. The lifetime of the given state is then the mean lifetime/exponential time constant. Physically, the lifetime is the time required for the system response to decay by $1/e \approx 36.8\,\%$. An excited state can decay to different energy levels. Then, those will have different probabilities of occurring, and thus occur at different rates with different lifetimes. The excited states that have longer lifetimes than a few tens of nanoseconds are called metastable states. These are associated with "forbidden" energy state transitions in quantum mechanics, where the provided energy undergoes an unusual intersystem crossing and becomes trapped with only “forbidden" transitions available to return to a lower energy state. However, these transitions, although “forbidden", will still occur in quantum mechanics, but with a significantly lower probability and therefore longer time scales. Knowledge on the process of de-excitation of forbidden transitions can be useful, for example to make toys glow in the dark. For the aurora, as we will come back to, the knowledge is crucial for understanding the auroral display and how the different emissions lines can be utilized in auroral studies.

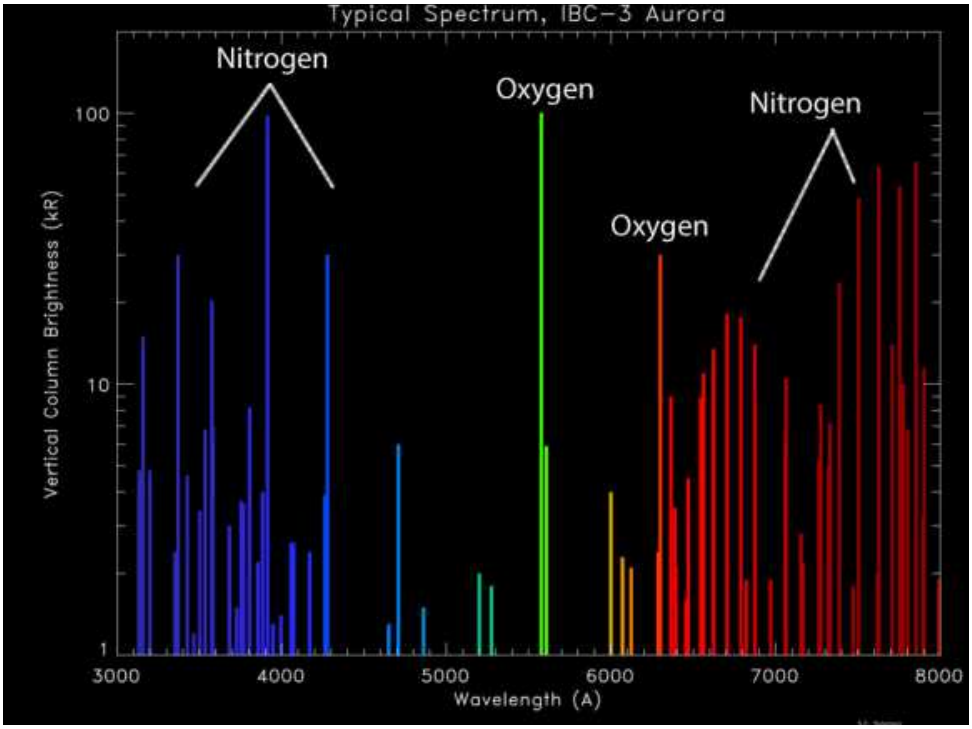

Figure 4.2: A typical spectrum of the visible bright aurora (IBC-3). The wavelengths of the auroral emission lines and bands are given in Ångstrøm, which equals 0.1 nm, and their brightness in kR. It is roughly indicated which emissions are due to Oxygen and Nitrogen (atomic, molecular or ionized is not differentiated). The source of this material is the COMET® Website at http://meted.ucar.edu/ of the University Corporation for Atmospheric Research (UCAR).

4.2 Important emissions for auroral studies

In Papers I-III we have utilized the 557.7 nm green aurora that is described in the next section. For comparison I first introduce two examples of red and blue aurora that are widely used in auroral studies.

4.2.1 Blue aurora at 427.8 nm

The blue-violet aurora in the form of the 427.8 nm band, is often used in the studies of auroral dynamics because it is the result of spontaneous decays with a lifetime of 70 ns. Collisions between electrons and molecular nitrogen, N_2^+, leaves some of the ionized molecules in the upper excited state of the first negative band ($N_2^+(B^2\sum_u^+)$) with an excitation potential energy above the ground state of 6.2 eV. This results in emissions with a maximum at 427.8 nm in a fraction of the decays. The intensity of

the 427.8 nm emissions can be used to determine the total energy flux carried by the precipitating electrons. This is possible because the emissions are prompt and result from precipitation of electrons at all energies above the excitation energy.

4.2.2 Red aurora at 630.0 nm

The most important red aurora is the ∼630.0 nm line. It is produced by the transition from the metastable excited atomic oxygen O(^{1}D) to the ground state O(^{3}P). It has two special properties: 1) A low excitation potential energy (1.96 eV), 2) a long lifetime of ∼110 s [*Rees and Roble*, 1975]. The increasingly denser atmosphere at lower altitudes causes the excited oxygen to easily lose its energy by collisions instead of emitting light (quenching). This is why the red aurora typically has its maximum intensity high in the atmosphere at around 250-300 km altitude, and results from the low-energy part of the electron precipitation. This means that the luminosity of the 630.0 nm typically depends strongly on the mean energy of the precipitating electrons. Figure 4.3 shows the height distribution of the excitations rate of the metastable states O(^{1}D), where the dashed curve also takes quenching into account.

During the relatively long lifetime, the atoms can move considerably from the location they were excited, resulting in a rather uniform aurora that is not suited to study dynamics. However, at some conditions the 630 nm emissions are observed as almost prompt emissions (private communication with Dr. Robert Michell). These possibly occur when the precipitation results in a sufficiently large amount of O(^{1}D) excitations at low altitudes. Then the part of the decay distribution with very short lifetimes can be detected, while the the rest is quenched. Also, *Liang et al.* [2016] found noticeable fluctuations in the red-line during dynamic pulsating aurora at lower altitudes than the uniform red aurora. However, he found evidence that some of the cases were due to the pulsating aurora being associated with low energy (< 1 keV) electron precipitation. In general, the red aurora is less visible, not only because of the smearing and quenching, but also because our eyes are less sensitive to the red light, compared to the green light.

4.3 Green aurora at 557.7 nm

The green aurora at 557.7 nm is the brightest emissions in the visible spectrum of most aurorae. It is produced by the transition from the second lowest excited state O(^{1}S) with an excitation potential energy above the ground state of 4.17 eV to the lowest excited state O(^{1}D) in atomic oxygen.

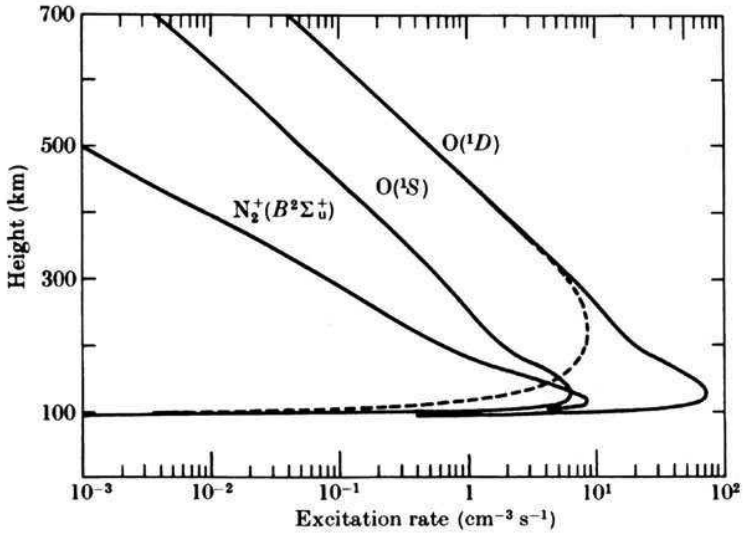

Figure 4.3: Height distribution of excitation rate of the $N_2^+(B^2\sum_u^+)$ state causing the 427.8 nm and 391.4 nm emissions and the metastable states $O(^1D)$ causing the 630.0 nm and 636.4 nm emissions and the $O(^1S)$ behind the 557.7 nm and 297.2 nm emissions. The dashed curve also takes quenching of the metastable $O(^1D)$ state into account. The excitation profiles are estimated from an example spectrum of precipitating electrons. The figure and details can be found in *Kamiyama* [1966].

Exactly how the excitation of the $O(^1S)$ occurs is still not clear. Possible sources are suggested to be direct electron excitation, dissociative recombination with an O_2 ion, and energy transfer from an excited N_2 molecule [*Brekke*, 2013], and dissociative excitation of O_2 [*LeClair and McConkey*, 1993]:

$$e + O \rightarrow e + O^* \qquad \text{Excitation}$$

$$e + O_2 \rightarrow e + O^* + O^* \qquad \text{Dissociative excitation}$$

$$N_2(A^2\sum_u^+) + O \rightarrow O^* + N_2 \qquad \text{Energy transfer}$$

$$e + O_2^+ \rightarrow e + O^* + O \qquad \text{Dissociative recombination}$$

The last two processes have a delay time with respect to the initial ionization and excitation processes. The relative contributions of the various possible excitation processes have been calculated by combining in-situ measurements of various species with atmospheric models and laboratory determined reaction rates, but the results differ [*Burns and Reid*, 1985]. Thus, the possible sources are not well understood and proba-

bly change with altitude and ionospheric conditions.

$O(^1S)$ is a metastable state with a lifetime of 0.75 s. Like the red 630.0 nm aurora, the green aurora can only exist because of the low density of the thermosphere. As the neutral density increases, the 557.7 nm emissions are quenched. However, this becomes important at relatively low altitudes below around 100 km altitude. The quenching and rapid decrease of concentration of atomic oxygen below around 100 km are probably responsible for the abrupt-looking end of the lower edges of green auroral curtains. In auroral rays the green aurora are can also be seen to lag behind the violet-blue aurora. This results from the effective lifetime of the green aurora at 557.7 nm compared to the prompt violet-blue aurora at 427.8 nm. The effective lifetime is a combination of the (radiative) lifetime, possible contributions from time delay excitation processes, and quenching, and can therefore vary slightly from depending on the controlling parameters.

In this thesis we have utilized the 557.7 nm emission because it is brighter than the 427.8 nm. In Papers I and II we utilize the green line to observe the dynamic pulsating aurora, and further discuss how the 557.7 nm emissions is limited by chemical effects compared to prompt emissions such as the violet-blue 427.8 nm. The ASI has a 3.3 Hz time resolution, meaning that the ASI data is limited by the Nyquist frequency of 1.65 Hz, which is comparable to the time delay and smoothing of the effective lifetime of the $O(^1S)$ states.

The 557.7 nm emissions are captured by a narrow band interference filter with a full width at half maximum of 2 nm. The interference filter selects the narrow frequency band by attenuating the other wavelengths in multiple reflections from two semi-reflective coatings on a transparent spacer resulting in destructive interference.

4.4 All-sky imager

The all-sky imager used is part of an experiment called Multi-Spectral Observatory Of Sensitive EMCCDs (MOOSE), designed by Marilia Samara and Robert Michell. It was installed at Poker Flat Research Range in Alaska (-147.4° geographic longitude, 65.1° geographic latitude) in September 2011. Since then the five low-light imagers have been run in many different modes and configurations, but typically with two ASI and three narrow-FOV imagers, and provided aurora images intended to be applied to a wide range of optical imaging science. Figure 4.4 shows the experiment configuration

with two ASIs mounted in the same dome, one capturing the green aurora (557.7 nm), and the other the violet-blue aurora (427.8 nm).

Figure 4.4: The two MOOSE all-sky imagers mounted in the same dome. One captures the green aurora (557.7 nm), and the other captures the violet-blue aurora (427.8 nm). Photo by Robert Michell.

4.4.1 Imager specifics and operation

The imager is an Andor Ixon DU-888 EMCCD (Electron Multiplying Charge Coupled Device). It has a 1024×1024 pixel chip with internal binning capabilities that allow trade-offs between temporal and spatial resolution. The CCD is cooled to -70°C to reduce thermal noise (dark current) and can detect single photons with a high quantum efficiency ($>90\,\%$). For our events the imager is set to 2×2 binning, resulting in a 512×512 image at 3.3 frames per second ($\sim$300 ms exposure time). This configuration was chosen because it provides adequate temporal resolution for the range of scale sizes captured by the all-sky FOV.

4.4.2 Calibration

Both the pointing and intensity need to be calibrated. This was performed by the MOOSE experiment, and the details of the calibration process can be found in the paper by *Grubbs et al.* [2016]. Here I provide a short introduction to the concepts.

The pointing direction is determined by matching the stars in the image with the known position of the stars. In this way the conversion factors and thus geographic coordinates and angular pixel sizes of the image are obtained.

The intensity calibration is done by comparing the measured count rate from the stars in the image (corrected for the background emissions of the sky) to the known spectral irradiance of the stars integrated over the ASI spectral selection. The ratio between the two provides the conversion factor for the intensity measured in counts/s to photon flux given in photons/cm^2 s. The next step is to determine how bright the aurora is in order to produce 1 count/s. Because the aurora is emitted from a range of altitudes in all directions where only a fraction will reach the imager, the conversion factor is basically based on the FOV of each imager pixel and the line-of-sight integrated emissions. For the 557.7 nm emissions the resulting conversion for one exposure time is linear: 1 count = 9.16 R, when the imager dark counts are subtracted. The uncertainty in the intensity is probably only 10–20 % and increasing towards the limb pixels, which is very good for auroral imagers. The uncertainty mainly comes from the calibration source and non-uniformity of the imager response (the center pixels have a higher gain, etc.).

Rayleigh is the unit for the intensity of airglow and aurora, which is based on the proportionality between the surface brightness of the aurora and the line-of-sight integrated emissions per unit of volume when absorption and scattering can be ignored. Rayleigh is basically the measured brightness multiplied by 4π, where one Rayleigh equals the column emissions rate of 10^6 photons per cm$^2 s$ [*Hunten et al.*, 1956]. The weakest aurora that we can see with our eyes is $\sim$1 kR, which means that the aurora must produced at a rate of one billion (10^9) photons per cm^2 from the "surface" of the aurora per second. In comparison, the medium intense aurora is 10 kR, while very intense aurora can reach more than 100 kR. At maximal intensity the emissions on the ground can be compared with the light reflected from the moon, which is around thousand times stronger than the light from the stars.

4.4.3 Fish-eye lens distortions

The fish-eye lens has a FOV of half of a sphere (180°) in order to capture the sky from horizon to horizon. This corresponds to around 600 km across at an altitude of $\sim$110 km, where the most green aurora is produced. If we include the sky near the horizon, which often can be covered by buildings, trees and mountains, it would be around 1000 km.

Equiangular projection

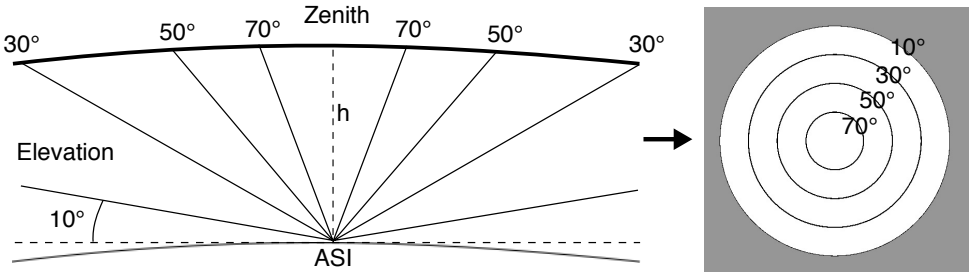

Figure 4.5: Illustration of the equiangular projection of the emissions onto the image. All elevation angles below 10° (grey) are set to 0 R, while the light from the sky is within the 160° FOV circle (white).

The resulting image of the sky is a circle within the square frame. The projection is equiangular, in which the distance along the radius of the circular image is proportional to elevation angle above the horizon, as illustrated in Figure 4.5.

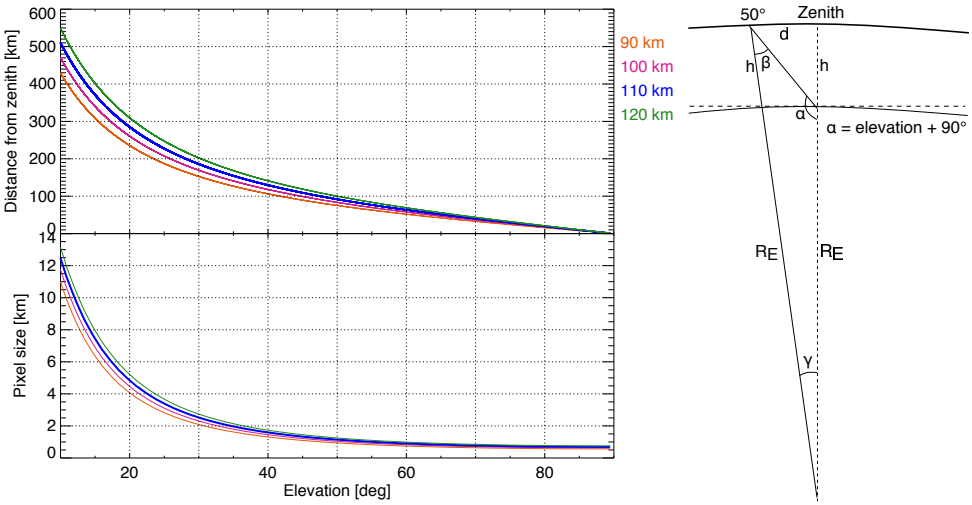

Figure 4.6: Distance from zenith and one-dimensional pixel size as a function of elevation for four different altitudes based on the angular pixel size of the ASI setup and the geometry (not to scale), where d is the distance from zenith, h is the altitude of the thin shell emission assumption, and R_E is the distance from the center of the Earth to the surface.

The data we use are in the format of the image in Figure 4.5. All elevation angles below 10° (grey) are set to 0 R, while the light from the sky is within the 160° FOV circle (white) of 444 pixels in diameter. The angular pixel size that follows is therefore 0.36°. From this we can calculate the pixel size in km at a certain altitude.

Figure 4.6 shows the distance from zenith and one-dimensional pixel size as a function of elevation for four different altitudes. The calculation takes into consideration the curvature of the atmosphere, as can be found from the simple geometry shown in Figure 4.6, where γ(elevation,h) is a function of elevation and altitude (h) and the distance from zenith $d = \gamma(R_E + h)$. The most obvious distortion is therefore the varying pixel size from $\sim$600 m in the centre of the image to 4–5 km at 20° elevation and quickly increasing to as high as 11–12 km for the most limb pixels. Figure 4.6 also shows that the the assumption of 110 km altitude [e.g. *Egeland and Burke*, 2013] for the nightside 557.7 nm auroral emissions causes a small error in the pixel size compared to the error due to elevation angle.

Column integration

A thin auroral form will look brighter when viewed at lower angles along the horizon, since more emission will be included in the line-of-sight. The ASI obtains column integrated emissions which typically originate from a range of altitudes and magnetic field lines, meaning that the intensity depends on the elevation and viewing angle across or along the magnetic field. If we assume that the aurora is a thin homogeneous layer and the magnetic field has a 90° elevation, we could do a correction of the line of sight integration. The intensity correction is $I_{corrected} = I_{measured} \cos(90°\text{-elevation})$ for a flat Earth and ionosphere. However, the aurora is normally very complex in both morphology, spacing and vertical thickness, which could introduce artificial intensities if the above correction is performed. For example a low elevation pixel could integrate emissions across a single arc, while pixel of higher elevation could sample emissions at different altitudes across several nearby arcs. Thus, the higher elevation pixel would have captured more emissions from along the line of sight, but got a smaller correction than the lower elevation pixel that captured less emissions along the line of sight. In addition, the magnetic field could have an elevation less than 90°, which introduce a secondary intensity distortion across the FOV. We have therefore not attempted to apply this correction. It should also be mentioned that the aurora close to the horizon needs to travel through more atmosphere, but this does not create a considerable scattering or absorption of the 557.7 nm auroral emissions.

Parallax effect

Emissions at different altitudes will be displaced with respect to each other when not monitored in the magnetic zenith. This is called the parallax effect defined as a displacement in the apparent position of an object viewed along two different lines of sight. When the line of sight has an angle to the magnetic field, the low altitude emis-

sions will have a larger parallax angle than higher altitude emissions from the same arc. The result is that the image displays an auroral arc that is wider than the original arc, as illustrated in Figure 4.7. Due to the already mentioned complexity in an auroral display, such as multiple arcs and variable vertical thickness, and because it is not possible to determine the vertical thickness of the aurora from one ASI alone, we have not attempted to correct for the parallax distortions. However, the parallax distortions are maybe more important in quantitative analysis of ratios of auroral emission lines from different heights, than the smearing they introduce in the scale-size dependent characteristics. In Papers II and III we do discuss the inherent limitations of the ASI distortions and give an estimate of the smearing based on the main distortion, thus size of the original pixels as shown in Figure 4.6.

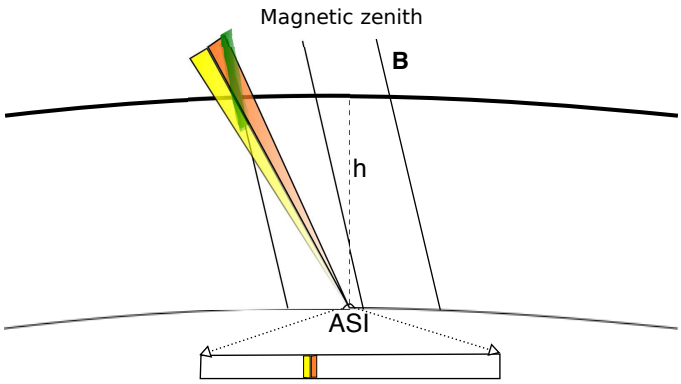

Figure 4.7: A Sketch of how the parallax effect can cause distortions in the resulting image. Here the line of sight has an angle to the magnetic magnetic field. Therefore, the low altitude emissions will have a larger parallax angle than higher altitude emissions from the same arc. In the resulting image the arc will be displayed as much wider than it is.

4.5 Image processing

To correct for the strongly distorted view of the night sky from the fish-eye lens of the all-sky imager we perform a projection of the image onto a cartesian grid with a uniform pixel resolution. The cartesian grid is oriented with geographical north on the top and east to the left, as if you were to lie flat on your back with your feet facing south to watch the night sky. The geographical orientation facilitates a straight forward correction of the ASI rotating with Earth below the aurora. Figure 4.8 shows the distorted view of the ASI (a), and the results of projection the emissions onto a cartesian grid with a uniform pixel resolution of 2.0×2.0 km (b) and 1.0×1.0 km. In Papers I and III we use a pixel size resolution of 2.0×2.0 km, and avoid the most distorted limb pixels

outside the centre FOV (∼500×500 km) as indicated by the white frame in image b. For Paper II we have used a pixel size resolution of 1.0×1.0 km. This projection samples pixel sizes from the original ASI image of maximum ∼3.5 km, where the patches have less smearing than ∼2.5 km (see Figure 4.6).

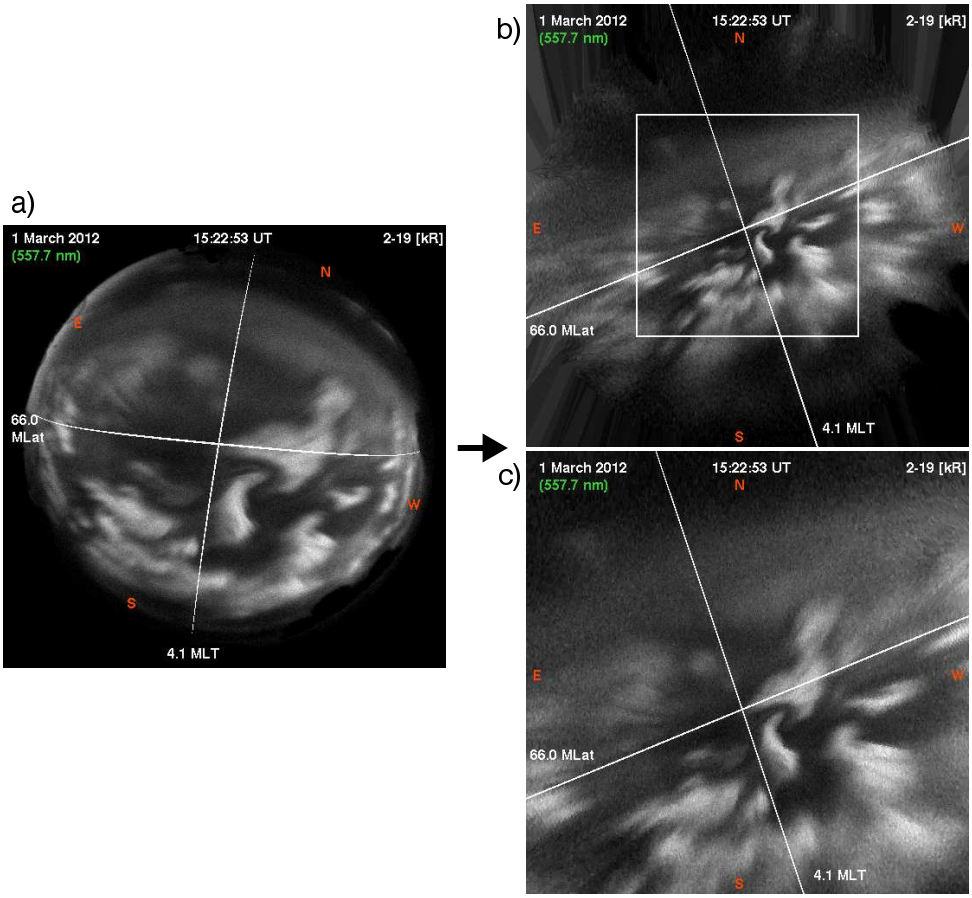

Figure 4.8: (a) The strongly distorted view of the ASI, and the results of projection the emissions onto a cartesian grid with a uniform pixel resolution of (b) 2.0×2.0 km and (c) 1.0×1.0 km. The images are of the pulsating auroral patches 1 March 2012 at 15:22:53 UT. The geographical orientation is indicated in red, and the magnetic (Altitude Adjusted Corrected Geomagnetic coordinate system, AACGM) orientation is indicated by a superposition of the 66.0 MLat and 4.1 MLT. We avoid the most distorted limb pixels outside the centre FOV (∼500×500 km) as indicated by the white frame in image b.

First we transform the original spherical geographical pixel coordinates (assuming 110 km altitude) to cartesian geographical coordinates (assuming r = 1). In this way we can use the scalar product to find the pixel vector in the original image that lies closest

in geographical coordinates to each pixel vector in the new image. The resolution is preserved and we do not need to make assumptions of the altitude of the emissions. The only artifact of the projection is that emissions in the center of the image are collected over a smaller area than covered by the new pixel size, and likewise that emissions in the outer parts of the image are collected over a larger area than covered by the new pixel size. Based on the discussion in the above Section 4.4.3, we do not attempt to do any further distortion corrections. However, while some projections shrink the limb pixels and do an interpolation, our projection is quite honest in the sense that the original limb pixels are projected onto several new pixels and therefore display the original pixel size with the original intensity, and thus the related distortions.

Chapter 5

Summary of papers

5.1 Paper I: Temporal characteristics and energy deposition of pulsating auroral patches

Science objective

Determine the characteristics of pulsating auroral patches in order to provide better observational constraints on the suggested mechanisms.

Why is it important?

The pulsating aurora has a broad definition. It includes all low-intensity aurorae that undergo repetitive, quasi-periodic, or occasionally periodic intensity fluctuations on time scales ranging from less than 1 second to several tens of seconds. These aurorae can occur in many different shapes, be persistent or short-lived, and also their mutual characteristics, such as their association with high energy precipitation and fast fluctuations superposed on the main on-off fluctuation, seems to vary from event to event. It is believed that the mechanism of the fluctuating aurora is a time-varying pitch-angle scattering located at the magnetic equator. However, what controls the time-variation is not clear, and there are also events of non-conjugacy that is hard to explain with a single mechanism at magnetic equator. It is a mystery whether pulsating aurorae can have different mechanisms, or whether the large variation can be explained by one mechanism. To understand the latter we also need to solve some fundamental questions on pulsating aurora, such as what underlying mechanism(s) controls their on-off fluctuation. This illustrates the need for better characterization in order to provide better observational constraints on the suggested mechanisms.

Key points

- Objective and quantitative characteristics of pulsating auroral patches.
- Pulsating aurora is highly variable in all measurable parameters and thus would be more accurately described as fluctuating aurora.
- Characteristics of pulsating auroral patches do not fit well with the Flow cyclotron maser theory.

Data and methodology

We utilize data from an all sky imager that captured a new image every $\sim$0.3 seconds of an event of bright green (557.7 nm) pulsating aurora located around 4.1 MLT and 65° MLat. Prior to the analysis we correct for the distorted fish-eye view of the ASI frames by performing a projection of the emissions onto a cartesian grid with uniform spatial resolution. Six well defined individual pulsating auroral patches are identified and extracted using an automatic contouring technique that facilitates a fixed point analysis. This allows us to derive objective quantitative parameters for each of the patches. These include patch duration (on-time and off-time), peak intensity and integrated intensity. Further, we found how the energy deposition relates to the on-time and off-time and how it varies over the on-time. Altogether we provide a series of observational constraints on the suggested mechanisms and discuss whether the auroral observational consequences of the suggested mechanisms can explain the characteristics of the pulsating auroral patches.

Conclusion

The results indicate that there are no clear candidates of the suggested mechanisms and drivers to explain the observational constraints set by the PA patches in a satisfactory manner, and that the use of the term “pulsating" is inappropriate since our findings and other published results are not regular periodic and thus a more appropriate term may be fluctuating aurora:

- The PA patches display a striking temporal variability. The on-time has a wide distribution of 2–21 s with a preferred (typical) on-time of $\sim$3-5 s. The distribution of the off-time is more confined (0-7 s) having a median of 0.6 s. Therefore, the frequently used period or quasi-period can not sufficiently describe the temporal characteristics. Instead, on-time and off-time serves as a more accurate description.

- The temporal constraints do not appear to support the variations of the Flow cyclotron maser theory, but fit better within the framework of the Nonlinear relaxation oscillator, largely because it predicts a temporal variability.

- The energy deposition is found to be highly variable from fluctuation to fluctuation. The constraints set by the the energy deposition and its relation to the on-time and off-time seem to indicate: 1) The pulse on-time is a composition of higher frequency pulsations, where the composition for some reason varies from pulse to pulse; 2) The off-time is not related to a loading but is related to the time it takes to lower the resonance threshold to start a new fluctuation; 3) The slightly quicker build up than decay of the energy deposition is opposite to the observational consequences that would be expected from the flow cyclotron maser (and backward wave oscillator), which in particular is suggested to create the pulsating aurora in the shape of patches.

Relation to thesis objective

Pulsating aurora is a phenomenon that occurs often, but are poorly understood. We therefore do not know where and how the pulsating aurora belongs in the large scale transport of energy and momentum in the M-I system. This paper therefore provides objective and quantitative characteristics of pulsating auroral patches in order to give better observational constraints on the suggested mechanisms.

5.2 Paper II: Do pulsating auroral patches vary in a coherent fashion?

Science objective

Provide objective and quantitative measurements of the extent to which pulsating auroral patches maintain their morphology and fluctuate in a coherent fashion. Does the patch maintain its shape? Does the entire patch vary with the same fluctuation and phase? Do the patches drift with the plasma convection $\mathbf{E} \times \mathbf{B}$ velocity?

Why is it important?

For the same reasons as described above for Paper I, we need to solve some fundamental questions on pulsating aurora, such as what controls the shape and coherency of fluctuating auroral patches. It has also been suggested that imaging of pulsating auroral patches can be used for remote sensing of the magnetospheric convection. It is

therefore important to establish if all patches are drifting solely with the plasma convection $\mathbf{E} \times \mathbf{B}$ velocity. Altogether, this illustrates the need for better characterization of pulsating aurorae.

Key points

- The shapes of the patches are remarkably persistent
- Only one of four patches behaves in a coherent fashion
- The patches appear to drift differently from the SuperDARN determined $\mathbf{E} \times \mathbf{B}$ velocity

Data and methodology

We utilize the same event and observations as described for Paper I. We do a careful analysis of four relatively well separated individual fluctuating auroral patches. Because the fluctuating auroral display is very complex, with adjacent patches, within patch variations, and relative movements, a manual contouring technique is used to capture the patches over a considerable part of their lifetime. This allows for a quantitative determination of the question: To what extent a patch maintains its shape. We follow the patches for $\sim$7–10 min and also determine how often the patches merge with nearby patches. Further, we determine the drift both in the patch frame of references, and in a reference frame co-rotating with Earth for comparison with the SuperDARN $\mathbf{E} \times \mathbf{B}$ drifts. The fixed point analysis also makes it possible to perform a time-position correlation analysis to estimate the extent to which each of the patches fluctuate in a coherent fashion.

Conclusion

The characteristics of four fluctuating auroral patches from a single event do not allow for general conclusions, but it ensures that the characteristics are not due to dependencies such as local time and geomagnetic activity. Based on this work we conclude:

- For all of the patches their shape can be considered remarkably persistent with 85–100 % of the patch being repeated for 4.5–8.5 minutes.
- For the three largest patches the temporal correlation coefficient show a negative dependence on distance. A time-delayed response within all of the patches indicate that the so called streaming spatiotemporal mode can explain part of the variability. Thus, only one of four patches behaves in a coherent fashion.

- The patches appear to drift differently from the SuperDARN determined $\mathbf{E} \times \mathbf{B}$ convection velocity. However, in a non-rotating reference frame the patches drift with 230–287 m/s in a north-eastward direction, which is what typically could be expected for the convection return flow.

Our interpretation of the findings is that the mechanism is located at lower altitudes and not in the plasma sheet, and that the patches likely drift with the $\mathbf{E} \times \mathbf{B}$ velocity. The only parameter which appears to be consistent for fluctuating auroral patches, is their shape, this supports the suggestion made in Paper I that pulsating aurora is a misnomer and that the name fluctuating aurora is more appropriate.

Relation to thesis objective

Same as described for Paper I.

5.3 Paper III: Scale size-dependent characteristics of the nightside aurora

Science objective

Describe the scale size dependent characteristics of the magnetosphere-ionosphere system as observed by an all sky imager measuring the 557.7 nm auroral emissions.

Why is it important?

The magnetosphere-ionosphere system is highly dynamic. However, due to the observational challenges, only a few studies have attempted to address the spatiotemporal behavior of any electrodynamic parameter of the magnetosphere-ionosphere system, such as plasma convection or electrical conductances. This indicates a need for analyses that can separate between changes in time and in space and to evaluate the importance of the different scale sizes. This is needed both to complement the few existing multipoint missions and provide quantitative measures to whether their assumptions are valid, and to provide quantitative measures for the many single satellite and rocket missions to evaluate their sampling rate and for how long they measure on the same phenomenon.

Key points

- An innovative 2D analysis of all-sky images revealing the characteristics of the magnetosphere-ionosphere system

- The largest auroral scale sizes are stable on time scales of minutes while the small scale sizes are more variable

- The characteristics of the nightside aurora and field-aligned currents are in remarkable agreement

Data and methodology

Observations at fixed positions for an extended period of time are provided by a ground based all-sky imager capturing a new image every $\sim$0.3 seconds of the green (557.7 nm) auroral emissions. We report on a single event of nightside aurora ($\sim$22:15 MLT and $\sim$66° MLat) during a period of fairly constant moderate geomagnetic disturbances preceding a substorm onset. Prior to the actual analysis we transform the ASI frames from the distorted fish-eye lens view to a cartesian grid with uniform spatial resolution, and ensure that the sky is clear, the moon is down and that there are no artifacts such as building and antennas in the FOV. To capture a large range of scale-sizes we only avoid the the most distorted limb pixels of the image we find the characteristics of the aurora within the centre 507 by 507 km FOV. The spatiotemporal characteristics of the auroral emissions are found by performing a simple, yet robust, analysis that combines a two-dimensional spatial fast Fourier transform (FFT) with a temporal correlation.

Conclusion

The single event studied in this paper provides an opportunity to prove the technique and provides a glimpse of the M-I system characteristics but it does not allow general conclusions. Below we summarize the findings.

- We find a scale size dependent variability where the largest scale sizes are stable on time scales of minutes while the small scale sizes are more variable. For example an auroral form of 1000 km^2 can be considered as static on time scales of about 10 s or less, while a 10,000 km^2 auroral form can be considered as static on time scales less than a minute.

- We question the assumption that the spatiotemporal characteristics are fairly constant by separating the movie into two smaller intervals of different types of auroral displays. We find that the spatiotemporal characteristics varies during the event. The interval of “less variable" aurora has more stable auroral forms of $\sim$2000–5000 km^2 and less stable large auroral forms ($>$9000 km^2) compared to the interval of “more variable" aurora. However, the trend of increasing variability towards the smaller scale sizes is similar.

- We have effectively found the scale size dependent total time derivate. However, an estimate shows that the source of the variability is mostly due to change in the partial derivative with respect to time and that we can largely ignore the convective term of the auroral arcs.

- The scale size of about 30,000 km^2 is the most significant, while the amplitude falls off towards larger and smaller scale sizes. For scale sizes less than about 800 km^2 the amplitudes are less than 10 kR.

- The average spatiotemporal characteristics of the auroral emissions are in remarkable agreement with the spatiotemporal characteristics of the nightside FACs during moderately disturbed times. Thus, two different electrodynamical parameters of the M-I system show similar behavior. This result is interpreted as an indication of a system that uses repeatable solutions to transfer energy and momentum from the magnetosphere to the ionosphere.

Relation to thesis objective

This paper describes the scale size dependent variability of the magnetosphere-ionosphere system as observed by auroral emissions.

Chapter 6

Discussion of papers

The overarching thesis objective is to provide new insight into the characteristics of the dynamic magnetosphere-ionosphere system as visually manifested by the aurora. This was motivated by a need to advance our understanding of how the magnetosphere-ionosphere system responds to the solar wind driver and how it internally transports and dissipates energy and momentum. This understanding does not only stem from scientific curiosity but also from humanity's ever increasing dependence on the conditions in our near space environment. A thorough discussion of the results of Papers I-III are found in the respective papers. The objective of this chapter is therefore to highlight the connection between the individual papers by discussing the overarching thesis objective and future prospects.

I would like to add an important note on importance of phenomena. It is often argued that if a process is not a significant mechanism for transporting energy and momentum within the M-I system it is of less importance. As an analogy the dominant precipitation mechanism in the atmosphere is most often dew since it falls everywhere and every night. That, however, does not imply that we should stop investigating hurricanes, tornadoes and other processes. While fluctuating aurora is unlikely to play any significant role in the energy-momentum transfer it is an often occurring phenomenon that provide a considerable challenge of our understanding of the M-I system. Likewise, we should be careful about equating societal impact with importance.

6.1 Inherent limitation

In this thesis we have utilized a ground based all-sky imager to investigate a wide range of auroral scale sizes with high time and spatial resolution. The limitations due to the all-sky imager distortions and green (557.7 nm) aurora were introduced in Chapter 4,

and discussed in Papers I-III. It is, however, important to highlight that this thesis focuses on the small to mesoscale auroral scale sizes of a few km to around 250 km. At the same time this effectively means that we neglect the micro scale-sizes from tens of meters to a few km, where the smallest scale size corresponds to the electron gyro radius [*Borovsky et al.*, 1991; *Maggs and Davis*, 1968]. The micro scales cover narrow arcs and filamentary structures associated with discrete aurorae and black aurorae, commonly appearing in a background of diffuse aurora [*Sandahl et al.*, 2008]. In fluctuating aurorae, there are both embedded small scale (<1 km) high-frequency fluctuations ($>\sim 3$ Hz) [*Samara and Michell*, 2010], and non-fluctuating coexisting discrete auroral filaments from lower-energy precipitation [*Dahlgren et al.*, 2015]. However, our result in Paper III and the studies of arc thickness and lifetimes by *Knudsen et al.* [2001] and *Partamies et al.* [2010], suggest that the lifetime decreases with the scale size, maybe indicating that they are of less importance in the transport of energy and momentum from the magnetosphere to the ionosphere. For example, *Trondsen and Cogger* [1998] found mean lifetimes of 0.9 s for bright, and 4.6 s for weak curls with scale sizes on the order of 0.1–10 km, while *Sandahl et al.* [2008] considered fine-scale aurorae with spatial scales smaller than around 1 km and temporal scales shorter than around 1 s.

In Paper III we tested the significance of the different auroral scale sizes as estimated by their amplitude found from the complex spectrum as the square root of the bandpass filtered power, and found that the smaller auroral scale sizes (two-dimensional) also have smaller amplitudes. However, earlier studies using other techniques, have indicated that small auroral scale sizes can have large amplitudes. For example, *Lanchester et al.* [1997] suggested that most of the precipitation energy density in a bright arc resides in an extremely narrow filament, and *Chaston et al.* [2003b] found that inertial Alfvén waves can drive aurora to optical intensities as high as 100 kR over ionospheric widths on the order of 1 km. The role of the micro-scale structures in the transport of energy and momentum in the magnetosphere-ionosphere system is not solved. It is often thought that the smallest auroral features are caused by more local processes that do not map far out into the magnetosphere, but the associated local structures in electron density and conductivity, as well as ionospheric feedback mechanisms can contribute to the M-I system [*Sandahl et al.*, 2008].

In summary, we test a wide range of auroral scale sizes, but effectively neglect the micro scale auroral features, mainly due to observational constrains (here the effective imager resolution). Further, we do not address the largest scale sizes, such as the auroral oval and substorm auroral bulge. A quantification over a wider range of spatial and

temporal scales can and should be performed by applying an analysis similar to the one developed in Paper III, to narrow-field of view imager data of micro-scale aurora, and maybe also satellite imaging of the largest auroral scale sizes.

6.2 Ways to characterize dynamics

6.2.1 Fixed point analysis

To get beyond the large-scale static picture, and to characterize the structure and dynamics of the ionosphere-magnetosphere system, we need to address the time-space ambiguity. Space measurements are challenged by the relative movement between the observer and the phenomena measured, and of course the limited number of multi-point satellite and rocket missions. One of the distinct advantages of an all-sky imager is that it provides multipoint observations over a wide range of auroral scale sizes. However, some non-trivial post-processing of the images is required since the imager rotates eastward with the Earth and thus moves the FOV across the night sky. The result is that aurorae fixed in a reference frame not rotating with the Earth (fixes in MLT) will get an apparent westward velocity component in the images that needs to be corrected for. The velocity of Earth's rotation is easily calculated from the Earth's rotational period and distance at the geographic latitude and altitude of the aurora. If the aurorae do not have a drift component in the geographic east-west direction, they move across the center FOV of the images (512 km at 65.1° geographic latitude and 110 km altitude) in only 43 min, corresponding to a speed of 198 m/s. Considering this limit, 10-20 min continuous observations at fixed positions in a non-rotating reference system, like the event analyzed in Paper III, is an extended period in time.

In Papers I and II we study persistent fluctuating auroral patches, while in Paper III we study the very dynamic display of auroral arcs. The distinct advantage of the fluctuating auroral patches is that they are relatively easy to track. In Papers I and II we therefore find the velocity of the auroral patch in the ASI frame of reference, which is a combination of the movement of the ASI FOV and drift of the patch in the fixed reference frame. To determine the apparent drift of the patch we make an outline around the patch and find the velocity which best follows the patch through its lifetime. This technique assumes that the velocity is constant during the lifetime of the patch ($\sim$10 min), which none of the patches appear to violate. Using the apparent drift velocity a new movie is made where the patch is centered at all times.

In Paper III we study a 507×507 km FOV (assuming 110 km altitude) where the au-

roral display varies from multiple slightly deformed east-west oriented arcs to relative dim and uniform arcs with slowly varying structures covering the entire FOV, followed by a brightening and transition to highly structured rapidly changing arcs. During the event parts of the FOV also includes dark sky, and diffuse and fluctuating aurora. It is likely that the auroral forms move relative to each other. We therefore do a correction for the movement of the FOV due to the ASI rotating with the Earth and only correlate the pixels in the frequency filtered images that overlap for the entire event. The resulting FOV is 283 km in the geographic east-west direction and 507 km in the north-south direction. This means that in the scale-size dependent variability analysis in Paper III, we effectively find the total time derivative:

$$\frac{dI}{dt} = \frac{\partial I}{\partial t} + \mathbf{U} \cdot \nabla I$$

where I is the auroral emissions and **U** is the velocity of the auroral arcs and forms. The variability in the auroral display can be due to changes in the partial derivative with respect to time as well as any movement of the auroral forms. Separating these terms in order to determine the cause of the observed dI/dt is not straight forward. Several studies have shown that during growth or recovery phases auroral arcs are found to move with the convective motion of the magnetosphere at relatively slow speeds of several 100 m/s, and slow down at the equator ward edge of the auroral oval [*Akasofu*, 1964; *del Pozo et al.*, 2002; *Paschmann et al.*, 2003; *Pulkkinen et al.*, 1991]. However, slow and fast drifts which are different from the magnetospheric convective motion (not frozen-in) are also reported [e.g. *del Pozo et al.*, 2002; *Frey et al.*, 1996; *Haerendel*, 1983; *Williams et al.*, 1998]. These are: 1) Slow motions, of the order of 100 m/s, which may be directed poleward or equatorward [e.g. *Haerendel et al.*, 1993]. 2) Fast poleward motions, on the order of 1 km/s, mainly found during substorm expansions [e.g. *Panov et al.*, 2016].

In Paper III we evaluate the relative importance of the two terms (partial derivative and convective term). We estimate the convective term by calculating the velocity vector (**U**) from the 2D shift in a simple cross-correlation analysis of images separated by 10 s. We found relatively slow speeds mostly below 130 m/s that have a southward component that increases towards the substorm onset, as shown in Figure 6.1. This fits well with the magnetospheric convection during a growth phase. However, there is also a magnetic eastward drift component that might not reflect the convection since the event is around 22.15 MLT where the convection often can be expected to be westward. The latter can therefore rather be the result of the aurora undergoing a mix of temporal changes, such as break ups into multiple arcs, which makes the convective

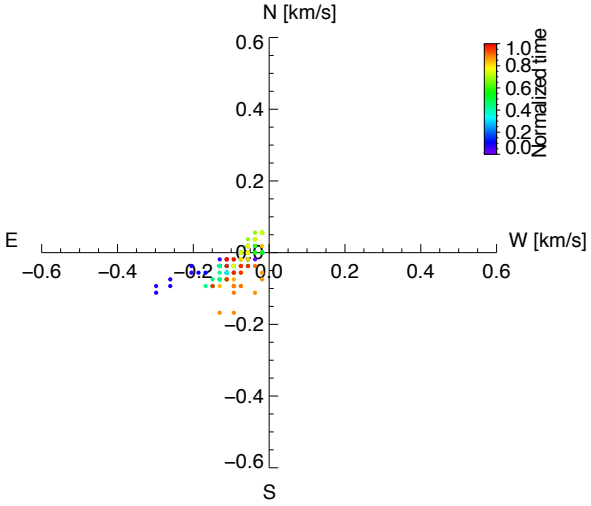

Figure 6.1: The auroral velocity vectors from Paper III on a geographic grid with the color scale denoting the event time until substorm onset (normalized).

term very difficult to determine. The weakness of this technique is, of course, that the cross-correlation is largely determined by the large-scales and thus it is assumed that all scale sizes are moving with the same velocity. For example, by comparing the speed of auroral arc distortions, *Partamies et al.* [2001] found indications that the speed of an auroral structure seems to anticorrelate with its size. Further, *Trondsen and Cogger* [1998] found that curls (0.1-10 km) exhibit extremely swift horizontal east-west aligned motions along arcs with a speed that increases with the brightness of the arc. This clearly indicates that the assumption of collective motion across scale-sizes is not true. However, due to the complexity of the ASI auroral display, there is no straight forward way to determine the contribution to the variability from the convective term. Despite the uncertainty in determining the convective term, the conclusion in Paper III that the largest source of the variability is due to the partial derivative seems reasonable.

6.2.2 Separate the auroral display into different scale sizes

The fluctuating auroral patches are by definition a certain scale size. However, as we point out in Paper II, even for the bright and well-defined fluctuating auroral patches there are adjacent patches that fluctuate differently. In addition, we found that only the smallest of the four well-defined patches behaves in a coherent fashion. This shows that extracting scale size information from a display of pulsating auroral patches requires a careful analysis.

In Paper III we use a 2D FFT technique to separate the auroral display into different frequencies estimating 2D auroral scale sizes. The frequencies inherent to the FFT is given by the resolution of the image, which in our case is the 512×512 pixels images. So when the FFT divides our signal into (phase shifted) sine waves of different frequencies we get $512/2 = 256$ frequencies in both the geographic east-west and north-south direction, where the highest frequency is the Nyquist frequency. The FFT is applied on the full frame images to best accommodate the boundary continuity assumption inherent to the FFT technique, without altering the data that we are interested in (the center frame, 256×256 pixels). We use a Hanning-type window to attenuate the image outside the center frame. The frequency filtering is done with a narrow band Hanning-type filter because it is simple and does the job of smoothing the frequency cut-off in order to avoid ringing in the space domain. We chose to use a narrow band 2D frequency filter, meaning that we bandpass filter all frequency combinations $f = f_{east-west} \cdot f_{north-south}$ of the same area, and thus can filter very different shapes if they appear in the original image.

Using a FFT narrow frequency bandpass to analyze scale sizes of course has its limitations. However, any artifacts and uncertainties to the scale sizes are likely minimized because we in the end are interested in the difference between the frequency filtered images. In Paper III we discuss the validation of the auroral scale sizes and conclude that the scale size dependent characteristics that we find indeed are real and not artifacts and uncertainties introduced by the technique. However, a FFT does not tell us where in the image the signal or feature is located and it assumes that the band-passed frequencies occur over the whole image. This artifact is clearly not dominating the above analysis, but it would be interesting to get a better visual representation of the auroral scale size. The next step can therefore be to further experiment with different types and widths of the frequency bandpass, and wavelet transform techniques, which can give a better idea of where in the image certain scale sizes occur. The analysis can also be tested on a smaller FOV in order to minimize the ASI distortions. This would, however, narrow the range of scale-sizes included in the analysis. A better solution would be to utilize images where the ASI distortions are minimized by combining observations of the same FOV from several ASI at different locations. A third approach could be to only address arc widths by utilizing a 1D instead of a 2D spatial FFT, and thereby supplement the analyses by e.g. *Knudsen et al.* [2001]; *Partamies et al.* [2010]. This approach is tested in a preliminary study of fluctuating aurora along different magnetic latitudes (not published). Finally, a space-borne high resolution imager would provide a superior dataset with far less inherent complexities.

6.3 M-I system dynamics

In the introduction I mentioned the challenge of investigating the fluctuating aurorae with satellite and sounding rockets. With the results in Paper III we can do a similar estimate for the nightside ($\sim$ 22.15 MLT) aurorae during a period of fairly constant moderate geomagnetic disturbances. Figure 6.2 shows the auroral scale-size dependent variability that we provide in Paper III. It shows the correlation distribution as a function of scale size and time separation between images, which reveals the time scales of change for different auroral scale sizes. The result show that the M-I system (as observed by 557.7 nm emissions) appears to display a scale size dependent variability where the small scale sizes are more variable and the larger scale sizes more stable.

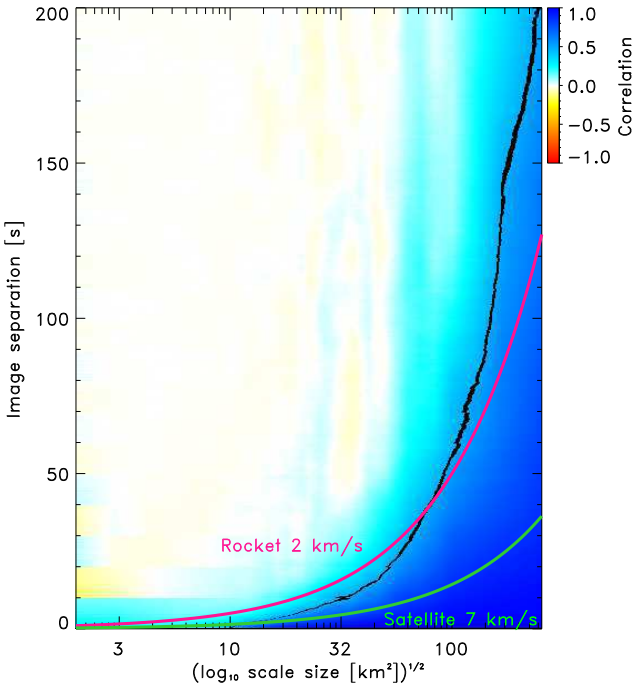

Figure 6.2: Correlation as a function of auroral scale size and image separation. The black line of 0.5 correlation coefficients provides a loose separation boundary between regions of 'high correlation' and 'low correlation', and the pink and green lines are the typical mean speeds of sounding rockets and satellites at ionospheric altitudes. The results are from Paper III.

I have further approximated the implications for observations with rockets and low earth orbit satellites by plotting their typical mean speeds on top of the correlation distribution in Figure 6.2. A sounding rocket crossing the nightside auroral display is typically in the poorly correlated region for a wide range of scale sizes, while a low Earth

orbit satellite pass will be in the region of good correlation. This basically means that we should be careful interpreting small-scale variations observed by sounding rockets. It should of course be mentioned that the degree of change in an auroral form is indicated by the linear Pearson correlation of 0.5 (black line), and the scale sizes are based on an altitude of 110 km. However, as we discuss in Paper III, the threshold of change could be raised to 0.6 or another reasonable number without any effect on the main conclusion. The scale sizes in Figure 6.2 are found to be in remarkable agreement with the scale size dependent variability of the magnetic field perturbations due to Birkeland currents scaled to 200 km altitude. However, for low Earth orbit satellites measuring e.g. particle precipitation or Birkeland currents at higher altitudes, the scale sizes should be scaled according to the magnetic field. The single event studied in Paper III does not allow general conclusions, but it proves that ASI can be used for more than the typical qualitative loose descriptions of the aurora (without any further data processing), and that a scale-size dependent analysis of the auroral emissions is a necessary supplement to in-situ observations, especially for measurements obtained from sounding rockets.

In order to understand and predict a dynamical system we need to know what drives the different parts of the system out of equilibrium and the evolution of restoring equilibrium. A plethora of studies have contributed to solve the fundamental behavior. One approach has been to describe the magnetosphere in a state of self-organized criticality (SOC) [*Angelopoulos et al.*, 1999; *Bak et al.*, 1988; *Bak*, 1999; *Klimas et al.*, 2000; *Lui*, 2002] or versions of SOC that allows a possible solution to the seemingly contradicting observations of the repeatable and coherent substorm phenomena with underlying complex behavior in the plasma sheet [*Valdivia et al.*, 2003]. There is also evidence that the discrete aurorae and their acceleration processes are nearly scale size invariant over much of the range of scales reported for auroral arc widths [*Chaston et al.*, 2011]. In this thesis, we advance our understanding by providing a description of the auroral dynamics. It may sound trivial that small scale sizes change more rapidly than larger scale sizes, but that implies a systematic behavior of the M-I system. The magnetosphere repeatedly uses the same solutions to dissipate its energy into the ionosphere. Of course, our study only provides a glimpse of the M-I system characteristics and it does not allow general conclusions. However, our results in Paper III are found in correspondence to a larger statistical study of Birkeland currents and thus give independent support to the claim of such an underlying magnetosphere-ionosphere (M-I) system behavior. For the fluctuating aurorae studied in Papers I-II, we found that their behavior, such as intensity fluctuation, energy deposition and coherency are highly variable. The only parameter which seems reasonably constant is their persistency of shape (and maybe

drift) that we quantified in Paper II. However, it is a mystery why the fluctuating auroral patches appear in these scale sizes and whether there is a scale-size dependent variability as found for the discrete aurorae. Further, the fluctuating auroral patches appear in a complex display of nearby and adjacent patches with different scale sizes. This raises the question whether they are caused by a large-scale mechanism or many nearby individual mechanisms. Therefore, in order to understand the fundamental question of how the different scale sizes of the M-I system are coupled, the techniques and methodologies of Papers I-III should be further improved and utilized on more events, and in conjunction with multi-point in-situ observations.

6.4 Future prospects

The fundamental understanding of the dynamic M-I system and the associated phenomena studied in this thesis still remains to be solved. In the above discussion we have suggested how fixed point analyses with ground-based ASI can be utilized to describe the dynamics of the M-I system. The concept should also be applied to other electrodynamic parameters of the system, for example electron densities and plasma flows by running radars in special modes that facilitates multipoint observations at fixed position in the ionosphere over an extended period of time.

Chapter 7

Conclusion

To get beyond the large-scale static picture and to characterize the structure and dynamics of the magnetosphere-ionosphere system, we have to overcome the time-space ambiguity of space observations. We have provided scale size-dependent characteristics of the magnetosphere-ionosphere system as visually manifested by the aurora. We utilize ground-based observations of auroral emissions since they provide extended periods of continuous observations at a fixed position in the ionosphere with high spatial and temporal resolution. The observations are made with an all-sky imager in order to capture a wide range of auroral scale sizes from small to mesoscale auroral scale sizes of a few km to around 250 km. The all-sky observations are projected onto a grid of uniform pixel size and further processed in order to get observations that are fixed in the reference frame of the ionosphere, and the reference frame of the individual auroral forms.

In order to separate between changes in time and space, we first make use of the distinct advantage of well-defined fluctuating auroral patches, that they relatively easily can be tracked in their frame of reference. Secondly, we separate the aurora into different scale sizes and quantify their lifetimes. In this way, we have provided objective and quantitative characteristics of fluctuating auroral patches in order to give better observational constraints on the suggested mechanisms, as well as described the scale size dependent characteristics of the magnetosphere-ionosphere system as observed by the nightside auroral emissions. The careful analyses of single events have the distinct advantage that their variability is likely not due to different geomagnetic conditions and other controlling parameters. They therefore provide glimpses of the M-I system characteristics under certain conditions, but at the same time do not allow for general conclusions. The quantitative characteristics can be found in Papers I-III. Below I summarize the overall findings.

- Fluctuating auroral patches display a striking variability. The patches do not fluctuate in a coherent fashion, the energy deposition is highly variable from one fluctuation to the next, the on-time varies wildly and does not show any correlation to the preceding off-time, nor the peak intensity. The only parameter which appears to be consistent for fluctuating auroral patches, is their shape. The frequently used terms “period" or “quasi-period", and the name “pulsating aurora" are therefore inappropriate, and the terms “on-time", “off-time" and “fluctuating aurora" is a more appropriate description of the phenomenon.

- There are no clear winning candidates of the suggested mechanisms to explain the observational constraints set by the fluctuating auroral patches in a satisfactory manner. Our interpretation of the findings is that the mechanism is located at lower altitudes and not in the plasma sheet.

- We have developed an innovative image analysis combining spatial frequency filtering to separate the images into 2D scale sizes, and a temporal correlation to reveal the time scales of change in the different scale sizes. The analysis was tested on an event of a pre-midnight auroral display during a period of fairly constant moderate geomagnetic disturbances. The resulting characteristics showed a scale size dependent variability where the largest scale sizes are stable on time scales of minutes while the small scale sizes are more variable. ASI should therefore be used for more than qualitative loose descriptions of the aurora (without any further data processing), and scale-size dependent image analysis are a necessary supplement to in-situ observations, especially by sounding rockets.

- The average spatiotemporal characteristics of the auroral emissions are in remarkable agreement with the spatiotemporal characteristics of the nightside Birkeland currents during moderately disturbed times. Thus, two different electrodynamical parameters of the M-I coupling show similar behavior. This result is interpreted as an indication of a system that uses repeatable solutions to transfer energy and momentum from the magnetosphere to the ionosphere.

Bibliography

Akasofu, S.-I., The development of the auroral substorm, *Planetary and Space Science*, *12*(4), 273–282, doi:10.1016/0032-0633(64)90151-5, 1964. 19, 68

Akasofu, S. I., *Physics of Magnetospheric Substorms*, 486–498 pp., D. Reidel Publishing Company, Norwell, Mass., 1977. 26

Alfvén, H., Existence of Electromagnetic-Hydrodynamic Waves, *Nature*, *150*(3805), 405–406, doi:10.1038/150405d0, 1942. 10

Andersson, L., J.-E. Wahlund, J. Clemmons, B. Gustavsson, and L. Eliasson, Electromagnetic waves and bursty electron acceleration: implications from Freja, *Annales Geophysicae*, *20*(2), 139–150, doi:10.5194/angeo-20-139-2002, 2002. 41

Angelopoulos, V., T. Mukai, and S. Kokubun, Evidence for intermittency in Earth's plasma sheet and implications for self-organized criticality, *Physics of Plasmas*, *6*(11), doi:10.1063/1.873681, 1999. 72

Bak, P., C. Tang, and K. Wiesenfeld, Self-organized criticality, *Physical Review A*, *38*(1), 364–374, doi:10.1103/PhysRevA.38.364, 1988. 72

Bak, P. P., *How nature works : the science of self-organized criticality*, 212 pp., Copernicus, 1999. 72

Baumjohann, W., and R. Treumann, *Advanced Space Plasma Physics*, Imperial College Press, London, 1997a. 9

Baumjohann, W., and R. A. Treumann, *Basic Space Plasma Physics*, Imperial College Press, London, 1997b. 9

Belon, A. E., N. Davis, and N. W. Glass, Conjugacy of Visual Auroras During Magnetically Disturbed Periods, *Antarc. J. U. S.*, *3*, 117–119, 1968. 31

Belon, A. E., J. E. Maggs, T. N. Davis, K. B. Mather, N. W. Glass, and G. F. Hughes, Conjugacy of visual auroras during magnetically quiet periods, *Journal of Geophysical Research*, *74*(1), 1–28, doi:10.1029/JA074i001p00001, 1969. 31

Birkeland, K., *The Norwegian Polaris Expedition 1902-1903. Vol. 1, On the cause of magnetic storms and the origin of terrestrial magnetism*, 1 ed., 305 pp., Aschhoug, Oslo, 1908. 17

Borovsky, J., D. Suszcynsky, M. Buchwald, and H. Dehaven, Measuring the Thicknesses of Auroral Curtains, *Arctic*, *44*, 231–238, 1991. 66

Boudouridis, A., and H. E. Spence, Separation of spatial and temporal structure of auroral particle precipitation, *Journal of Geophysical Research*, *112*(A12), 1–12, doi: 10.1029/2007JA012591, 2007. 5

Brekke, A., *Physics of the upper polar Atmopshere*, second ed., Springer, Berlin, Heidelberg, 2013. 9, 12, 13, 15, 47

Brown, N. B., T. N. Davis, T. J. Hallinan, and H. C. Stenbaek-Nielsen, altitude of pulsating aurora determined by a new instrumental technique, *Geophysical Research Letters*, *3*(7), 403–404, doi:10.1029/GL003i007p00403, 1976. 24, 25

Bryant, D., G. Courtier, and G. Bennett, Equatorial modulation of electrons in a pulsating aurora, *Journal of Atmospheric and Terrestrial Physics*, *33*(6), 859–867, doi: 10.1016/0021-9169(71)90086-9, 1971. 33

Bryant, D., M. Smith, and G. Courtier, Distant modulation of electron intensity during the expansion phase of an auroral substorm, *Planetary and Space Science*, *23*(5), 867–878, doi:10.1016/0032-0633(75)90022-7, 1975. 29

Bryant, D. A., H. L. Collin, G. M. Courtier, and A. D. Johnstone, Evidence for Velocity Dispersion in Auroral Electrons, *Nature*, *215*(5096), 45–46, doi:10.1038/215045a0, 1967. 29

Burns, G. B., and J. S. Reid, A comparison of methods for calculating O(1S) lifetimes, *Australian Journal of Physics*, *38*(4), 647–656, 1985. 47

Chamberlain, J. W., *Physics of the aurora and airglow*, Academic Press, New York, 1961. 14

Chaston, C. C., C. W. Carlson, R. E. Ergun, and J. P. McFadden, Alfvén Waves, Density Cavities and Electron Acceleration Observed from the FAST Spacecraft, *Physica Scripta*, *2000*(T84), 64, doi:10.1238/Physica.Topical.084a00064, 2000. 41

Chaston, C. C., J. W. Bonnell, C. W. Carlson, J. P. McFadden, R. E. Ergun, and R. J. Strangeway, Properties of small-scale Alfvén waves and accelerated electrons from FAST, *Journal of Geophysical Research*, *108*(A4), 8003, doi:10.1029/2002JA009420, 2003a. 41

Chaston, C. C., L. M. Peticolas, J. W. Bonnell, C. W. Carlson, R. E. Ergun, J. P. McFadden, and R. J. Strangeway, Width and brightness of auroral arcs driven by inertial Alfven waves, *Journal of Geophysical Research: Space Physics*, *108*(A2), doi:10.1029/2001JA007537, 2003b. 66

Chaston, C. C., K. Seki, T. Sakanoi, K. Asamura, and M. Hirahara, Evidence for a Multi-scale Aurora, in *The Dynamic Magnetosphere*, pp. 271–280, Springer Netherlands, Dordrecht, doi:10.1007/978-94-007-0501-2_15, 2011. 72

Colpitts, C. A., Investigations of the Many Distinct Types of Auroras, in *Auroral Dynamics and Space Weather*, pp. 1–18, John Wiley & Sons, Inc, Hoboken, NJ, doi:10.1002/9781118978719.ch1, 2015. 40

Colpitts, C. A., S. Hakimi, C. A. Cattell, J. Dombeck, and M. Maas, Simultaneous ground and satellite observations of discrete auroral arcs, substorm aurora, and Alfvénic aurora with FAST and THEMIS GBO, *Journal of Geophysical Research: Space Physics*, *118*(11), 6998–7010, doi:10.1002/2013JA018796, 2013. 41

Coroniti, F. V., and C. F. Kennel, Auroral micropulsation instability, *Journal of Geophysical Research*, *75*(10), 1863–1878, doi:10.1029/JA075i010p01863, 1970a. 34

Coroniti, F. V., and C. F. Kennel, Electron precipitation pulsations, *Journal of Geophysical Research*, *75*(7), 1279–1289, doi:10.1029/JA075i007p01279, 1970b. 34

Dahlgren, H., B. S. Lanchester, and N. Ivchenko, Coexisting structures from high- and low-energy precipitation in fine-scale aurora, *Geophysical Research Letters*, *42*(5), 1290–1296, doi:10.1002/2015GL063173, 2015. 66

Davidson, G., Self-modulated VLF wave-electron interactions in the magnetosphere: A cause of auroral pulsations, *Journal of Geophysical Research*, *84*(A11), 6517, doi:10.1029/JA084iA11p06517, 1979. 34

Davidson, G., Pitch-angle diffusion and the origin of temporal and spatial structures in morningside aurorae, *Space Science Reviews*, *53*(1-2), 45–82, doi:10.1007/BF00217428, 1990. 37

Davidson, G. T., Pitch angle diffusion in morningside aurorae: 2. The formation of repetitive auroral pulsations, *Journal of Geophysical Research*, *91*(A4), 4429, doi:10.1029/JA091iA04p04429, 1986a. 34

Davidson, G. T., Pitch Angle Diffusion in Morningside Aurorae 1. The Role of the Loss Cone in the Formation of Impulsive Bursts of Precipitation, *Journal of Geophysical Research: Space Physics*, *91*, 4413–4427, 1986b. 34

Davis, N. T., Observed characteristics of auroral forms, *Space Science Reviews*, *22*(1), 77–113, doi:10.1007/BF00215814, 1978. 24, 30, 31

Deehr, C., and G. Romick, Pulsating aurora induced by upper atmospheric barium releases, *Nature*, *267*(5607), 135–136, doi:10.1038/267135a0, 1977. 36

del Pozo, C., P. Williams, N. Gazey, P. Smith, F. Honary, and M. Kosch, Multi-instrument observations of the dynamics of auroral arcs: a case study, *Journal of Atmospheric and Solar-Terrestrial Physics*, *64*(15), 1601–1616, doi:10.1016/S1364-6826(02)00083-4, 2002. 68

Demekhov, A. G., and V. Y. Trakhtengerts, A mechanism of formation of pulsating aurorae, *Journal of Geophysical Research*, *99*(A4), 5831–5841, doi:10.1029/93JA01804, 1994. 34

Dungey, J., Interplanetary Magnetic Field and the Auroral Zones, *Physical Review Letters*, *6*(2), 47–48, doi:10.1103/PhysRevLett.6.47, 1961. 11

Eather, R. H., and S. B. Mende, Airborne observations of auroral precipitation patterns, *Journal of Geophysical Research*, *76*(7), 1746–1755, doi:10.1029/JA076i007p01746, 1971. 22

Egeland, A., and W. J. Burke, Størmer's Auroral Studies, in *Carl Størmer, Auroral Pioneer*, 1 ed., pp. 29–107, Springer-Verlag Berlin Heidelberg, doi:10.1007/978-3-642-31457-5, 2013. 52

Escoubet, C. P., M. Fehringer, and M. Goldstein, Introduction The Cluster mission, *Annales Geophysicae*, *19*(10/12), 1197–1200, doi:10.5194/angeo-19-1197-2001, 2001. 5

Evans, D. S., Precipitating electron fluxes formed by a magnetic field aligned potential difference, *Journal of Geophysical Research*, *79*(19), 2853–2858, doi:10.1029/JA079i019p02853, 1974. 40

Evans, D. S., G. T. Davidson, H. D. Voss, W. L. Imhof, J. Mobilia, and Y. T. Chiu, Interpretation of electron spectra in morningside pulsating aurorae, *Journal of Geophysical Research*, *92*(A11), 12,295, doi:10.1029/JA092iA11p12295, 1987. 29

Fedorov, E. N., V. A. Pilipenko, M. J. Engebretson, and T. J. Rosenberg, Alfven wave modulation of the auroral acceleration region, *Earth Planets Space*, *56*(7), 649–661, doi:10.1186/BF03352527, 2004. 37

Frank, L. A., J. B. Sigwarth, J. D. Craven, J. P. Cravens, J. S. Dolan, M. R. Dvorsky, P. K. Hardebeck, J. D. Harvey, and D. W. Muller, The visible imaging system (VIS) for the Polar spacecraft, *Space Science Reviews*, *71*(1-4), 297–328, doi: 10.1007/BF00751334, 1995. 43

Frey, H., G. Haerendel, D. Knudsen, S. Buchert, and O. Bauer, Optical and radar observations of the motion of auroral arcs, *Journal of Atmospheric and Terrestrial Physics*, *58*(1-4), 57–69, doi:10.1016/0021-9169(95)00019-4, 1996. 68

Fritz, B. A., M. L. Lessard, M. J. Blandin, and P. A. Fernandes, Structure of black aurora associated with pulsating aurora, *Journal of Geophysical Research: Space Physics*, *120*(11), 10,096–10,106, doi:10.1002/2015JA021397, 2015. 24, 38

Fujii, R., N. Sato, T. Ono, H. Fukunishi, T. Hirasawa, S. Kokubun, T. Araki, and T. Saemundsson, Conjugacies of pulsating auroras by all-sky TV observations, *Geophysical Research Letters*, *14*(2), 115–118, doi:10.1029/GL014i002p00115, 1987. 31

Fukuda, Y., R. Kataoka, Y. Miyoshi, Y. Katoh, T. Nishiyama, K. Shiokawa, Y. Ebihara, D. Hampton, and N. Iwagami, Quasi-periodic rapid motion of pulsating auroras, *Polar Science*, *10*(3), 183–191, doi:10.1016/j.polar.2016.03.005, 2016. 35

Gjerloev, J. W., S. Ohtani, T. Iijima, B. Anderson, J. Slavin, and G. Le, Characteristics of the terrestrial field-aligned current system, *Annales Geophysicae*, *29*(10), 1713–1729, doi:10.5194/angeo-29-1713-2011, 2011. 5

Grubbs, G., R. Michell, M. Samara, D. Hampton, and J.-M. Jahn, A synthesis of star calibration techniques for ground-based narrowband electron-multiplying charge-coupled device imagers used in auroral photometry, *Journal of Geophysical Research: Space Physics*, *121*(6), 5991–6002, doi:10.1002/2015JA022186, 2016. 49

Haerendel, G., An Alfven Wave Model of Auroral Arcs, in *High-Latitude Space Plasma Physics*, edited by B. Hultqvist and T. Hagfors, pp. 515–535, Springer US, Boston, MA, doi:10.1007/978-1-4613-3652-5_27, 1983. 68

Haerendel, G., S. Buchert, C. La Hoz, B. Raaf, and E. Rieger, On the proper motion of auroral arcs, *Journal of Geophysical Research: Space Physics*, *98*(A4), 6087–6099, doi:10.1029/92JA02701, 1993. 68

Hallinan, T. J., H. C. Stenbaek-Nielsen, and C. S. Deehr, Enhanced aurora, *Journal of Geophysical Research*, *90*(A9), 8461–8475, doi:10.1029/JA090iA09p08461, 1985. 30, 36

Hardy, D. A., M. S. Gussenhoven, and D. Brautigam, A statistical model of auroral ion precipitation, *Journal of Geophysical Research*, *94*(A1), 370, doi:10.1029/JA094iA01p00370, 1989. 23

Hoffman, R. A., R. Fujii, and M. Sugiura, Characteristics of the field-aligned current system in the nighttime sector during auroral substorms, *Journal of Geophysical Research*, *99*(A11), 21,303, doi:10.1029/94JA01659, 1994. 18

Holmgren, G., R. Boström, M. Kelley, P. Kintner, R. Lundin, U. Fahleson, E. Bering, and W. Sheldon, Trigger, An active release experiment that stimulated auroral particle precipitation and wave emissions, *Journal of Geophysical Research: Space Physics*, *85*(A10), 5043–5053, doi:10.1029/JA085iA10p05043, 1980. 36

Hosokawa, K., and Y. Ogawa, Ionospheric variation during pulsating aurora, *Journal of Geophysical Research: Space Physics*, *120*(7), 5943–5957, doi:10.1002/2015JA021401, 2015. 30

Hosokawa, K., Y. Ogawa, A. Kadokura, H. Miyaoka, and N. Sato, Modulation of ionospheric conductance and electric field associated with pulsating aurora, *Journal of Geophysical Research*, *115*(A3), A03,201, doi:10.1029/2009JA014683, 2010. 29

Hosokawa, K., Y. Miyoshi, and W. Li, Introduction to special section on pulsating aurora and related magnetospheric phenomena, *Journal of Geophysical Research: Space Physics*, *120*(7), 5341–5343, doi:10.1002/2015JA021453, 2015. 5, 28, 39

Hughes, W. J., The magnetopause, magnetotail, and magnetic reconnection, in *Introduction to Space Physics*, chap. 9, pp. 227–287, Cambridge University Press, New York, 1995. 10

Humberset, B. K., J. W. Gjerloev, M. Samara, R. G. Michell, and I. R. Mann, Temporal characteristics and energy deposition of pulsating auroral patches, *Journal of Geophysical Research: Space Physics*, *121*(7), 7087–7107, doi:10.1002/2016JA022921, 2016. iii, 1, 24

Humberset, B. K., J. W. Gjerloev, I. R. Mann, R. G. Michell, and M. Samara, Does pulsating auroral patches vary in a coherent fashion?, *Submitted to Journal of Geophysical Research: Space Physics*, *X*, 2017a. iii

Humberset, B. K., J. W. Gjerloev, M. Samara, and R. G. Michell, Scale Size Dependent Characteristics of the Nightside Aurora, *Journal of Geophysical Research: Space Physics*, *122*(2), 2455–2466, doi:10.1002/2016JA023695, 2017b. iv

Hunten, D., F. Roach, and J. Chamberlain, A photometric unit for the airglow and aurora, *Journal of Atmospheric and Terrestrial Physics*, *8*(6), 345–346, doi:10.1016/0021-9169(56)90111-8, 1956. 50

Iijima, T., and T. A. Potemra, Field-aligned currents in the dayside cusp observed by Triad, *Journal of Geophysical Research*, *81*(34), 5971–5979, doi:10.1029/JA081i034p05971, 1976. 17

Iijima, T., and T. A. Potemra, Large-scale characteristics of field-aligned currents associated with substorms, *Journal of Geophysical Research*, *83*(A2), 599, doi:10.1029/JA083iA02p00599, 1978. 3, 17, 18

Jaynes, A. N., M. R. Lessard, J. V. Rodriguez, E. Donovan, T. M. Loto'aniu, and K. Rychert, Pulsating auroral electron flux modulations in the equatorial magnetosphere, *Journal of Geophysical Research: Space Physics*, *118*(8), 4884–4894, doi:10.1002/jgra.50434, 2013. 29, 32, 35

Jaynes, A. N., et al., Correlated Pc4-5 ULF waves, whistler-mode chorus, and pulsating aurora observed by the Van Allen Probes and ground-based systems, *Journal of Geophysical Research: Space Physics*, *120*(10), 8749–8761, doi:10.1002/2015JA021380, 2015. 34

Jones, S., et al., PFISR and ROPA observations of pulsating aurora, *Journal of Atmospheric and Solar-Terrestrial Physics*, *71*(6-7), 708–716, doi:10.1016/j.jastp.2008.10.004, 2009. 30

Jones, S. L., M. R. Lessard, K. Rychert, E. Spanswick, and E. Donovan, Large-scale aspects and temporal evolution of pulsating aurora, *Journal of Geophysical Research*, *116*(A3), A03,214, doi:10.1029/2010JA015840, 2011. 26

Jones, S. L., M. R. Lessard, K. Rychert, E. Spanswick, E. Donovan, and A. N. Jaynes, Persistent, widespread pulsating aurora: A case study, *Journal of Geophysical Research: Space Physics*, *118*(6), 2998–3006, doi:10.1002/jgra.50301, 2013. 27

Kaila, K., R. Rasinkangas, P. Pollari, R. Kuula, J. Kangas, T. Turunen, and T. Bösinger, High resolution measurements of pulsating aurora by EISCAT, optical instruments and pulsation magnetometers, *Advances in Space Research*, *9*(5), 53–56, doi:10.1016/0273-1177(89)90340-2, 1989. 30

Kamiyama, H., Ionization and excitation by precipitating electrons, *Rep. Ionosph. Space Res. Japan*, *20*(2), 171–187, 1966. 47

Karlsson, T., G. T. Marklund, S. Figueiredo, T. Johansson, and S. Buchert, Separating spatial and temporal variations in auroral electric and magnetic fields by Cluster multipoint measurements, *Annales Geophysicae*, *22*(7), 2463–2472, doi: 10.5194/angeo-22-2463-2004, 2004. 5

Kataoka, R., Y. Miyoshi, D. Hampton, T. Ishii, and H. Kozako, Pulsating aurora beyond the ultra-low-frequency range, *Journal of Geophysical Research: Space Physics*, *117*(A8), doi:10.1029/2012JA017987, 2012. 28

Kennel, C. F., and H. E. Petschek, Limit on stably trapped particle fluxes, *Journal of Geophysical Research*, *71*(1), 1–28, doi:10.1029/JZ071i001p00001, 1966. 19

Kivelson, M. G. M. G., and C. T. C. T. Russell, *Introduction to space physics*, 568 pp., Cambridge University Press, 1995. 9

Klimas, A. J., J. A. Valdivia, D. Vassiliadis, D. N. Baker, M. Hesse, and J. Takalo, Self-organized criticality in the substorm phenomenon and its relation to localized reconnection in the magnetospheric plasma sheet, *Journal of Geophysical Research: Space Physics*, *105*(A8), 18,765–18,780, doi:10.1029/1999JA000319, 2000. 72

Knudsen, D. J., E. F. Donovan, L. L. Cogger, and B. Jackel, Width and structure of mesoscale optical auroral arcs, *Geophysical Research Letters*, *28*(4), 705–708, doi: 10.1029/2000GL011969, 2001. 66, 70

Lanchester, B. S., M. H. Rees, D. Lummerzheim, A. Otto, H. U. Frey, and K. U. Kaila, Large fluxes of auroral electrons in filaments of 100 m width, *Journal of Geophysical Research: Space Physics*, *102*(A5), 9741–9748, doi:10.1029/97JA00231, 1997. 66

Le, G., Y. Wang, J. a. Slavin, and R. J. Strangeway, Space Technology 5 multipoint observations of temporal and spatial variability of field-aligned currents, *Journal of Geophysical Research*, *114*(A8), 1–14, doi:10.1029/2009JA014081, 2009. 5

LeClair, L. R., and J. W. McConkey, Selective detection of O(1S0) following electron impact dissociation of O2 and N2O using a XeO* conversion technique, *The Journal of Chemical Physics*, *99*(6), 4566–4577, doi:10.1063/1.466056, 1993. 47

Lessard, M., A Review of Pulsating Aurora, in *Auroral Phenomenology and Magnetospheric Processes: Earth And Other Planets*, edited by A. Keiling, E. Donovan, F. Bagenal, and T. Karlsson, pp. 55–68, American Geophysical Union, Washington, D. C., doi:10.1029/2011GM001187, 2012. 5, 24, 29, 37, 39

Li, W., J. Bortnik, R. M. Thorne, Y. Nishimura, V. Angelopoulos, and L. Chen, Modulation of whistler mode chorus waves: 2. Role of density variations, *Journal of Geophysical Research*, *116*(A6), A06,206, doi:10.1029/2010JA016313, 2011a. 36

Li, W., R. M. Thorne, J. Bortnik, Y. Nishimura, and V. Angelopoulos, Modulation of whistler mode chorus waves: 1. Role of compressional Pc4âĂŞ5 pulsations, *Journal of Geophysical Research*, *116*(A6), A06,205, doi:10.1029/2010JA016312, 2011b. 34

Li, W., J. Bortnik, Y. Nishimura, R. M. Thorne, and V. Angelopoulos, The origin of pulsating aurora: Modulated whistler mode chorus waves, in *Auroral Phenomenology and Magnetospheric Processes: Earth and Other Planets*, edited by A. Keiling, E. Donovan, F. Bagenal, and T. Karlsson, pp. 379–388, American Geophysical Union, Washington, D. C., 2012. 29, 39

Li, W., et al., Global distribution of whistler-mode chorus waves observed on the THEMIS spacecraft, *Geophysical Research Letters*, *36*(9), L09,104, doi:10.1029/2009GL037595, 2009. 23

Liang, J., E. Donovan, B. Ni, C. Yue, F. Jiang, and V. Angelopoulos, On an energy-latitude dispersion pattern of ion precipitation potentially associated with magnetospheric EMIC waves, *Journal of Geophysical Research: Space Physics*, *119*(10), 8137–8160, doi:10.1002/2014JA020226, 2014. 23

Liang, J., E. Donovan, Y. Nishimura, B. Yang, E. Spanswick, K. Asamura, T. Sakanoi, D. Evans, and R. Redmon, Low-energy ion precipitation structures associated with pulsating auroral patches, *Journal of Geophysical Research: Space Physics*, *120*(7), 5408–5431, doi:10.1002/2015JA021094, 2015. 29, 36

Liang, J., E. Donovan, B. Jackel, E. Spanswick, and M. Gillies, On the 630âĂL'nm red-line pulsating aurora: Red-line Emission Geospace Observatory observations and model simulations, *Journal of Geophysical Research: Space Physics*, *121*(8), 7988–8012, doi:10.1002/2016JA022901, 2016. 46

Luhmann, J., Auroral pulsations from atmospheric waves, *Journal of Geophysical Research*, *84*(9), 4224–4228, 1979. 37

Lui, A., Multiscale phenomena in the near-Earth magnetosphere, *Journal of Atmospheric and Solar-Terrestrial Physics*, *64*(2), 125–143, doi:10.1016/S1364-6826(01)00079-7, 2002. 72

Lui, A., and C. Anger, A uniform belt of diffuse auroral emission seen by the ISIS-2 scanning photometer, *Planetary and Space Science*, *21*(5), 799–809, doi:10.1016/0032-0633(73)90097-4, 1973. 21

Lundblad, J., and F. Søraas, Proton observations supporting the ion cyclotron wave heating theory of SAR arc formation, *Planetary and Space Science*, *26*(3), 245–254, doi:10.1016/0032-0633(78)90090-9, 1978. 23

Lynch, K. A., D. Pietrowski, R. B. Torbert, N. Ivchenko, G. Marklund, and F. Primdahl, Multiple-point electron measurements in a nightside auroral arc: Auroral Turbulence II particle observations, *Geophysical Research Letters*, *26*(22), 3361–3364, doi:10.1029/1999GL900599, 1999. 5

Lynch, K. A., et al., Structure and dynamics of the nightside poleward boundary: Sounding rocket and ground-based observations of auroral electron precipitation in a rayed curtain, *Journal of Geophysical Research: Space Physics*, *117*(A11), n/a–n/a, doi:10.1029/2012JA017691, 2012. 5

Maggs, J., and T. Davis, Measurements of the thicknesses of auroral structures, *Planetary and Space Science*, *16*(2), 205 – 209, doi:10.1016/0032-0633(68)90069-X, 1968. 66

McEwen, D. J., E. Yee, B. A. Whalen, and A. W. Yau, Electron energy measurements in pulsating auroras, *Canadian Journal of Physics*, *59*(8), 1106–1115, doi:10.1139/p81-146, 1981. 29

McPherron, R. L., Growth phase of magnetospheric substorms, *Journal of Geophysical Research*, *75*(28), 5592–5599, doi:10.1029/JA075i028p05592, 1970. 20

Mende, S. B., Observing the magnetosphere through global auroral imaging: 1. Observables, *Journal of Geophysical Research: Space Physics*, *121*(10), 10,623–10,637, doi:10.1002/2016JA022558, 2016. 41

Mende, S. B., C. W. Carlson, H. U. Frey, T. J. Immel, and J. Gérard, IMAGE FUV and in situ FAST particle observations of substorm aurorae, *Journal of Geophysical Research*, *108*(A4), 8010, doi:10.1029/2002JA009413, 2003. 41

Minatoya, H., N. Sato, T. Saemundsson, and T. Yoshino, Absence of Correlation between Periodic Pulsating Auroras in Geomagnetically Conjugate Areas, *J. Geomag. Geoelectr.*, *47*, 583–598, 1995. 31

Miyoshi, Y., Y. Katoh, T. Nishiyama, T. Sakanoi, K. Asamura, and M. Hirahara, Time of flight analysis of pulsating aurora electrons, considering wave-particle interactions with propagating whistler mode waves, *Journal of Geophysical Research*, *115*(A10), A10,312, doi:10.1029/2009JA015127, 2010. 34

Miyoshi, Y., et al., Energetic electron precipitation associated with pulsating aurora: EISCAT and Van Allen Probe observations, *Journal of Geophysical Research: Space Physics*, *120*(4), 2754–2766, doi:10.1002/2014JA020690, 2015. 30

Murphree, J. S., R. A. King, T. Payne, K. Smith, D. Reid, J. Adema, B. Gordon, and R. Wlochowicz, The Freja ultraviolet imager, *Space Science Reviews*, *70*(3-4), 421–446, doi:10.1007/BF00756880, 1994. 18

Nakajima, A., et al., Electron and wave characteristics observed by the THEMIS satellites near the magnetic equator during a pulsating aurora, *Journal of Geophysical Research*, *117*(A3), A03,219, doi:10.1029/2011JA017066, 2012. 32

Nakamura, R., and T. Oguti, Drifts of auroral structures and magnetospheric electric fields, *Journal of Geophysical Research*, *92*(A10), 11,241, doi:10.1029/JA092iA10p11241, 1987. 30

Nemzek, R. J., R. Nakamura, D. N. Baker, R. D. Belian, D. J. McComas, M. F. Thomsen, and T. Yamamoto, The relationship between pulsating auroras observed from the ground and energetic electrons and plasma density measured at geosynchronous orbit, *Journal of Geophysical Research*, *100*(A12), 23,935, doi:10.1029/95JA01756, 1995. 31, 35

Newell, P. T., T. Sotirelis, and S. Wing, Diffuse, monoenergetic, and broadband aurora: The global precipitation budget, *Journal of Geophysical Research: Space Physics*, *114*(A9), n/a–n/a, doi:10.1029/2009JA014326, 2009. 21, 41

Ni, B., et al., Origins of the Earth's Diffuse Auroral Precipitation, *Space Science Reviews*, *200*(1-4), 205–259, doi:10.1007/s11214-016-0234-7, 2016. 22, 23

Nishimura, Y., J. Bortnik, W. Li, J. Liang, R. M. Thorne, V. Angelopoulos, O. Le Contel, U. Auster, and J. W. Bonnell, Chorus intensity modulation driven by time-varying field-aligned low-energy plasma, *Journal of Geophysical Research: Space Physics*, *120*(9), 7433–7446, doi:10.1002/2015JA021330, 2015. 36

Nishimura, Y., et al., Identifying the driver of pulsating aurora., *Science (New York, N.Y.)*, *330*(6000), 81–4, doi:10.1126/science.1193186, 2010. 32, 33

Nishimura, Y., et al., Multievent study of the correlation between pulsating aurora and whistler mode chorus emissions, *Journal of Geophysical Research*, *116*(A11), A11,221, doi:10.1029/2011JA016876, 2011. 32

Nishiyama, T., T. Sakanoi, Y. Miyoshi, Y. Katoh, K. Asamura, S. Okano, and M. Hirahara, The source region and its characteristic of pulsating aurora based on the

Reimei observations, *Journal of Geophysical Research*, *116*(A3), A03,226, doi:10.1029/2010JA015507, 2011. 34

Nishiyama, T., T. Sakanoi, Y. Miyoshi, D. L. Hampton, Y. Katoh, R. Kataoka, and S. Okano, Multiscale temporal variations of pulsating auroras: On-off pulsation and a few Hz modulation, *Journal of Geophysical Research: Space Physics*, *119*(5), 3514–3527, doi:10.1002/2014JA019818, 2014. 35

Nishiyama, T., Y. Miyoshi, Y. Katoh, T. Sakanoi, R. Kataoka, and S. Okano, Substructures with luminosity modulation and horizontal oscillation in pulsating patch: Principal component analysis application to pulsating aurora, *Journal of Geophysical Research: Space Physics*, *121*(3), 2360–2373, doi:10.1002/2015JA022288, 2016. 35

Oguti, T., Recurrent Auroral Patterns, *Journal of Geophysical Research*, *81*(10), 1782–1786, doi:10.1029/JA081i010p01782, 1976. 29

Oguti, T., and T. Watanabe, Quasi-periodic poleward propagation of on-off switching aurora and associated geomagnetic pulsations in the dawn, *Journal of Atmospheric and Terrestrial Physics*, *38*(5), 543–551, doi:10.1016/0021-9169(76)90013-1, 1976. 26

Olsen, N., et al., The Swarm Satellite Constellation Application and Research Facility (SCARF) and Swarm data products, *Earth, Planets and Space*, *65*(11), 1189–1200, doi:10.5047/eps.2013.07.001, 2013. 5

Oyama, S., K. Shiokawa, J. Kurihara, T. T. Tsuda, S. Nozawa, Y. Ogawa, Y. Otsuka, and B. J. Watkins, Lower-thermospheric wind fluctuations measured with an FPI during pulsating aurora at Tromsø, Norway, *Annales Geophysicae*, *28*(10), 1847–1857, doi:10.5194/angeo-28-1847-2010, 2010. 25

Panov, E. V., W. Baumjohann, R. A. Wolf, R. Nakamura, V. Angelopoulos, J. M. Weygand, and M. V. Kubyshkina, Magnetotail energy dissipation during an auroral substorm, *Nat Phys*, *12*(12), 1158–1163, doi:10.1038/nphys3879, 2016. 68

Partamies, N., K. Kauristie, T. I. Pulkkinen, and M. Brittnacher, Statistical study of auroral spirals, *Journal of Geophysical Research: Space Physics*, *106*(A8), 15,415–15,428, doi:10.1029/2000JA900172, 2001. 69

Partamies, N., M. Syrjäsuo, E. Donovan, M. Connors, D. Charrois, D. Knudsen, and Z. Kryzanowsky, Observations of the auroral width spectrum at kilometre-scale size, *Annales Geophysicae*, *28*(3), 711–718, doi:10.5194/angeo-28-711-2010, 2010. 66, 70

Paschmann, G., S. Haaland, and R. Treumann, *Auroral Plasma Physics*, 486 pp., Springer Netherlands, 2003. 21, 40, 68

Pedersen, T., E. Mishin, and K. Oksavik, Observations of structured optical emissions and particle precipitation equatorward of the traditional auroral oval, *Journal of Geophysical Research: Space Physics*, *112*(A10), n/a–n/a, doi:10.1029/2007JA012299, 2007. 24

Peticolas, L. M., T. J. Hallinan, H. C. Stenbaek-Nielsen, J. W. Bonnell, and C. W. Carlson, A study of black aurora from aircraft-based optical observations and plasma measurements on FAST, *Journal of Geophysical Research: Space Physics*, *107*(A8), SMP 30–1–SMP 30–11, doi:10.1029/2001JA900157, 2002. 23, 24

Pilipenko, V. A., S. L. Shalimov, E. N. Fedorov, M. J. Engebretson, and W. J. Hughes, Coupling between field-aligned current impulses and Pi1 noise bursts, *Journal of Geophysical Research*, *104*(A8), 17,419–17,430, doi:10.1029/1999JA900190, 1999. 37

Pollock, C., et al., The Role and Contributions of Energetic Neutral Atom (ENA) Imaging in Magnetospheric Substorm Research, *Space Science Reviews*, *109*(1-4), 155–182, doi:10.1023/B:SPAC.0000007518.93331.d5, 2003. 12

Pulkkinen, T. I., R. J. Pellinen, H. E. J. Koskinen, H. J. Opgenoorth, J. S. Murphree, V. Petrov, A. Zaitzev, and E. Friis-Christensen, Auroral Signatures of Substorm Recovery Phase: A Case Study, in *Magnetospheric Substorms*, edited by J. R. Kan, T. A. Potemra, S. Kokubun, and T. Iijima, American Geophysical Union, Washington D. C., doi:10.1029/GM064p0333, 1991. 68

Rees, M. H., *Physics and chemistry of the upper atmosphere*, Cambridge University Press, Cambridge, doi:10.1017/CBO9780511573118, 1989. 14, 15

Rees, M. H., and R. G. Roble, Observations and theory of the formation of stable auroral red arcs, *Reviews of Geophysics*, *13*(1), 201, doi:10.1029/RG013i001p00201, 1975. 46

Royrvik, O., and T. N. Davis, Pulsating Aurora: Local and Global Morphology, *Journal of Geophysical Research*, *82*(29), 4720–4740, doi:10.1029/JA082i029p04720, 1977. 25, 26, 28

Sætre, C., The effect of energetic electron precipitation on the nitric oxide density in the lower thermosphere, Phd, The University of Bergen, 2007. 13

Saito, Y., S. Machida, M. Hirahara, T. Mukai, and H. Miyaoka, Rocket observation of electron fluxes over a pulsating aurora, *Planetary and Space Science*, *40*(8), 1043–1054, doi:10.1016/0032-0633(92)90033-K, 1992. 29

Samara, M., and R. G. Michell, Ground-based observations of diffuse auroral frequencies in the context of whistler mode chorus, *Journal of Geophysical Research*, *115*, A00F18, doi:10.1029/2009JA014852, 2010. 28, 66

Samara, M., R. G. Michell, and R. J. Redmon, Low-altitude satellite measurements of pulsating auroral electrons, *Journal of Geophysical Research: Space Physics*, *120*(9), 8111–8124, doi:10.1002/2015JA021292, 2015. 29

Sandahl, I., L. Eliasson, and R. Lundin, Rocket observations of precipitating electrons over a pulsating aurora, *Geophysical Research Letters*, *7*(5), 309–312, doi:10.1029/GL007i005p00309, 1980. 29

Sandahl, I., T. Sergienko, and U. Brändström, Fine structure of optical aurora, *Journal of Atmospheric and Solar-Terrestrial Physics*, *70*(18), 2275–2292, doi:10.1016/j.jastp.2008.08.016, 2008. 66

Sandholt, P. E. P. E., H. C. Carlson, and A. Egeland, *Dayside and polar cap aurora*, 1 ed., 287 pp., Springer Netherlands, 2002. 21

Sato, N., M. Morooka, K. Minatoya, and T. Saemundsson, Nonconjugacy of pulsating auroral patches near L=6, *Geophysical Research Letters*, *25*(20), 3755–3758, doi:10.1029/1998GL900002, 1998. 31

Sato, N., D. M. Wright, C. W. Carlson, Y. Ebihara, M. Sato, T. Saemundsson, S. E. Milan, and M. Lester, Generation region of pulsating aurora obtained simultaneously by the FAST satellite and a Syowa-Iceland conjugate pair of observatories, *Journal of Geophysical Research*, *109*(A10), A10,201, doi:10.1029/2004JA010419, 2004. 29, 31, 37, 38

Sato, N., A. Kadokura, T. Motoba, K. Hosokawa, G. Bjornsson, and T. Saemundsson, Ground-Based Aurora Conjugacy and Dynamic Tracing of Geomagnetic Conjugate Points, in *Auroral Phenomenology and Magnetospheric Processes: Earth And Other Planets*, edited by A. Keiling, E. Donovan, F. Bagenal, and T. Karlsson, pp. 91–98, American Geophysical Union, Washington, D. C., 2012. 31, 32

Sato, N., et al., Direct comparison of pulsating aurora observed simultaneously by the FAST satellite and from the ground at Syowa, *Geophysical Research Letters*, *29*(21), 2041, doi:10.1029/2002GL015615, 2002. 37

Scourfield, M., W. Innes, and N. Parsons, Spatial coherency in pulsating aurora, *Planetary and Space Science*, *20*(11), 1843–1848, doi:10.1016/0032-0633(72)90117-1, 1972. 29

Scourfield, M. W. J., and N. R. Parsons, Pulsating auroral patches exhibiting sudden intensity-dependent spatial expansion, *Journal of Geophysical Research*, *76*(19), 4518–4524, doi:10.1029/JA076i019p04518, 1971. 29

Scourfield, M. W. J., J. G. Keys, E. Nielsen, C. K. Goertz, and H. Collin, Evidence for the ExB drift of pulsating auroras, *Journal of Geophysical Research*, *88*(A10), 7983, doi:10.1029/JA088iA10p07983, 1983. 30

Sergeev, V., E. Sazhina, N. Tsyganenko, J. Lundblad, and F. Søraas, Pitch-angle scattering of energetic protons in the magnetotail current sheet as the dominant source of their isotropic precipitation into the nightside ionosphere, *Planetary and Space Science*, *31*(10), 1147–1155, doi:10.1016/0032-0633(83)90103-4, 1983. 23

Sergienko, T., I. Sandahl, B. Gustavsson, L. Andersson, U. Brändström, and Å. Steen, A study of fine structure of diffuse aurora with ALIS-FAST measurements, *Annales Geophysicae*, *26*(11), 3185–3195, doi:10.5194/angeo-26-3185-2008, 2008. 23, 24

Shi, R., D. Han, B. Ni, Z.-J. Hu, C. Zhou, and X. Gu, Intensification of dayside diffuse auroral precipitation: contribution of dayside Whistler-mode chorus waves in realistic magnetic fields, *Annales Geophysicae*, *30*(9), 1297–1307, doi:10.5194/angeo-30-1297-2012, 2012. 23

Slavin, J. a., G. Le, R. J. Strangeway, Y. Wang, S. a. Boardsen, M. B. Moldwin, and H. E. Spence, Space Technology 5 multi-point measurements of near-Earth magnetic fields: Initial results, *Geophysical Research Letters*, *35*, L02,107, doi:10.1029/2007GL031728, 2008. 5

Smith, M., D. Bryant, and T. Edwards, Pulsations in auroral electrons and positive ions, *Journal of Atmospheric and Terrestrial Physics*, *42*(2), 167–178, doi:10.1016/0021-9169(80)90077-X, 1980. 29

Søraas, F., K. Aarsnes, J. Lundblad, and D. Evans, Enhanced pitch angle scattering of protons at mid-latitudes during geomagnetic storms, *Physics and Chemistry of the Earth, Part C: Solar, Terrestrial & Planetary Science*, *24*(1-3), 287–292, doi:10.1016/S1464-1917(98)00041-5, 1999. 23

Stenbaek-Nielsen, H., and T. Hallinan, Pulsating auroras: Evidence for noncollisional thermalization of precipitating electrons, *Journal of Geophysical Research*, *84*(A7), 3257–3271, doi:10.1029/JA084iA07p03257, 1979. 30, 36

Stenbaek-Nielsen, H. C., Pulsating aurora: The importance of the ionosphere, *Geophysical Research Letters*, *7*(5), 353–356, doi:10.1029/GL007i005p00353, 1980. 37

Stenbaek-Nielsen, H. C., T. N. Davis, and N. W. Glass, Relative motion of auroral conjugate points during substorms, *Journal of Geophysical Research*, *77*(10), 1844–1858, doi:10.1029/JA077i010p01844, 1972. 31

Stenbaek-Nielsen, H. C., E. M. Wescott, and R. W. Peterson, Pulsating auroras over conjugate areas, *Antarc. J. U. S.*, *8*, 246–247, 1973. 31

Störmer, C., Statistics of heights of various auroral forms from Southern Norway: Second communication, *Journal of Geophysical Research*, *53*(3), 251, doi:10.1029/TE053i003p00251, 1948. 30

Störmer, C., *The polar aurora*, XVII, 403 s., pl. ill., Clarendon Press, Oxford, doi:10.1002/qj.49708235123, 1955. 25

Swift, D., and D. Gurnett, Direct comparison between satellite electric field measurements and the visual aurora, *Journal of Geophysical Research*, *78*(31), 7306–7313, doi:10.1029/JA078i031p07306, 1973. 30

Tagirov, V. R., V. S. Ismagilov, E. E. Titova, V. A. Arinin, A. M. Perlikov, J. Manninen, T. Turunen, and K. Kaila, Auroral pulsations and accompanying VLF emissions, *Annales Geophysicae*, *17*(1), 66–78, doi:10.1007/s00585-999-0066-9, 1999. 38

Thieman, J. R., and R. A. Hoffman, Determination of inverted-V stability from Dynamics Explorer satellite data, *Journal of Geophysical Research*, *90*, 3511–3516, doi:10.1029/JA090iA04p03511, 1985. 41

Trondsen, T. S., and L. L. Cogger, A survey of small-scale spatially periodic distortions of auroral forms, *Journal of Geophysical Research: Space Physics*, *103*(A5), 9405–9415, doi:10.1029/98JA00619, 1998. 66, 69

Tsurutani, B. T., and E. J. Smith, Postmidnight chorus: A substorm phenomenon, *Journal of Geophysical Research*, *79*(1), 118–127, doi:10.1029/JA079i001p00118, 1974. 34

Valdivia, J. A., A. Klimas, D. Vassiliadis, V. Uritsky, and J. Takalo, Self-Organization in a Current Sheet Model, in *Advances in Space Environment Research - Volume I*, pp. 515–522, Springer Netherlands, Dordrecht, doi:10.1007/978-94-007-1069-6_52, 2003. 72

Wahlund, J.-E., H. J. Opgenoorth, and P. Rothwell, Observations of thin auroral ionization layers by EISCAT in connection with pulsating aurora, *Journal of Geophysical Research*, *94*(A12), 17,223–17,233, doi:10.1029/JA094iA12p17223, 1989. 30, 36

Wallis, D. D., J. R. Burrows, M. C. Moshupi, C. D. Anger, and J. S. Murphree, Observations of particles precipitating into detached arcs and patches equatorward of the auroral oval, *Journal of Geophysical Research*, *84*(A4), 1347, doi:10.1029/JA084iA04p01347, 1979. 24

Watanabe, M., A. Kadokura, N. Sato, and T. Saemundsson, Absence of geomagnetic conjugacy in pulsating auroras, *Geophysical Research Letters*, *34*(15), L15,107, doi:10.1029/2007GL030469, 2007. 31, 32, 38

Weimer, D. R., Models of high-latitude electric potentials derived with a least error fit of spherical harmonic coefficients, *Journal of Geophysical Research*, *100*(A10), 19,595, doi:10.1029/95JA01755, 1995. 3

Wescott, E. M., H. C. Stenbaek-Nielsen, T. N. Davis, and H. M. Peek, The Skylab Barium Plasma Injection Experiments, 1. Convection observations, *Journal of Geophysical Research*, *81*(25), 4487–4494, doi:10.1029/JA081i025p04487, 1976. 30

Williams, J. D., An Investigation into Pulsating Aurora, Ph. d. thesis, University of Washington, Seattle, WA, 2002. 37

Williams, P. J. S., C. F. del Pozo, I. Hiscock, and R. Fallows, Velocity of auroral arcs drifting equatorward from the polar cap, *Annales Geophysicae*, *16*(10), 1322–1331, doi:10.1007/s00585-998-1322-0, 1998. 68

Winningham, J. D., F. Yasuhara, S. I. Akasofu, and W. J. Heikkila, The latitudinal morphology of 10-eV to 10-keV electron fluxes during magnetically quiet and disturbed times in the 2100-0300 MLT sector, *Journal of Geophysical Research*, *80*(22), 3148–3171, doi:10.1029/JA080i022p03148, 1975. 22

Yamamoto, T., and T. Oguti, Recurrent fast motions of pulsating auroral patches: 1. A case study on optical and quantitative characteristics during a slightly active period, *Journal of Geophysical Research*, *87*(A9), 7603, doi:10.1029/JA087iA09p07603, 1982. 28

Yang, B., E. Donovan, J. Liang, J. M. Ruohoniemi, and E. Spanswick, Using patchy pulsating aurora to remote sense magnetospheric convection, *Geophysical Research Letters*, *42*(13), 5083–5089, doi:10.1002/2015GL064700, 2015. 30

Yang, B., E. Donovan, J. Liang, and E. Spanswick, A statistical study of the motion of pulsating aurora patches: using the THEMIS All-Sky Imager, *Annales Geophysicae*, *35*(2), 217–225, doi:10.5194/angeo-35-217-2017, 2017. 30

Yau, A. W., B. A. Whalen, and D. J. McEwen, Rocket-borne measurements of particle pulsation in pulsating aurora, *Journal of Geophysical Research*, *86*(A7), 5673, doi:10.1029/JA086iA07p05673, 1981. 29, 33

Zhang, X.-J., V. Angelopoulos, B. Ni, and R. M. Thorne, Predominance of ECH wave contribution to diffuse aurora in Earth's outer magnetosphere, *Journal of Geophysical Research: Space Physics*, *120*(1), 295–309, doi:10.1002/2014JA020455, 2015. 23

Zheng, Y., K. A. Lynch, M. Boehm, R. Goldstein, H. Javadi, P. Schuck, R. L. Arnoldy, and P. M. Kintner, Multipoint measurements of field-aligned current density in the auroral zone, *Journal of Geophysical Research*, *108*(A5), 1–20, doi:10.1029/2002JA009450, 2003. 5

Zmuda, A. J., J. H. Martin, and F. T. Heuring, Transverse magnetic disturbances at 1100 kilometers in the auroral region, *Journal of Geophysical Research*, *71*(21), 5033–5045, doi:10.1029/JZ071i021p05033, 1966. 17

Zmuda, A. J., F. T. Heuring, and J. H. Martin, Dayside magnetic disturbances at 1100 kilometers in the auroral oval, *Journal of Geophysical Research*, *72*(3), 1115–1117, doi:10.1029/JZ072i003p01115, 1967. 17

I

Paper I

Temporal characteristics and energy deposition of pulsating auroral patches

B. K. Humberset, J. W. Gjerloev, M. Samara, R. G. Michell, and I. R. Mann

Journal of Geophysical Research: Space physics, 121, doi:10.1002/2016JA022921 (2016)

AGU PUBLICATIONS

JGR

Journal of Geophysical Research: Space Physics

RESEARCH ARTICLE
10.1002/2016JA022921

Key Points:
- Objective and quantitative characteristics of pulsating auroral patches
- Pulsating aurora is highly variable in all measurable parameters and thus would be more accurately described as fluctuating aurora
- Characteristics of pulsating auroral patches do not fit well with the flow cyclotron maser theory

Correspondence to:
B. K. Humberset,
Beate.Humberset@uib.no

Citation:
Humberset, B. K., J. W. Gjerloev, M. Samara, R. G. Michell, and I. R. Mann (2016), Temporal characteristics and energy deposition of pulsating auroral patches, *J. Geophys. Res. Space Physics*, *121*, 7087–7107, doi:10.1002/2016JA022921.

Received 7 MAY 2016
Accepted 1 JUL 2016
Accepted article online 11 JUL 2016
Published online 23 JUL 2016

Temporal characteristics and energy deposition of pulsating auroral patches

B. K. Humberset[1], J. W. Gjerloev[1,2], M. Samara[3], R. G. Michell[3,4], and I. R. Mann[5]

[1] Birkeland Centre for Space Science, Department of Physics and Technology, University of Bergen, Bergen, Norway, [2] The Johns Hopkins University Applied Physics Laboratory, Laurel, Maryland, USA, [3] NASA Goddard Space Flight Center, Greenbelt, Maryland, USA, [4] Department of Astronomy, University of Maryland, College Park, Maryland, USA, [5] Department of Physics, University of Alberta, Edmonton, Alberta, Canada

Abstract We present a careful statistical analysis of pulsating aurora (PA) using all-sky green line (557.7 nm) images obtained at 3.3 Hz. Six well-defined individual PA patches are identified and extracted using a contouring technique. Quantitative parameters such as the patch duration (on-time and off-time), peak intensity, and integrated intensity are determined for each patch and each pulsation. The resulting characteristics serve as strict observational constraints that any of the many competing theories attempting to explain PA must predict. The purpose of this paper is to determine the characteristics of PA patches in order to provide better observational constraints on the suggested mechanisms. All aspects of the temporal behavior of the individual patches appear to be erratic. Historically, PA has been defined very loosely and we argue that the use of the term "pulsating" is inappropriate since our findings and other published results are not regularly periodic and thus a more appropriate term may be fluctuating aurora. Further, we find that the observational constraints do not fit well with the flow cyclotron maser theory, which in particular is suggested to create PA patches. There is no clear candidate of the suggested mechanisms and drivers to explain the observational constraints set by the PA patches in a satisfactory manner.

1. Introduction

Pulsating aurora (PA) is a phenomenon of irregularly shaped patches and bands of low-intensity aurora that undergoes rapid alternating increases and decreases in luminosity. Patches of different sizes and shapes switch on and off or vary in intensity independently of each other. The broad definition of pulsating aurora covers auroral arcs, arc segments, and patches of fixed and variable area having horizontal sizes of a few to hundreds of kilometers with repetitive, quasiperiodic, or occasionally, periodic intensity variations on time scales ranging from less than 1 s to several tens of seconds [*Royrvik and Davis*, 1977].

The pulsating aurora is generally considered to be quasiperiodic with an average period of 8 ± 2 s [*Royrvik and Davis*, 1977]. It is called quasiperiodic because in a single train of pulsations the spacing between successive maxima is not even but varies noticeably from one pulsation to the next. The range 2–20 s has been chosen because observations falling within the chosen definition apparently form a uniform data set and are concerned with a single magnetospheric process, while there are temporal changes in the aurora with both shorter and longer periods which seem to have different characteristics [*Johnstone*, 1978]. The light intensity is often described having rapid rise and decay times compared to the duration of the pulse, as if it were switching on and off, in addition to the sometimes simultaneous ~3 Hz pulsations on top. In general, there is a characteristic variety in the shape of a train of pulsations. Both "on-time" and "off-time" (see Figure 6) can vary from pulse to pulse, with the larger variations probably found in the off-time [*Davidson and Chiu*, 1991]. Attempts have been made to relate pulsation periods to latitude. *Thomas and Rothwell* [1979] found a relation interpreted as being consistent with the latitude variation of the bounce period. However, in a later study, *Duncan et al.* [1981] found no consistent, simultaneous change in period with latitude, which have discouraged further investigations of a connection to bounce period or Alfvén communication. *Royrvik and Davis* [1977] were unable to find any significant trends that relate pulsating behavior to form type, level of activity, time within the auroral substorm, local time, or latitude. It seem like this conclusion still stands, although there are indications that PA with shorter periodicity can have a near-Earth origin [e.g., *Johnstone*, 1971], while longer periodicity PA is linked to a magnetospheric source [e.g., *Jaynes et al.*, 2013].

AGU Journal of Geophysical Research: Space Physics 10.1002/2016JA022921

There is an agreement that the high-energy precipitating electrons result from pitch angle scattering. However, exactly how the modulation causing the pulsating aurora occurs is still up for discussion. Most studies point toward a time-varying pitch angle scattering close to the magnetic equator. In situ studies have observed lower band chorus [*Nishimura et al.*, 2010] and continuous measurements of electron flux modulations [*Jaynes et al.*, 2013] correlated with a single pulsating patch located through cross-correlation analysis of image pixels from an all-sky imager having the mapped footpoint within its field of view. The nonlinear relaxation oscillator [*Davidson*, 1979, 1986a, 1986b] and the flow cyclotron maser [*Demekhov and Trakhtengerts*, 1994] are theoretical candidates explaining the time-varying pitch angle scattering, the latter theory in a more quantitative manner which makes it easier to compare with observations. Since then, an increasing number of observations at the magnetic equator have made it possible to compare local plasma parameters (chorus waves, electron cyclotron harmonic waves, plasma densities, and ULF waves) in order to understand the time-varying pitch angle scattering. For example, depletions in the total electron density, probably attributed to changes in cold electron fluxes of unknown origin, are found to correlate with increases in chorus wave amplitude [*Li et al.*, 2012]. This kind of studies will probably make new advances in understanding the processes behind pulsating aurora, but there are also well-known characteristics such as nonconjugate pulsating aurora that are hard to explain with a single mechanism at the magnetic equator. *Sato et al.* [2002, 2004] showed observations of velocity-dispersed high-energy electron precipitation in correlation with nonconjugate pulsating aurora and anticorrelated with the proton flux, suggesting that it was due to a time-varying field-aligned electric field far from the magnetic equator and possibly a good fit to the mechanism of auroral acceleration region modulation by Alfvén waves [*Fedorov et al.*, 2004]. There seems to be an agreement that the ionosphere is not entirely passive, but exactly what role it has is largely unclear. There are not many suggestions of a source local to lower altitudes, such as the concept of how neutral atmosphere pressure waves could cause quasiperiodic fluctuations in auroral intensity described by *Luhmann* [1979]. It is more likely that the lower ionosphere and atmosphere have an alternating component, such as an ionospheric feedback mechanism based on the flow cyclotron maser theory suggested by *Tagirov et al.* [1999]. Pulsating aurora is more complicated than can probably be explained by time-varying pitch angle scattering alone. It remains to find how one or more ionospheric or near-Earth mechanisms contribute, if they act as a secondary control mechanism on the time-varying electron flux scattered near the magnetic equator or if they are entirely responsible for some aurora that falls within the broad category of pulsating aurora.

A satellite at low-Earth orbit altitudes crosses a pulsating patch in less than a pulsating period, while a slower-moving rocket would cross the patch within a few on-off cycles. Within that time, the observed variation is likely both temporal and spatial, and the sampling rate is limited. For high-altitude satellites (e.g., geostationary) the magnetic field line mapping is very challenging and thus we must question the relationship between the auroral form and the satellite observations.

The purpose of this paper is to determine the characteristics of PA patches in order to provide better observational constraints on the suggested mechanisms. We use ground-based all-sky imager observations which provide good spatial and temporal resolution of a PA patch. The two-dimensional images of the night sky allow us to objectively separate spatial and temporal variations, thereby avoiding the space-time ambiguity which complicate rocket or satellite measurements. In section 2 we describe the event and data used; section 3 outlines the technique and methodology; in section 4 we show two typical examples of PA patches; section 5 shows statistical results; in section 6 we discuss our results, and finally, in section 7 we summarize and draw conclusions.

2. Data and Conditions

This study utilizes all-sky imager data obtained at Poker Flat Research Range in Alaska, located at 147.4/65.1° geographic longitude/latitude (~65.5° magnetic latitude). The full-frame 512 by 512 pixels images have a 1000 km field of view (FOV) of the sky at the assumed altitude (110 km) of the emissions. Throughout the recorded movies, the sky is clear, the moon is down, and there are no artifacts such as street lamps. The all-sky imager was filtered for the 557.7 nm green line from atomic oxygen and was operated at 3.3 Hz frame rate, resulting in spatial and temporal resolution that are well suited to study the diffuse pulsating aurora.

AGU Journal of Geophysical Research: Space Physics 10.1002/2016JA022921

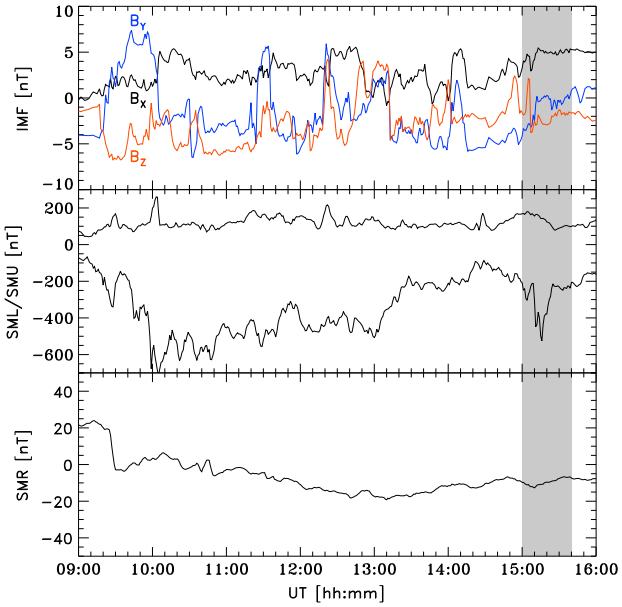

Figure 1. (top) IMF, (middle) SML/SMU indices, and (bottom) SMR. The time of the movie is indicated by the grey box. We use the SuperMAG data set of indices and time shifted IMF.

2.1. The 1 March 2012 15:00–15:40 UT

Our event occurred on 1 March 2012 during the late expansion and recovery phase of a substorm, as evident from the SMU index in Figure 1 (middle). We use the SuperMAG data set [*Gjerloev*, 2012; *Newell and Gjerloev*, 2011a, 2011b] of indices and propagated interplanetary magnetic field (IMF), which can be obtained through the SuperMAG website. The geomagnetic conditions are quiet to moderately disturbed with a moderately southward interplanetary magnetic field (IMF) and almost no ring current activity, as shown in Figure 1 (top and bottom). However, the SMU index shows 4.5 h of almost continuous substorm activity starting with the onset at 9:41 UT preceding our event. According to the SuperMAG substorm database [*Newell and Gjerloev*, 2011a], a second substorm onset happens at 14:48 UT. Before 15:00 UT the pulsating aurora covers the southern part of the sky with large east-west structures which seem to pulsate in a streaming fashion. At about 15:00 UT the pulsating aurora starts to break up into smaller more distinct and persistent patches. Our selected patches are located postmidnight around 4 magnetic local time (MLT).

3. Technique

To determine the characteristics of individual pulsating patches, we perform a five-step analysis:

1. Perform a cartesian projection.
2. Manually identify a pulsating patch.
3. Correct for Earth's rotation.
4. Contour and extract the patch.
5. Determine the patch properties.

These steps require a brief explanation.

3.1. Step 1: Cartesian Projection

The fisheye lens of the all-sky imager provides the maximum spatial coverage, but it also produces a strongly distorted view of the night sky. To correct for this, we transform each of the images to a square frame with

AGU Journal of Geophysical Research: Space Physics 10.1002/2016JA022921

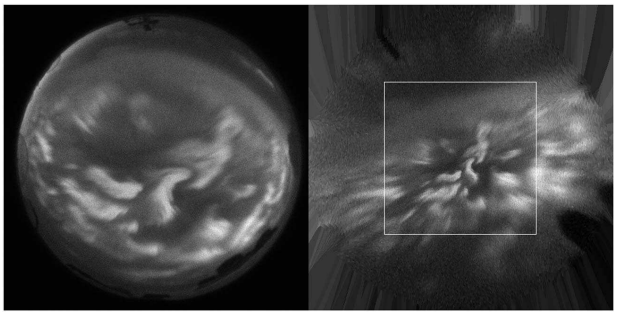

Figure 2. (left) Distorted fisheye view ASI image (right) transformed to a uniform 4 km^2 pixel grid. Patches outside the white frame are not analyzed to avoid the most distorted limb pixels.

a uniform pixel resolution of 2.0 by 2.0 km as shown in Figure 2. First, we transform the original spherical geographical pixel coordinates (at 110 km altitude) to Cartesian geographical coordinates (assuming $r = 1$). In this way we can use the scalar product to find the pixel vector in the original image that lies closest in geographical coordinates to each pixel vector in the new image. The resolution is preserved, and we do not need to make any assumptions of the altitude of the emissions. The only artifact is that the emissions in the outer parts of the image are collected over a larger area than covered by the new pixel size and likewise that emissions in the center of the image are collected over a smaller area than covered by the new pixel size. To avoid the most distorted limb pixels of the images, we only include patches located within the center of the FOV (a 500 by 500 km square).

3.2. Step 2: Patch Identification

Individual patches are manually identified from the movie and a keogram (see Figure 3). The keogram is merely used to decide if the patch is pulsating and for how long we can follow it before it either disappears or, for example, joins together with an adjacent patch.

3.3. Step 3: Correct for Earth's Rotation

The apparent drift of a patch in the movie frame of reference can be due to a combination of the Earth rotation (moving the FOV across the night sky) and the drift of the patch in an inertial frame. This latter frame is effectively GSE coordinates. We determine a rough contour around the patch for its entire lifetime to determine the apparent drift of the patch. A new movie of each individual patch is made where the patch is centered at all times (see Figure 4). This technique assumes that the velocity is constant during the lifetime of the patch and none of the patches appear to violate this assumption. The Earth's rotation is known and is easily subtracted from the apparent drift velocity to allow for a determination of the patch inertial frame velocity.

3.4. Step 4: Contour and Extract the Patch

The extracted patch is expected to vary during the train of pulsations. A new contour of the patch is determined for each pulsation. First, we identify an intensity level L where the patch intensity falls off; $L = (I_{max} - I_{min}) \times P$, where I_{max} is the maximum intensity during the pulsation, I_{min} is the minimum background intensity, and P is the percentage value which best captures the patch contour, for example, to avoid

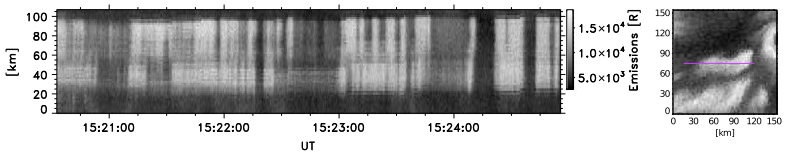

Figure 3. Geographic east-west keogram of the resulting time interval for a specific patch (#2). In Step 2 of the technique a keogram through a patch is used to decide if the patch is pulsating and for how long we can follow it.

AGU Journal of Geophysical Research: Space Physics 10.1002/2016JA022921

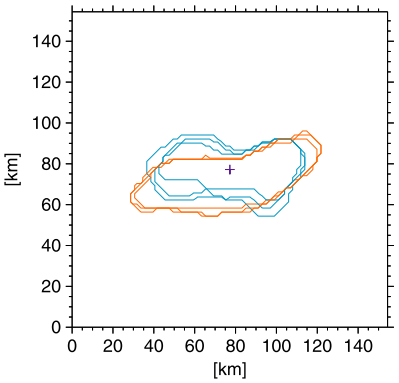

Figure 4. Contours of a patch (#2) for the three first (blue) and last (orange) on-times of a patch. In Step 3 of the technique the net velocity of the rotation of Earth and assumed constant drift is corrected for, resulting in centered contours.

capturing an adjacent patch. For each pulsation the contour is defined as the outermost edge of the sum of contours found for the ±2 images (±0.6 s) around maximum intensity as illustrated in Figure 5. For the times between pulsations the contours are interpolated using a square function.

In this study we only discuss individual patches. However, it happens that patches merge with one or several nearby patches. Exactly how frequently under which conditions and why this happens are not known. If the patch merges with a neighboring patch, we end the analysis. If a contour cannot be determined because of weak emissions, we use the average of the previous and following contours. To avoid capturing adjacent patches and background emissions, we visually check each contour.

3.5. Step 5: Patch Properties

With the patch identified and contoured, we can objectively determine the temporal characteristics and the energy deposition of the patches. For each image we calculate the patch total intensity (units of Rayleigh) as well as the patch median intensity (units of Rayleigh per square kilometer). The properties are calculated from the median intensity because it is less affected by the contouring technique and thus less sensitive to the background emissions.

First, possible pulsations are identified by finding the maxima and minima of the median intensity (we use a 1.5 s boxcar filter to remove local minima). An actual pulsation is defined as having a buildup or decay larger than the pulse threshold. The pulse threshold is 5% of the difference between the maximum and minimum median intensity in the time series. Second, the off-time is the time between pulsations defined as the interval around the minima where the intensity does not vary more than the pulse threshold. The on-time for an individual pulsation is further defined as the time between off-times. Figure 6 shows an example interval of a patch median intensity where the terms on-time and off-time are indicated. Figure 7 (top) also shows the smoothed median intensity (black curve) and the resulting maxima and off-time intervals for a train of pulsations.

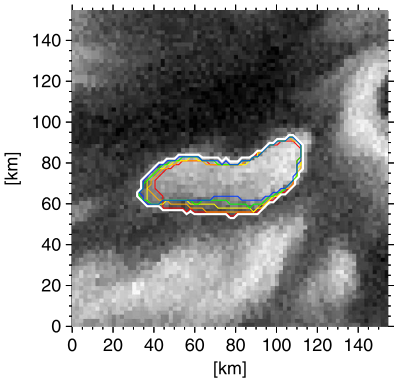

Figure 5. For each on-time the contour of the patch is found defined as the outermost edge (white) of the contours (red, orange, yellow, and green blue) found for the maximum intensity image ±2 images, as described in Step 4 of the technique.

To determine the intensity of an individual pulse, we must subtract the background emissions or offset. This may be due to diffuse aurora at higher altitudes, or in other words, we assume that a pulsating patch is superposed onto a background. The offset is estimated from the off-time values, and a linear fit is used to find the offset during the on-time (see Figures 6 and 7 (dashed lines)).

The energy deposition of the patch is referred to as intensity, defined as the median intensity corrected for the offset. Figure 7 (bottom) shows an example of the resulting intensity and train of pulses (highlighted in grey). The resulting off-times are indicated with shaded green

AGU Journal of Geophysical Research: Space Physics 10.1002/2016JA022921

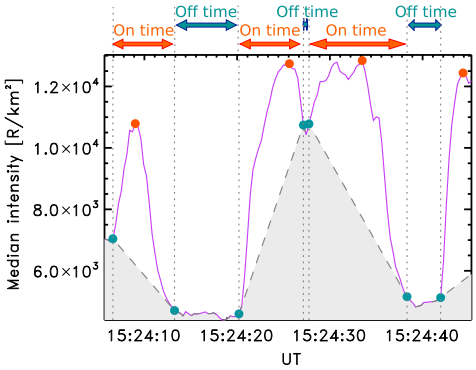

Figure 6. An example interval of a patch (#2) median intensity with examples of the defined on-time, off-time, and offset (dashed line).

areas in the background. In relation to the temporal characteristics, the integrated intensity is the energy deposited over one pulsation/on-time, while the maximum intensity is the peak energy deposition.

Using this technique, we identified, extracted, and quantified six patches.

4. Typical Example

This section is intended to give an example of what a pulsating patch is as well as to show some typical events supporting the statistical results (section 5).

To illustrate our technique and the behavior of a typical patch (#2), we show eight images from a ~4 min interval (Figure 8). Figure 8 (middle) shows its train of pulsations both in median and total intensity. The images

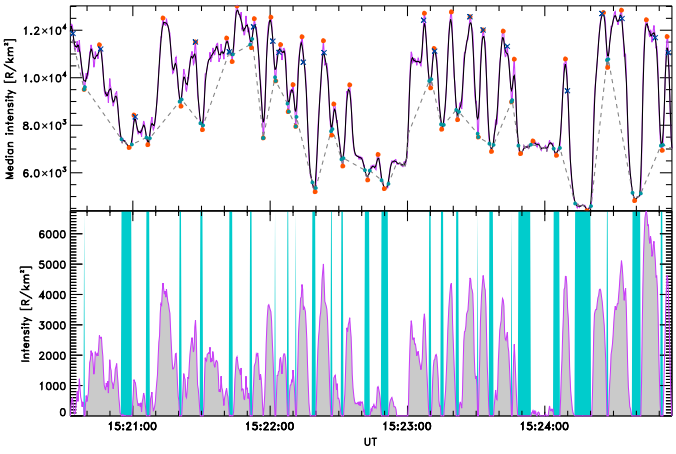

Figure 7. (top) The median intensity (purple), smoothed median intensity (black), the resulting maxima (orange) and the corrected minima (green) which define the off-times and on-times of the pulses, and the offset (dashed line). The crosses (dark blue) are the times for which the contours were found as described in Step 4 of the technique. (bottom) The resulting pulses (highlighted in grey) defined as the median intensity corrected for the offset. The off-times are indicated with shaded green areas in the background.

AGU Journal of Geophysical Research: Space Physics 10.1002/2016JA022921

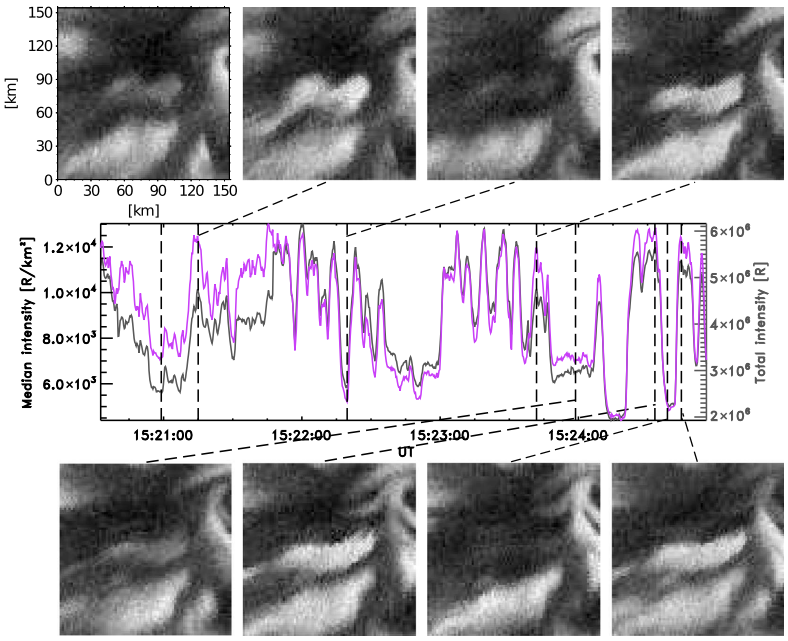

Figure 8. The train of pulsations for a typical patch (#2). Median (purple) and total intensity (grey) within the patch and eight image samples where the patch is either considered on/bright or off/dim.

are alternating peak and off-times, and it is apparent that during the off-time the patch still has emissions slightly higher than the surrounding background. We follow the patch for about 250 s or 26 pulses after which it merges with an adjacent patch and we terminate our analysis. It is evident from the median as well as the total intensity that the intensity during the on-times varies from pulse to pulse. The pulsating behavior is highly complex with pulsation on-times ranging from about 3 to 18 s. The patch certainly falls within the broad definition of "pulsating aurora," but the variable period does not appear to be in agreement with the term "pulsating" which by definition is a regular periodic behavior. A more appropriate term may be *fluctuating* aurora which by definition is irregular. Figure 9 shows another typical patch (#4) in the same format as Figure 8. In agreement with the previous example we find a striking variability in basically all measurable parameters. The patch shape may be the only parameter that remains relatively constant throughout the lifetime of the patch (in itself a remarkable observational fact).

5. Statistical Results

With the above definitions we can now determine the temporal characteristics and the characteristics of the energy deposition from each of the six patches.

5.1. Temporal Characteristics

As mentioned, Figure 8 displayed a striking temporal variability. Using all six patches, we show in Figure 10 the PDF (probability density function) of the on-times. The distribution shows a large spread of on-times, which vary from 2 to 21 s, with a peak at about 4 s. This reflects the highly variable total and median intensity through the lifetime of a patch, as, for example, shown in Figure 8 of example patch #2. The average on-time is 5.67 ± 0.14 s, and the average off-time is 0.80 ± 0.04 s. The average on-time and off-time combined form an approximate average period of 6.5 ± 0.2 s. Although the spread is wide, the distribution is clearly not scaleless and thus indicates that there is a preferred (typical) on-time of ~3–5 s.

AGU Journal of Geophysical Research: Space Physics 10.1002/2016JA022921

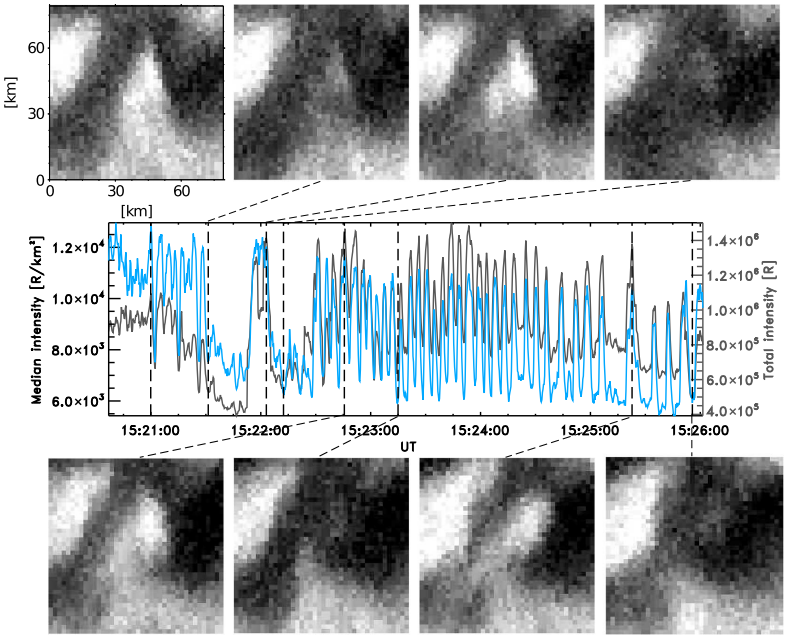

Figure 9. The train of pulsations for a typical patch (#4). Median (blue) and total intensity (grey) within the patch and eight image samples where the patch is either considered on/bright or off/dim.

Table 1 lists the duration (time and number of pulses) of the analysis for each of the patches. The exact lifetimes of the patches are probably longer because we start to capture most of the patches a bit into their lifetime and our technique is sensitive for neighboring patches which might terminate the analysis before the patch has disappeared. It is, however, clear that most of the patches are incredibly persistent.

5.2. Energy Deposition

We estimate the energy deposition for each pulse by integrating the intensity over the on-time interval. For this we use the median intensity rather than an actual 2-D spatial integration since this is less sensitive to uncertainties in the contouring procedure. This simplification can be described as $E_{\mathrm{tot}} = \sum_{i=1}^{n}\sum_{j=1}^{512}\sum_{k=1}^{512} I_{i,j,k}A_{\mathrm{pixel}} \approx \sum_{i=1}^{n}\tilde{I}_i A_{\mathrm{patch}}$ where the summation is over time or frame (i), the x coordinate (j), and the y coordinate (k), A_{pixel} is the pixel area, A_{patch} is the patch area, and finally, $\tilde{I}_i$ is the median of the total intensity within the patch.

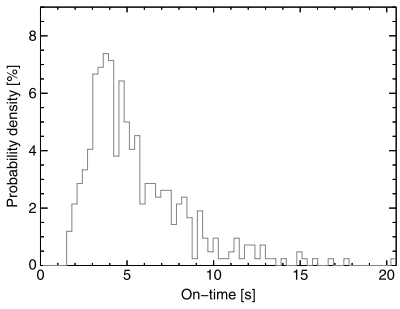

Figure 10. On-time probability density of the pulsating auroral patches.

The result, of course, does not have units of energy although the intensity of the green line is roughly proportional to the total energy flux of precipitating electrons. Further, this analysis does not include Poynting flux. We should, thus, be careful of interpreting it as a measure of energy deposition, but for the purpose of estimating

AGU Journal of Geophysical Research: Space Physics 10.1002/2016JA022921

Table 1. The Duration (Time and Number of Pulses) of the Analysis for Each of the Patches

Patch No.	Time (min:s)	No. of Pulses
1	12:05	127
2	4:12	26
3	14:35	132
4	5:16	54
5	4:23	40
6	5:05	36

the precipitating electron energy deposition, this technique should produce representative results.

Figure 11 shows the integrated intensity for all patches and all on-times. The scatterplot indicates a weak correlation ($r = 0.7$), but this is to be expected since the duration of the on-time (X axis) is obviously linearly correlated with the integrated intensity (Y axis). The simple linear fit suggests that the energy dissipated can be approximated by $f(T_{on}) = (5800 \pm 300)T_{on} - (1900 \pm 1800)$ R/km^2. However, the linear relationship is purely extrapolation as significant scatter is present, especially for longer on-times (exceeding ~6 s).

We could hypothesize that for the lifetime of a patch each pulsation (on-time) would involve the same amount of energy deposited. That would imply that a longer on-time would be associated with a weaker intensity. Figure 12 shows the maximum intensity as a function of on-time. What we find is virtually no correlation ($r = 0.27$) between the on-time and maximum intensity. Although the significance of the relationship is so that we can reject the null hypothesis, the very weak relationship implies that for the lifetime of the patch the energy deposition of the patch varies from one pulsation to another. It is also revealed that the maximum intensity varies through a train of pulsations, implying that the PA patches do not have a preferred maximum intensity.

Further, we could hypothesize that the off-time (wait time) is related to the subsequent energy deposition. The idea here is a storage and release which would then lead to a relationship where longer off-times lead to larger energy deposition. In Figure 13 we show the energy deposition as a function of the preceding off-time. The steps on the x axis represent the time resolution of the ASI data. A longer off-time does not imply a larger amount of energy deposited over the next on-time.

Finally, we test how the energy deposited changes during the on-times. Figure 14 shows the median of the on-times normalized in time and intensity. We separate the on-times into "long" duration (on-time >6 s, green line) and "short" duration (on-time ≤6 s, pink line). The latter captures the bulk of on-times (see Figure 10). This is done in an attempt to decrease the scattering due to double peaks and multipeaks, which likely are

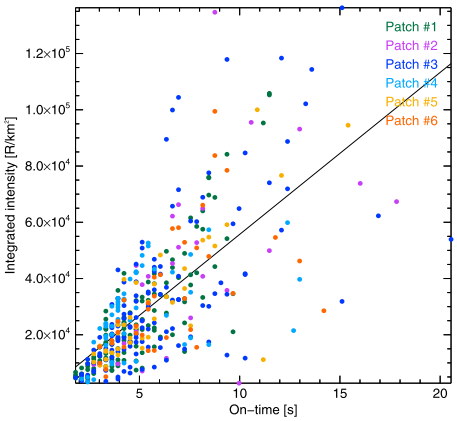

Figure 11. The intensity integrated over the on-time compared to the on-time. The different colors represent the different patches.

AGU Journal of Geophysical Research: Space Physics 10.1002/2016JA022921

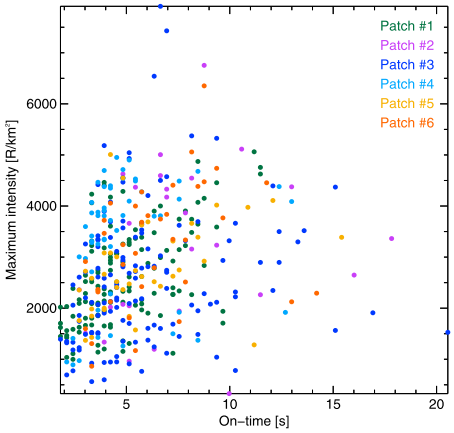

Figure 12. Maximum intensity during the on-time compared to the on-time. The different colors represent the different patches.

more frequent the longer the on-time is. However, also relatively short on-times have these characteristics (see, for example, second pulse at about 15:21 UT in Figure 7, bottom). In general, the energy deposition is highly irregular which results in considerable scatter for both short- and long-duration on-times. There is a tendency for short on-times (pink) to have a more well-defined peak, reaching an intensity level of about 0.95, compared to the long on-times (green) that stabilizes at an intensity level slightly less than 0.8 for roughly 35% of the on-time. The short-duration energy deposition (pink) is remarkably symmetric. The long-duration energy deposition (green) is symmetric below a normalized intensity level of about 0.55, but if we look at the entire on-time, the energy deposition has a quicker buildup than decay. The asymmetric distribution could be interpreted as indicative of a rapid release and slower decay in support of a loading-unloading process.

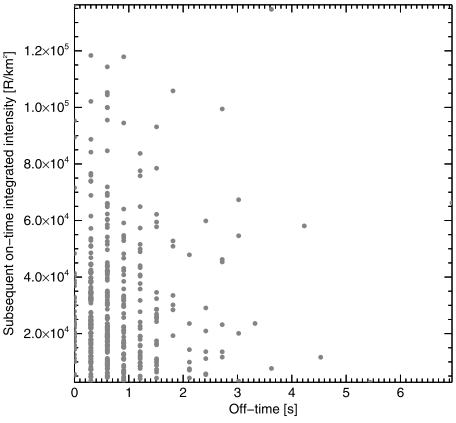

Figure 13. Off-time compared to the intensity integrated over the subsequent on-time.

AGU Journal of Geophysical Research: Space Physics 10.1002/2016JA022921

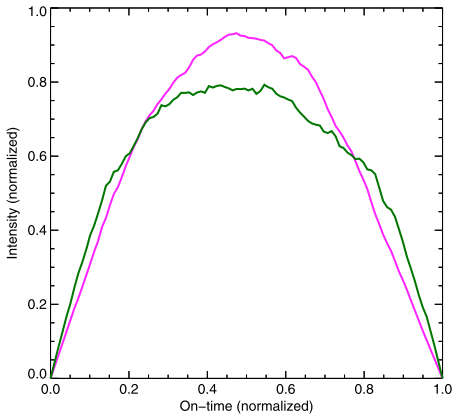

Figure 14. The median energy deposition of all pulses normalized in time and intensity. The on-time is separated into long on-times greater than 6 s (green) and short on-times less or equal to 6 s (pink).

6. Discussion

To interpret our results, we must first address the inherent limitations of the ASI data set and technique. The main limitations are as follows: (1) observations are limited to six patches, (2) 3.31 Hz time resolution, (3) 557.7 nm emissions, and (4) finding the exact area of the patches. The resulting characteristics and observational constraints of PA patches on the suggested mechanism will then be discussed. Finally, we discuss the majority of the most frequently mentioned theories of pulsating aurora that are listed in Table 2.

6.1. Inherent Limitations

The six patches analyzed are carefully selected adjacent patches. The amount of data available is large, but the technique chosen for this study is time consuming. The limited observations (1) of course result in limited statistics, and we cannot address how the characteristics depend on geomagnetic conditions, especially substorm phases, local time, latitude, or any other parameter that may vary from event to event. The pulsating auroras are observed under a wide variety of conditions [e.g., *Jones et al.*, 2013], meaning that this study may only address a small subset. Acknowledging this opens up another question as to the external or solar wind control of the patch evolution and behavior, a topic well beyond the scope of this paper. The limited observations could therefore be argued to be a distinct advantage since all occur during the same event and thus any variability cannot be due to dependencies such as geomagnetic activity, local time, and so on.

The 3.31 Hz time resolution (2) of the ASI data used is limited by the Nyquist frequency of 1.65 Hz. Therefore, we cannot distinguish rapid temporal behavior such as the ~3 Hz modulations often found to be superimposed on the slower variations and so-called flashes. Flashes are burst-like fluctuations where the on-time is shorter than 1 s, while the off-time can reach several minutes [*Tsuruda et al.*, 1981; *Yamamoto*, 1988]. Running the all-sky cameras at a higher cadence is possible, but the pulsating aurora that occurs with higher-frequency fluctuations, such as the 3 Hz modulations, occurs at small spatial scales on top of the large-scale pulsations. Therefore, to fully investigate the properties of the higher frequencies, a narrow field of view imager is more appropriate as was done in *Samara and Michell* [2010], where pulsations up to 10 to 15 Hz were reported. It is entirely possible that these higher-frequency pulsations are caused by completely different mechanisms, and therefore, it would make sense to investigate them independently.

The 557.7 nm emissions (3) are limited by a chemical effect. Compared to prompt emissions, the 557.7 nm emissions are found to have a mean lifetime of 0.3 to 0.59 s in pulsating aurora, the highest values of mean lifetime found in observations of sharp-edged patches *Scourfield et al.* [1971]. The important result is then a temporal smoothing over the same time scale, meaning that the 557.7 nm filter used could smooth out possible impulsive behavior. This study therefore focuses on the main on-off (bright/dim) modulation of the PA patches.

AGU Journal of Geophysical Research: Space Physics 10.1002/2016JA022921

Table 2. The Most Frequently Mentioned Theories of Pulsating Aurora, Their Auroral Observational Consequences, and How They Fit Within the Observational Constraints of Pulsating Auroral Patches

Theory	Summary	Auroral Observational Consequences	Can It Explain PA Patches?
Nonlinear relaxation oscillator [*Davidson*, 1979, 1986a, 1986b]	The control of wave growth is attributed to changes in the anisotropy as the loss cone is filled and emptied. The particles that are lost need to be replenished for the cycle to start again.	- Periods of 3 to 30 s - Rapid rise in energy deposition corresponding to wave growth times of ~0.1–1 s - The most probable period is near 10 s.	Yes
Nonlinear pulsation model [*Davidson and Chiu*, 1991]	Temporal variations may be driven by spatial variations in plasma density through a nonlinear pulsation model.	- Irregular pulsations - Trains of pulsations that begin between the pulses of a train that started several cycles earlier - Fourier spectrum of mainly broad features	Yes
Flow cyclotron maser [*Demekhov and Trakhtengerts*, 1994]	A continuous stream of energetic electrons enters a flux tube with enhanced cold plasma density that serves as a resonance cavity. Low-frequency waves start to scatter the high-energy electrons into the loss cone. The scattering moves toward higher wave frequencies and lower energy electrons and thus includes more particles. This continues until a maximum of the electrons participates and the waves are damped.	- On-time is determined by the nonlinear dynamics and is on the order of wave travel time between the ionospheres ~1–5 s. - Off-time is nearly equal to the time of energetic electron accumulation in the duct, suggesting a repetition period of ~5–30 s. - Slower buildup than decay of the energy deposition	No
Backward wave oscillator [*Trakhtengerts*, 1995, 1999]	Waves propagate opposite to the motion of interacting electrons resulting in step-like interactions and the generation of chorus bursts composited of chorus elements.	Rapid fluctuations superimposed on the on-time of quasiperiodic variations	Unknown
Flow cyclotron maser with ionospheric feedback [*Tagirov et al.*, 1999]	The feedback is due to the local increase in ionospheric electron density that reduces the waves and thus the scattering process at magnetic equator until it stops. This effect lags several seconds to the ionization by precipitating particles. As the electron density decreases due to recombination, it allows waves to begin to grow once again.	- Relaxation time is about twice the buildup time. - Whole cycle of the order 5–15 s - PA patch lifetime of 1–3 min	No
ULF waves [*Coroniti and Kennel*, 1970]	ULF waves act to modulate the velocity distribution of resonant electrons and thus the pitch angle scattering at magnetic equator.	- Relative periodic scattering dependent on diffusion rate and ULF wave frequency - Modulation should be superposed on an already enhanced precipitation background.	Unknown

AGU Journal of Geophysical Research: Space Physics 10.1002/2016JA022921

Table 2. (continued)

Theory	Summary	Auroral Observational Consequences	Can It Explain PA Patches?
Fermi-type acceleration [*Nakajima et al.*, 2012]	Field-aligned electrons are already generated by Fermi-type accelerations associated with earthward plasma flow at substorm onset. Pulsations of the field-aligned electrons are further suggested to be created by small pitch angle modulations by weak whistler mode waves, ECH waves, and/or magnetosonic waves, or alternatively Alfvén waves.		Unknown
Ionospheric ion-acoustic instability [*Pilipenko et al.*, 1999]	Ion-acoustic instability can arise when densities of local field-aligned currents in the topside ionosphere reach the threshold for excitation of high-frequency turbulence. Further, the ion-acoustic instability gives rise to quasi-oscillatory variations of parallel electric fields and consequently particle acceleration and precipitation.	Quasi-oscillatory particle precipitation	Unknown
Auroral acceleration region modulation by Alfvén waves [*Fedorov et al.*, 2004]	Magnetospheric Alfvén waves penetrating into the auroral acceleration region can produce oscillatory variations of the field-aligned potential drop in the auroral topside ionosphere	May cause oscillatory frequency dependence of electron acceleration modulations in the range around fractions of a hertz.	Unknown
Atmospheric pressure waves [*Luhmann*, 1979]	Pressure waves in the neutral atmosphere cause quasiperiodic fluctuations in the auroral intensity by changes in the altitude at which particles are lost to the atmosphere and thus the size of the loss cone.	– Quasiperiodic fluctuations in auroral intensity dependent on the frequency of the atmospheric density fluctuations and magnitude and direction of the local neutral wind – Can only explain PA periods longer than the bounce time	Unknown

AGU Journal of Geophysical Research: Space Physics 10.1002/2016JA022921

The main technique limitation is finding the exact area of the patches (4) using the contouring technique as outlined in Step 4. For each image we calculate the patch total intensity (units of Rayleigh) as well as the patch median intensity (units of Rayleigh per square kilometer). To limit the uncertainty in finding the exact area of the patches, we use the median intensity which is less affected by the contouring technique. It could also be discussed whether it is right to use the whole patch area compared to, for example, defining a core. The temporal variation we show is a smoothing over the scale size of the patch, which effectively smooth out any spatiotemporal variability within the patch and can make it difficult to put a threshold on what is considered sufficient rise and decay in intensity used to define the on-time and off-time of the patch. Then again, it is equally or more difficult to define, for example, a core area.

6.2. What Is the Temporal Variability of PA Patches?

We have defined an on-time and off-time of the patches and do not use the common term period because we find the temporal variation of the brightness of pulsating aurora to be highly variable and far from periodic or even quasiperiodic. Our technique has the advantage that it objectively determines the intensity variation using the patch area. It also provides a clear definition of the on-time and off-time and removes the unwanted variations that are due to the Earth's rotation and drift of the patches. In comparison, other published studies used simple north-south keogram or a sampling box around a central portion of the patch.

In the literature typical pulsating periods are referred to range from 2 to 20 s [*Royrvik and Davis*, 1977]. The results shown in Figure 10 show on-times in the range of 2 to 21 s, which is in good agreement with other published studies. We do, however, find more of the shorter than longer on-times. The average on-time (5.67 ± 0.14 s) and off-time (0.80 ± 0.04 s) combined form an approximate average period of 6.5 ± 0.2 s, which is shorter than the typical average period of 8 ± 2 s found by *Royrvik and Davis* [1977]. It should be mentioned here that our skewed PDFs indicate that the use of average is not appropriate. Rather, we should use typical (or mode), which may be more appropriate in describing the behavior. This means either that the pulsating auroral patches have a different characteristic compared to other kinds of pulsating aurora or that the use of the term period is simply not a characteristic for the pulsating aurora.

The large difference in on-times and off-times also suggests that the use of the terms on-time and off-time fits the fundamental characteristics of pulsating aurora better than the frequently used terms period, recurrence period, and on-off period. A similar conclusion was drawn by *Yamamoto* [1988] based on findings of mostly individual isolated pulses where the pulsation on-time therefore became the most essential quantity. He found that the standing and streaming forms combined have a median on-time of 3–4 s and a median off-time of 4.5–7 s for the *Kp* indices 3–4. The median of the 420 on-times shown in Figure 10 is 4.8 s, and the median off-time is 0.6 s (based on 426 off-times, not shown). The median on-time is thus slightly longer, while the median off-time is much shorter and the variance in the data set is larger for the on-times than the off-times, opposite to what was found by *Yamamoto* [1988]. He defined the on-time as the width of the pulse and off-time as the separation of individual pulsations, similar to what we do, but used a correlation to find the times. There are, however, factors that can explain the difference. The most important one is that the so-called type 1 pulsations are included in their statistics, while the type 3 pulsations might not be included. The type 1 is classified as a series of pulses having shorter on-times than off-times, type 2 as quasiperiodic fade-outs or decreases in luminosity from the on level having longer on-times than off-times, while the type 3 pulsations show neither full luminosity changes nor a clear distinction of on-times and off-times. When simply comparing the typical example in Figure 8 to the example Figures 1–3 and 5 in the paper by *Yamamoto* [1988] showing the different types of pulsations, the best fit is found to be either type 2 or type 3, consistent with a typically longer on-time than off-time. The different median on-times and off-times reported can therefore result from our observations of the type 2 and type 3 pulsations and not the type 1 pulsations. It should, however, be noted that the pulsating aurora analyzed in this study is relatively well-separated patches of either standing or streaming mode, while *Yamamoto* [1988] also included the moving mode, which is far more difficult to objectively identify. This example also illustrates how complicated it is to find the temporal characteristics, and not to mention a classification, of the pulsating aurora.

Although the spread is wide, the distribution is clearly not scaleless and thus indicates that there is a preferred (typical) on-time of ~3–5 s. Most later studies such as *Nishiyama et al.* [2014] and *Sato et al.* [2015] avoided the difficulties of defining the on-time and off-times by using the recurrence period and on-off period, respectively, as temporal characteristics of the main pulsation. *Sato et al.* [2015] found recurrent periods of ~9–12 s estimated from auroral intensities along a north-south keogram, but as they clearly point out, they investigate

AGU Journal of Geophysical Research: Space Physics 10.1002/2016JA022921

the characteristics of omega band pulsating aurora, which is significantly different in their shapes and structure compared to PA patches and possibly have a different generation and modulation mechanism. *Nishiyama et al.* [2014] studied the dual-scale temporal characteristics of PAs, meaning the relationship between the on-off periods and rapid modulations. The on-off periods, which were estimated with a fast Fourier transform analysis with a 60 s data window, ranged from 1.6 to 15 s. PA with on-off periods shorter than 10 s accounted for 72% of the total events in their statistical analysis, and as can be seen from their Figure 4, they find most on-off periods from 4.0 to 8.0 s, which is consistent with our result and thus supports the suggestion of a preferred (typical) on-time of ~3–5 s. Both the preferred on-time and short off-time are characteristics that should be explained by the suggested mechanism(s) of pulsating auroral patches.

6.3. PA Patches Energy Deposition in Relation to Their Temporal Characteristics

This is the first study attempting to estimate the energy deposition in association with the on-time and off-time of PA patches. We have done an analysis of the energy deposition, where the auroral intensity is used as an indicator of the actual energy deposition by the energy flux of downward electrons. Although we may argue that the emissions are related to the particle precipitation, they do not include Poynting flux. However, a comparison between precipitating energy flux and the relative intensity of the auroral luminosity extracted from a corresponding all-sky image was found to agree well [*Stenbaek-Nielsen et al.*, 1998]. The analysis of estimating the energy deposition from auroral emissions is out of scope of this study. A few simple hypotheses relevant for the suggested mechanisms and drivers of the pulsating aurora are tested. We find the following: (1) A weak correlation between the length of the on-time and the energy deposition. This is as expected, but there is significant scatter, especially for longer on-times. (2) No correlation between the on-time and maximum intensity. (3) PA patches have no preferred maximum energy deposition. (4) The off-time does not have a relation to the amount of energy that is deposited over the next on-time. (5) Evidence of a slightly quicker build up than decay of the energy deposition.

According to our observations, the PA patches have no preferred maximum energy deposition. However, it has been reported that the intensities of the PA patches have relatively constant maximum amplitude. The difference might be due to the offset subtracted, which has a slower variation. For example, *Yamamoto* [1988] reported that the amplitude was fairly constant throughout the train of pulsations and noted that the maximum intensity showed much slower changes than the period of pulsation, indicating that the background conditions, which may relate to the causal instability, vary little during several cycles of pulsations. The train of pulsations in Figure 8 shows evidence of the same, where the on-off pulsations seem to be superposed on a slower variation in the background intensity. We have taken this into account and subtracted the offset before investigating the energy deposition (see Figure 7). A further investigation of the background emissions are out of scope of this paper, but the observation can be of interest in the ongoing research on the role of the background plasma as driver of the chorus emissions. For example, *Li et al.* [2011a] did find a one-to-one variation in the ULF and chorus modulations with periods ranging from tens of seconds to a few minutes, and *Jaynes et al.* [2015] link chorus modulations with ~45 s to 1 min periods to ULF waves having periods closer to 2 min. Interestingly, the train of pulsations of patch #2 in Figures 7 and 8 indicates that the offset has a rise and decay over about one to four on-times. In addition, purely visually, it looks like there also exists a slower background variability of about 70 s (15:21:00–15:22:20 UT), 30 s (15:22:20–15:22:50 UT), and 90 s (15:22:50–15:24:20 UT). Also, the train of pulsations of example patch #4 in Figure 9 gives an indication of this dual-temporal characteristic of the background emission. In contrast to the results by *Yamamoto* [1988], we find that the maximum intensity varies through a train of pulsations, revealing that the PA patches do not have a preferred maximum intensity and that there probably are complex varying precipitation fluxes behind the on-off pulsations. The different results likely arise because we subtract the offset to study the characteristics of the on-off pulsations, while the maximum amplitude by *Yamamoto* [1988] included the slower varying background emissions.

Our results in Figure 12 show that there is virtually no correlation between the on-time and maximum intensity. One might simplistically expect a relationship if the total energy deposited by the patch was approximately constant from pulse to pulse. It has been suggested that the on-off pulsations are closely correlated to the amplitudes of lower band chorus waves [*Nishimura et al.*, 2010, 2011] or electron cyclotron harmonics [*Liang et al.*, 2010] at the magnetic equator. The amplitude of the waves at magnetic equator tells us how effective the pitch angle scattering rate is. This implies that the available energy simply would be deposited over a shorter on-time (negatively correlated), which is not the case. Interestingly, this seems to disagree with a recent study by *Samara and Michell* [2010]. They found that the frequency of the pulsations correlates to

AGU Journal of Geophysical Research: Space Physics 10.1002/2016JA022921

the intensity of the aurora, with the brighter aurora being associated with the higher frequencies. The disagreement between the observations is likely because the higher frequencies correlate to the intensity and not the on-time. This is confirmed by a later observation of the auroral intensity being correlated to the ~3 Hz frequencies and not the on-off periods [*Nishiyama et al.*, 2014]. The observations combined support the proposed explanation that the higher frequencies superposed on the on-time intensity are related to the chorus elements and that closer spacing between the chorus elements corresponds to higher-energy resonant electrons [*Nunn et al.*, 2009; *Samara and Michell*, 2010]. Our finding suggests that the total energy deposited by the patch varies from pulse to pulse. The variable energy deposition can possibly be due to the on-off pulse being a composition of higher-frequency pulsations, where the composition for some reason varies from pulse to pulse. We find no preferred relationship between maximum intensity and the on-time in support of the auroral intensity being correlated to the superimposed higher frequencies and not the frequencies in the on-off regime.

Figure 14 indicates a slightly quicker buildup than decay of the energy deposition for the longer on-times (>6 s). This is the opposite of the results by *Samara and Michell* [2010] that also found the intensity profile of the pulsating structures to be asymmetric, but with the intensity increasing at a slower rate than it decreases. They suggest that this could be consistent with the backward wave oscillator chorus generation mechanism [*Trakhtengerts*, 1995, 1999], where the chorus bursts increase in frequency until they reach a cutoff and no longer resonate with the plasma sheet electrons of the correct energy range (few keV to tens of keV). They find it to be a common feature in the many different pulsating auroral structures examined but most pronounced during a time period where our observations are not entirely comparable. The main differences being the magnetic local time (~0400 MLT versus ~0030 MLT), the time from a substorm onset (1.5 versus 0.5 h), and their observation of several distinct pulsating structures and pulsations forming at the southern edge of a brighter auroral arc, but not well-separated pulsating patches. It is, however, unclear how these differences would explain or influence the generation mechanisms. Further, the above general picture of chorus generation can be verified utilizing pulsating aurora, especially the pulsating patches as manifested in the flow cyclotron maser theory [*Trakhtengerts*, 1999]. Hence, we find it puzzling that we do not observe evidence of the bursts of several chorus elements which are suggested to appear in the final stage of a so-called optical flash. The indication of the energy deposition having a slightly quicker buildup than decay for the longer on-times (>6 s) and a symmetric buildup and decay for the shorter on-times (≤6 s) might therefore not support the observational constraints set by the flow cyclotron maser theory, which is suggested to create the pulsating auroral patches.

The slightly quicker buildup than decay of the longer on-times (> 6 s, green line) in Figure 14 agrees with the observations by *Jaynes et al.* [2013]. They often found a sawtooth component in their observation of the electron precipitation close to the magnetic equator. The same feature was also evident in the luminosity of the pulsating auroral patches that correlated to the particle measurements. Their observations were interpreted as a possible loading and dumping cycle for the particle populations that fit well within the framework of the nonlinear relaxation oscillator theory. They sketch a scenario where the diffusion becomes less and less effective after the initial filling and emptying of the loss cone, possibly multiple times, as the electrons at adjacent pitch angles continue to diffuse into the loss cone during multiple bounces through the near-equatorial interaction region. The duration of the sawtooth with a rapid rise of 0–4 s and more gradual decrease of about 20 s does not fit to the on-times that we detect (6–21 s where most are less than 10 s and only one above 20 s), and we do not see a clear sawtooth in Figure 14. However, the indications of a slightly quicker buildup than decay of the energy deposition for the longer on-times (>6 s) can still be indicative of a rapid release and slower decay in support of the nonlinear relaxation oscillator theory.

When comparing auroral emissions to the suggested mechanisms and drivers of PA, there are a few effects we should keep in mind. As already mentioned, we observe the 557.7 nm emissions, which introduce a time lag (<0.6 s) and more importantly a smoothing over the same time scale, and we perform a quantitative analysis using the auroral intensity as indicative of the energy deposition. Additionally, there is the effect from time dispersion. In a beam of energetic electron precipitation the highest-energy electrons reach the atmosphere first and will at ionospheric altitudes result in an energy dispersion. This has been used to trace the source region of the pulsations assuming that the pulsations are imposed at one point. A simple exercise using the experimental measurements of bounce times above Poker Flat during moderate disturbed times [*Nemzek et al.*, 1992] shows that the lag of 10 keV to 30 keV electrons traveling from the magnetic equator could be in the order of ~0.4 s. In situ measurements by sounding rockets detected pulsating precipitation

AGU Journal of Geophysical Research: Space Physics 10.1002/2016JA022921

of electrons with energies from a few keV to tens of keV [*Bryant et al.*, 1975; *Sandahl et al.*, 1980; *Yau et al.*, 1981]. *Bryant et al.* [1975] observed pulsations in energies from 3 keV and up, the most pronounced pulsations >9 keV, while *Sandahl et al.* [1980] found clear pulsations in electron flux from 5 to 40 keV, the most pronounced around 20 keV. We also calculated the length of a magnetic field line from Poker Flat to magnetic equator using the Tsyganenko 2001 (T01) field model [*Tsyganenko*, 2002a, 2002b] and found that the electron precipitation times were comparable to the results by *Nemzek et al.* [1992]. The assumption here is of course that no field-aligned potential drops are located between the plasma sheet and the observed ionospheric emissions. The travel times we calculated were 1.5 s for 3 keV, 0.9 s for 10 keV, 0.5 s for 30 keV, 0.4 s for 50 keV, and 0.3 s for 100 keV precipitating electrons traveling 7.8 R_E. This means that the time lag between the 3 keV and the 100 keV pulsation could reach a considerable 1.2 s. However, the most probable time lags are 0.6 s or less if we assume, according to the in situ measurements, that the pulsations mostly occur above 10 keV. The dispersion effect is further complicated if we account for details of the suggested pitch angle scattering mechanism, for which the wave packet originates at the magnetic equator and propagates toward higher latitudes, resonating with electrons of increasing energy traveling the opposite way [*Miyoshi et al.*, 2010]. Even though the resonance of higher-energy electrons occurs after that of lower energy electrons and the higher-energy electrons travel a longer path, *Miyoshi et al.* [2010] found that the scattered electrons at higher energies overtake the electrons at lower energies before reaching the atmosphere. Taking into account this effect therefore acts to decrease the time dispersion. The effect of dispersion has also been used to explain features that we see in optical aurora. For example, *Samara and Michell* [2010] proposed that an alternative explanation to the common feature they observed in pulsating patches could be the result of higher-energy electrons arriving first followed by a greater flux of lower energy electrons, where the steep decrease in luminosity corresponds to the emptying of the loss cone. *Nishiyama et al.* [2014] suggested that the dispersion effect can explain why their ground-based data do not show any strong modulation with frequency higher than 3 Hz. The explanation being that the time difference between high-energy and low-energy electrons can easily fill the time gap of precipitating electron flux due to the quiet period between chorus elements. They further used the results of *Saito et al.* [2012] to explain that this effect seems to be larger on modulations generated by chorus elements with a repetition rate of 10 Hz compared to 3 Hz. *Saito et al.* [2012], however, explain their simulation results differently. Count rates of precipitated 1 MeV electrons detected at 100 km altitude show a pulse structure for 300 ms chorus element repetition, which is not seen for a 100 ms repetition. They explain that this is due to the precipitation of one chorus element overlapping the next for a time gap as short as 100 ms. Hence, it is not a time dispersion effect. In any case, it is clear that it is not straightforward to deduce the exact effect of dispersion in pulsating aurora. However, because the most probable time lag due to time dispersion is 0.6 s or less, and this is possibly further decreased by the effects of the pitch angle scattering mechanism, it is likely that the observed characteristics in the energy deposition are due to the generation mechanism and not a dispersion effect.

6.4. Observational Constraints on the Suggested Mechanisms

The auroral observational consequences of the most frequently mentioned theories of PA and how they fit within the observational constraints of PA patches are listed in Table 2. In the recent years, there has been an increase in the observations at the magnetic equator resulting in many studies relating different local plasma parameters (chorus waves, electron cyclotron harmonic waves, plasma densities, and ULF waves) and linking these to characteristics of PA. Below we will further discuss observational constraints set by the PA characteristics on the proposed theories and studies.

A significant result from our analysis is the highly variable on-time and the short off-times. This begs the fundamental question: What controls the variable on-time and off-time? In section 6.3 we found that the frequently cited theoretical candidates explaining the time-varying pitch angle scattering did not appear to provide likely explanations, although our findings fit better within the framework of the nonlinear relaxation oscillator, compared to the flow cyclotron maser. A similar conclusion can be drawn from a simple comparison to the expected on-time and off-time of the models. The nonlinear relaxation oscillator could give pulsation periods of order 3 to 30 s mainly determined by the strong diffusion time, the bounce period, or the loss cone filling time; most calculations yield values closest to the bounce period [*Davidson*, 1990]. If the latter is the case, it could possibly explain the preferred (typical) on-time of ~ 3–5 s, which according to our event-specific calculations are close to 3.6 s for 10 keV electrons, 2.4 s for 20 keV electrons, and 1.2 s for 100 keV electrons. Interestingly, *Davidson and Chiu* [1991] later described a system that even for a purely sinusoidal driver could result in extremely complex electron precipitation pulsations. The measurable consequences could be trains

AGU Journal of Geophysical Research: Space Physics 10.1002/2016JA022921

of pulsations that begin between the pulses of a train that started several cycles earlier and a Fourier spectrum of mainly broad features rather than narrow peaks associated with periodic behavior. Both the periods and the variability of the pulsations that we observe could fit within this framework. The flow cyclotron maser explicitly includes the effect of the entry of new energetic electrons into a flux tube with enhanced cold plasma density which serves as a resonance cavity and deals with details of the wave-particle interactions which makes the theory easier to compare with observations [*Nemzek et al.*, 1995]. The on-time is determined by the nonlinear dynamics and is on the order of wave travel time between the ionospheres ~1–5 s, whereas the off-time is nearly equal to the time of energetic electron accumulation in the duct, suggesting a repetition period of ~5–30 s [*Demekhov and Trakhtengerts*, 1994]. These relatively short on-times do not fit our observations. In a later study *Tagirov et al.* [1999] explain observations of pulsating patches based on the flow cyclotron maser theory and an ionospheric feedback. In this process the relaxation time is about twice the buildup time and the whole cycle of the order 5–15 s. Our observations show weak evidence of a quicker buildup than decay but have a wider temporal range. The observations described in section 6.3 show an agreement with the nonlinear relaxation oscillator, while here the observation could be found in favor of a mechanism based on the flow cyclotron maser theory. Based on the expected temporal characteristics, our observations fit better within the framework of the nonlinear relaxation oscillator. However, this is mainly because the model predicts a large temporal variability, which also could make it fit to almost any observation.

The temporal characteristics of our observations can be compared to the chorus bursts which are found to correlate with plasma density depletions, but the agreement is not convincing. An additional factor suggested to play a dominant role in determining the on-off duration is temporal variations in the plasma density at the magnetic equator. Observations at geosynchronous orbit have revealed that quasiperiodic chorus waves can arise from changes in the plasma density probably attributed to changes in cold electron (less than a few eV) fluxes [*Li et al.*, 2011b, 2012]. A visual comparison of the temporal characteristics of the chorus magnetic wave amplitude is in good correlation with the density depletions by *Li et al.* [2011b] which show ~10 s on-times and short off-times in one case but ~15–30 s on-times and even longer off-times in the other case. Hence, the temporal characteristics of the wave bursts correlating with plasma density depletions can compare to our observations, but the agreement is not convincing.

Further, we find that the observation of ULF waves driving the pulsating aurora does not fit well within the observational constraints of pulsating auroral patches. Observations of low-energy ion precipitation by low-Earth orbit satellites have further suggested that the changes in the cold plasma in relation to pulsating auroral patches might owe its origin to the ion outflows from the ionosphere [*Liang et al.*, 2015], while other studies have related the growth of quasiperiodic chorus waves directly to the dynamics of ultralow-frequency (ULF) waves [*Li et al.*, 2011a; *Jaynes et al.*, 2015]. *Jaynes et al.* [2015] suggest that substorm-driven Pc4–Pc5 magnetospheric ULF pulsations (field line resonance as a result of a substorm injection) modulate chorus waves and thus are driver of pulsating particle precipitation. They link chorus modulations with ~45 s to 1 min periods to ULF waves having periods closer to 2 min, thus occurring with twice the periodicity as the chorus. On the other hand, *Li et al.* [2011a] found a one-to-one variation in the ULF and chorus modulations, but also, they focused on the modulation of whistler mode waves by long-period compressional pulsations in the Pc4–Pc5 range and did not investigate individual chorus elements, but rather a group of chorus elements showing intensification over a time scale of tens of seconds to a few minutes. Thus, these time scales are too long to explain the on-times and off-times of pulsating auroral patches.

Our findings provide some strict observational constraints that any of the published theories must be able to explain. As such the wave-particle scattering mechanism where the off-time is the time it takes to reach the resonance threshold appears to be the leading candidate of PA patches. In Figure 13 we found that the off-time does not have a relation to the amount of energy that is deposited over the next on-time. This supports the wave-particle scattering mechanisms for which the scattered energy is not controlled by a preceding period of loading and where the off-time rather is the time it takes to reach the resonance threshold. For the flow cyclotron maser this is nearly equal to the time it takes for energetic electrons to accumulate in the flux tube and result in anisotropic velocity distribution. However, satellite observations of energetic electrons with large pitch angles are found to not change drastically between on and off stages [*Jaynes et al.*, 2013]. Further, *Nishiyama et al.* [2014] suggested that the on-off period of the pulsating aurora having ~3 Hz modulations superimposed was likely due to ULF compressional waves creating temporal variations in the cold plasma density affecting the conditions for nonlinear wave growth and consequently switch strong pitch angle scattering on and off repeatedly. The off-time can then be the time it takes for the cold plasma to lower

AGU Journal of Geophysical Research: Space Physics 10.1002/2016JA022921

the resonance threshold. If the suggested ULF waves act as a quasiperiodic driver, we would expect the temporal range of the off-time to be relatively narrow, which is exactly what we observe. However, the ULF waves described in the above paragraph of course have too long periods to explain the 0.6 s median off-time of PA patches. In summary, the characteristics of the energy deposition indicates that the off-time is the time it takes to reach the resonance threshold, and the relative narrow temporal range of the off-time can fit with the idea that the latter is controlled by a driver which is relatively periodic. We realize that any of the suggested drivers can account for a lack of agreement with our results by claiming changes in the plasma properties (e.g., density) in the generation region. We, however, argue that such support is a patchy unsatisfactory argument.

Alternative drivers to the traditional idea of a pitch angle scattering by chorus or electron cyclotron harmonic waves likely do not fit within the observational constraint of pulsating auroral patches. The most recent suggestions are (1) Fermi-type accelerations accompanying earthward plasma flow [*Nakajima et al.*, 2012] and (2) near-Earth time-varying field-aligned potential [*Sato et al.*, 2002, 2004]. *Nakajima et al.* [2012] observed pulsating aurora which traces to the midtail equatorial plane region at a much further distance than most other studies on pulsating aurora. They find that the local plasma conditions are not favorable to the generation of whistler and ECH waves through the electron temperature anisotropy and suggest that field-aligned electrons are already generated by Fermi-type accelerations associated with earthward plasma flow at substorm onset. However, the pulsations of the field-aligned electrons are further suggested to be created by small pitch angle modulations by weak whistler mode waves, ECH waves, and/or magnetosonic waves, or alternatively Alfvén waves. *Sato et al.* [2002, 2004] observed nonconjugate east-west aligned arc type of pulsating aurora and suggested that they are driven by near-Earth time-varying field-aligned electric fields. These studies do not go into detail on the proposed driver; however, there are other studies that go into detail on how quasi-oscillatory variation of parallel electric fields can arise. *Pilipenko et al.* [1999] discuss how ion-acoustic instabilities can arise when densities of local field-aligned currents in the topside ionosphere reach the threshold for excitation of high-frequency turbulence. These are related to nightside substorm onset. Further, the ion-acoustic instability gives rise to quasi-oscillatory variations of parallel electric fields and consequently particle acceleration and precipitation. Alternatively, *Fedorov et al.* [2004] discuss how magnetospheric Alfvén waves penetrating into the auroral acceleration region can produce oscillatory variations of the field-aligned potential drop in the auroral topside ionosphere that may cause oscillatory frequency dependence of electron acceleration modulations in the range around fractions of a hertz. In conclusion, the recently suggested alternative drivers are not sufficiently mature to provide any observational predictions and thus we cannot discuss them in a quantitative manner. Further, they are likely to result in a quasi-oscillatory particle precipitation which do not fit well within the observational constraint of pulsating auroral patches.

7. Summary and Conclusions

We presented a careful study of PA patches using green line all-sky images obtained at 3.3 Hz. We identified six individual pulsating patches and extracted them using a contouring technique. This allowed us to derive objective quantitative parameters for each of the patches. These included patch duration (on-time and off-time), peak intensity, and integrated intensity. Further, we found how the temporal characteristics related to the characteristics of the energy deposition. Altogether, we provide a series of observational constraints on the suggested mechanisms.

The PA patches display a striking temporal variability. The distribution of on-times shows a large spread (2–21 s) but is clearly not scaleless indicating that there is a preferred (typical) on-time of ~3–5 s. The distribution of the off-time is more confined (0–7 s) having a median of 0.6 s. This clearly states that the frequently used period or quasiperiod cannot sufficiently describe the temporal characteristics. On-time and off-time serve as a more accurate description of the observational constraint. We argue that the naming of pulsating aurora should be changed to fluctuating aurora since it is not periodic but rather erratic.

The temporal constraints do not appear to support the variations of the flow cyclotron maser theory but fit better within the framework of the nonlinear relaxation oscillator, largely because it predicts a temporal variability.

The energy deposition is found to be highly variable from pulse to pulse. The constraints set by the temporal characteristics in relation to the energy deposition seem to indicate the following: (1) The pulse on-time is a composition of higher-frequency pulsations, where the composition for some reason varies from pulse to

AGU Journal of Geophysical Research: Space Physics 10.1002/2016JA022921

pulse. (2) The off-time is not related to a loading but is related to the time it takes to lower the resonance threshold to start a new pulsation. (3) The slightly quicker buildup than decay of the energy deposition is opposite to the observational consequences that would be expected from the flow cyclotron maser (and backward wave oscillator), which is suggested to create the PA patches in particular.

It is clear that the suggested mechanisms and drivers of PA do not explain the observational constraints set by the PA patches in a satisfactory manner. Further, observations of PA patches and other types of PA with ground-based instruments are required to obtain a large set of observational constraints that any suggested driver or mechanism of PA must explain.

Acknowledgments
This study was supported by the Research Council of Norway under contract 223252/F50. The authors acknowledge the use of SuperMAG indices and all-sky imager data from the Multi-spectral Observatory of Sensitive EMCCDs (MOOSE). The SuperMAG indices were obtained freely from supermag.uib.no. MOOSE all-sky imager data were obtained from R. Michell and M. Samara. The data analyzed in this study are available upon request from the authors.

References

Bryant, D., M. Smith, and G. Courtier (1975), Distant modulation of electron intensity during the expansion phase of an auroral substorm, *Planet. Space Sci., 23*(5), 867–878, doi:10.1016/0032-0633(75)90022-7.
Coroniti, F. V., and C. F. Kennel (1970), Auroral micropulsation instability, *J. Geophys. Res., 75*(10), 1863–1878, doi:10.1029/JA075i010p01863.
Davidson, G. (1979), Self-modulated VLF wave-electron interactions in the magnetosphere: A cause of auroral pulsations, *J. Geophys. Res., 84*(A11), 6517–6523, doi:10.1029/JA084iA11p06517.
Davidson, G. (1990), Pitch-angle diffusion and the origin of temporal and spatial structures in morningside aurorae, *Space Sci. Rev., 53*(1–2), 45–82, doi:10.1007/BF00217428.
Davidson, G. T. (1986a), Pitch angle diffusion in morningside aurorae: 2. The formation of repetitive auroral pulsations, *J. Geophys. Res., 91*(A4), 4429–4436, doi:10.1029/JA091iA04p04429.
Davidson, G. T. (1986b), Pitch angle diffusion in morningside aurorae: 1. The role of the loss cone in the formation of impulsive bursts of precipitation, *J. Geophys. Res., 91*, 4413–4427.
Davidson, G. T., and Y. T. Chiu (1991), An unusual nonlinear system in the magnetosphere: A possible driver for auroral pulsations, *J. Geophys. Res., 96*(A11), 19,353–19,362, doi:10.1029/91JA01826.
Demekhov, A. G., and V. Y. Trakhtengerts (1994), A mechanism of formation of pulsating aurorae, *J. Geophys. Res., 99*(A4), 5831–5841, doi:10.1029/93JA01804.
Duncan, C. N., F. Creutzberg, R. L. Gattinger, F. R. Harris, and A. V. Jones (1981), Latitudinal and temporal characteristics of pulsating auroras, *Can. J. Phys., 59*(8), 1063–1069, doi:10.1139/p81-140.
Fedorov, E. N., V. A. Pilipenko, M. J. Engebretson, and T. J. Rosenberg (2004), Alfven wave modulation of the auroral acceleration region, *Earth Planets Space, 56*, 649–661.
Gjerloev, J. W. (2012), The SuperMAG data processing technique, *J. Geophys. Res., 117*(A9), A09213, doi:10.1029/2012JA017683.
Jaynes, A. N., M. R. Lessard, J. V. Rodriguez, E. Donovan, T. M. Loto'aniu, and K. Rychert (2013), Pulsating auroral electron flux modulations in the equatorial magnetosphere, *J. Geophys. Res. Space Physics, 118*(8), 4884–4894, doi:10.1002/jgra.50434.
Jaynes, A. N., et al. (2015), Correlated Pc4-5 ULF waves, whistler-mode chorus, and pulsating aurora observed by the Van Allen Probes and ground-based systems, *J. Geophys. Res. Space Physics, 120*(10), 8749–8761, doi:10.1002/2015JA021380.
Johnstone, A. D. (1971), Correlation between electron and proton fluxes in postbreakup aurora, *J. Geophys. Res., 76*(22), 5259–5267, doi:10.1029/JA076i022p05259.
Johnstone, A. D. (1978), Pulsating aurora, *Nature, 274*, 119–126.
Jones, S. L., M. R. Lessard, K. Rychert, E. Spanswick, E. Donovan, and A. N. Jaynes (2013), Persistent, widespread pulsating aurora: A case study, *J. Geophys. Res. Space Physics, 118*(6), 2998–3006, doi:10.1002/jgra.50301.
Li, W., R. M. Thorne, J. Bortnik, Y. Nishimura, and V. Angelopoulos (2011a), Modulation of whistler mode chorus waves: 1. Role of compressional Pc45 pulsations, *J. Geophys. Res., 116*(A6), A06205, doi:10.1029/2010JA016312.
Li, W., J. Bortnik, R. M. Thorne, Y. Nishimura, V. Angelopoulos, and L. Chen (2011b), Modulation of whistler mode chorus waves: 2. Role of density variations, *J. Geophys. Res., 116*(A6), A06206, doi:10.1029/2010JA016313.
Li, W., J. Bortnik, Y. Nishimura, R. M. Thorne, and V. Angelopoulos (2012), The origin of pulsating aurora: Modulated whistler mode chorus waves, in *Auroral Phenomenology and Magnetospheric Processes: Earth and Other Planets*, edited by A. Keiling et al., pp. 379–388, AGU, Washington, D. C.
Liang, J., V. Uritsky, E. Donovan, B. Ni, E. Spanswick, T. Trondsen, J. Bonnell, A. Roux, U. Auster, and D. Larson (2010), THEMIS observations of electron cyclotron harmonic emissions, ULF waves, and pulsating auroras, *J. Geophys. Res., 115*(A10), A10235, doi:10.1029/2009JA015148.
Liang, J., E. Donovan, Y. Nishimura, B. Yang, E. Spanswick, K. Asamura, T. Sakanoi, D. Evans, and R. Redmon (2015), Low-energy ion precipitation structures associated with pulsating auroral patches, *J. Geophys. Res. Space Physics, 120*(7), 5408–5431, doi:10.1002/2015JA021094.
Luhmann, J. (1979), Auroral pulsations from atmospheric waves, *J. Geophys. Res., 84*(9), 4224–4228.
Miyoshi, Y., Y. Katoh, T. Nishiyama, T. Sakanoi, K. Asamura, and M. Hirahara (2010), Time of flight analysis of pulsating aurora electrons, considering wave-particle interactions with propagating whistler mode waves, *J. Geophys. Res., 115*(A10), A10312, doi:10.1029/2009JA015127.
Nakajima, A., et al. (2012), Electron and wave characteristics observed by the THEMIS satellites near the magnetic equator during a pulsating aurora, *J. Geophys. Res., 117*(A3), A03219, doi:10.1029/2011JA017066.
Nemzek, R. J., P. R. Malcolm, and J. R. Winckler (1992), Comparison of Echo 7 field line length measurements to magnetospheric model predictions, *J. Geophys. Res., 97*(A2), 1279–1287, doi:10.1029/91JA02658.
Nemzek, R. J., R. Nakamura, D. N. Baker, R. D. Belian, D. J. McComas, M. F. Thomsen, and T. Yamamoto (1995), The relationship between pulsating auroras observed from the ground and energetic electrons and plasma density measured at geosynchronous orbit, *J. Geophys. Res., 100*(A12), 23,935–23,944, doi:10.1029/95JA01756.
Newell, P. T., and J. W. Gjerloev (2011a), Evaluation of SuperMAG auroral electrojet indices as indicators of substorms and auroral power, *J. Geophys. Res., 116*(A12), 1–12, doi:10.1029/2011JA016779.
Newell, P. T., and J. W. Gjerloev (2011b), Substorm and magnetosphere characteristic scales inferred from the SuperMAG auroral electrojet indices, *J. Geophys. Res., 116*(A12), 1–15, doi:10.1029/2011JA016936.
Nishimura, Y., et al. (2010), Identifying the driver of pulsating aurora, *Science, 330*(6000), 81–84, doi:10.1126/science.1193186.

AGU Journal of Geophysical Research: Space Physics 10.1002/2016JA022921

Nishimura, Y., et al. (2011), Multievent study of the correlation between pulsating aurora and whistler mode chorus emissions, *J. Geophys. Res.*, *116*(A11), A11221, doi:10.1029/2011JA016876.
Nishiyama, T., T. Sakanoi, Y. Miyoshi, D. L. Hampton, Y. Katoh, R. Kataoka, and S. Okano (2014), Multiscale temporal variations of pulsating auroras: On-off pulsation and a few Hz modulation, *J. Geophys. Res. Space Physics*, *119*(5), 3514–3527, doi:10.1002/2014JA019818.
Nunn, D., O. Santolik, M. Rycroft, and V. Trakhtengerts (2009), On the numerical modelling of VLF chorus dynamical spectra, *Ann. Geophys.*, *27*(6), 2341–2359, doi:10.5194/angeo-27-2341-2009.
Pilipenko, V. A., S. L. Shalimov, E. N. Fedorov, M. J. Engebretson, and W. J. Hughes (1999), Coupling between field-aligned current impulses and Pi1 noise bursts, *J. Geophys. Res.*, *104*(A8), 17,419–17,430, doi:10.1029/1999JA900190.
Royrvik, O., and T. N. Davis (1977), Pulsating aurora: Local and global morphology, *J. Geophys. Res.*, *82*(29), 4720–4740.
Saito, S., Y. Miyoshi, and K. Seki (2012), Relativistic electron microbursts associated with whistler chorus rising tone elements: GEMSIS-RBW simulations, *J. Geophys. Res.*, *117*(A10), A10206, doi:10.1029/2012JA018020.
Samara, M., and R. G. Michell (2010), Ground-based observations of diffuse auroral frequencies in the context of whistler mode chorus, *J. Geophys. Res.*, *115*, A00F18, doi:10.1029/2009JA014852.
Sandahl, I., L. Eliasson, and R. Lundin (1980), Rocket observations of precipitating electrons over a pulsating aurora, *Geophys. Res. Lett.*, *7*(5), 309–312, doi:10.1029/GL007i005p00309.
Sato, N., D. M. Wright, Y. Ebihara, M. Sato, Y. Murata, H. Doi, T. Saemundsson, S. E. Milan, M. Lester, and C. W. Carlson (2002), Direct comparison of pulsating aurora observed simultaneously by the FAST satellite and from the ground at Syowa, *Geophys. Res. Lett.*, *29*(21), 2041, doi:10.1029/2002GL015615.
Sato, N., D. M. Wright, C. W. Carlson, Y. Ebihara, M. Sato, T. Saemundsson, S. E. Milan, and M. Lester (2004), Generation region of pulsating aurora obtained simultaneously by the FAST satellite and a Syowa-Iceland conjugate pair of observatories, *J. Geophys. Res.*, *109*(A10), A10201, doi:10.1029/2004JA010419.
Sato, N., A. Kadokura, Y. Tanaka, T. Nishiyama, T. Hori, and A. S. Yukimatu (2015), Omega band pulsating auroras observed onboard THEMIS spacecraft and on the ground, *J. Geophys. Res. Space Physics*, *120*(7), 5524–5544, doi:10.1002/2015JA021382.
Scourfield, M. W. J., N. R. Parsons, L. P. Dennis, and W. F. Innes (1971), Effective lifetime of O(1 S) in pulsating aurora, *J. Geophys. Res.*, *76*(16), 3692–3699, doi:10.1029/JA076i016p03692.
Stenbaek-Nielsen, H. C., T. J. Hallinan, D. L. Osborne, J. Kimball, C. Chaston, J. McFadden, G. Delory, M. Temerin, and C. W. Carlson (1998), Aircraft observations conjugate to FAST: Auroral arc thicknesses, *Geophys. Res. Lett.*, *25*(12), 2073–2076, doi:10.1029/98GL01058.
Tagirov, V. R., V. S. Ismagilov, E. E. Titova, V. A. Arinin, A. M. Perlikov, J. Manninen, T. Turunen, and K. Kaila (1999), Auroral pulsations and accompanying VLF emissions, *Ann. Geophys.*, *17*(1), 66–78, doi:10.1007/s00585-999-0066-9.
Thomas, R., and P. Rothwell (1979), A latitude effect in the periodicity of auroral pulsating patches, *J. Atmos. Terr. Phys.*, *41*(12), 1179–1184, doi:10.1016/0021-9169(79)90020-5.
Trakhtengerts, V. Y. (1995), Magnetosphere cyclotron maser: Backward wave oscillator generation regime, *J. Geophys. Res.*, *100*(A9), 17,205–17,210, doi:10.1029/95JA00843.
Trakhtengerts, V. Y. (1999), A generation mechanism for chorus emission, *Ann. Geophys.*, *17*(1), 95–100, doi:10.1007/s00585-999-0095-4.
Tsuruda, K., S. Machida, T. Oguti, S. Kokubun, K. Hayashi, T. Kitamura, O. Saka, and T. Watanabe (1981), Correlations between the very low frequency chorus and pulsating aurora observed by low-light-level television at L=4.4, *Can. J. Phys.*, *59*(8), 1042–1048, doi:10.1139/p81-137.
Tsyganenko, N. A. (2002a), A model of the near magnetosphere with a dawn-dusk asymmetry: 1. Mathematical structure, *J. Geophys. Res.*, *107*(A8), 1179, doi:10.1029/2001JA000219.
Tsyganenko, N. A. (2002b), A model of the near magnetosphere with a dawn-dusk asymmetry: 2. Parameterization and fitting to observations, *J. Geophys. Res.*, *107*(A8), 1176, doi:10.1029/2001JA000220.
Yamamoto, T. (1988), On the temporal fluctuations of pulsating auroral luminosity, *J. Geophys. Res.*, *93*(A2), 897–911, doi:10.1029/JA093iA02p00897.
Yau, A. W., B. A. Whalen, and D. J. McEwen (1981), Rocket-borne measurements of particle pulsation in pulsating aurora, *J. Geophys. Res.*, *86*(A7), 5673–5681, doi:10.1029/JA086iA07p05673.

Paper III

Scale size-dependent characteristics of the nightside aurora

B. K. Humberset, J. W. Gjerloev, M. Samara, and R. G. Michell

Journal of Geophysical Research: Space physics, 122, doi:10.1002/2016JA023695 (2017)

III

AGU PUBLICATIONS

JGR

Journal of Geophysical Research: Space Physics

RESEARCH ARTICLE
10.1002/2016JA023695

Key Points:
- An innovative 2-D analysis of all-sky images revealing the characteristics of the magnetosphere-ionosphere coupling
- The largest auroral scale sizes are stable on timescales of minutes while the small scale sizes are more variable
- The characteristics of the nightside aurora and field-aligned currents are in remarkable agreement

Supporting Information:
- Movie S1
- Text S1

Correspondence to:
B. K. Humberset,
beate.humberset@uib.no

Citation:
Humberset, B. K., J. W. Gjerloev, M. Samara, and R. G. Michell (2017), Scale size-dependent characteristics of the nightside aurora, *J. Geophys. Res. Space Physics*, *122*, doi:10.1002/2016JA023695.

Received 14 NOV 2016
Accepted 27 JAN 2017
Accepted article online 1 FEB 2017

Scale size-dependent characteristics of the nightside aurora

B. K. Humberset[1], J. W. Gjerloev[1,2], M. Samara[3], and R. G. Michell[3,4]

[1] Birkeland Centre for Space Science, Department of Physics and Technology, University of Bergen, Bergen, Norway, [2] The Johns Hopkins University Applied Physics Laboratory, Laurel, Maryland, USA, [3] NASA Goddard Space Flight Center, Greenbelt, Maryland, USA, [4] Department of Astronomy, University of Maryland, College Park, Maryland, USA

Abstract We have determined the spatiotemporal characteristics of the magnetosphere-ionosphere (M-I) coupling using auroral imaging. Observations at fixed positions for an extended period of time are provided by a ground-based all-sky imager measuring the 557.7 nm auroral emissions. We report on a single event of nightside aurora (~22 magnetic local time) preceding a substorm onset. To determine the spatiotemporal characteristics, we perform an innovative analysis of an all-sky imager movie (19 min duration, images at 3.31 Hz) that combines a two-dimensional spatial fast Fourier transform with a temporal correlation. We find a scale size-dependent variability where the largest scale sizes are stable on timescales of minutes while the small scale sizes are more variable. When comparing two smaller time intervals of different types of auroral displays, we find a variation in their characteristics. The characteristics averaged over the event are in remarkable agreement with the spatiotemporal characteristics of the nightside field-aligned currents during moderately disturbed times. Thus, two different electrodynamical parameters of the M-I coupling show similar behavior. This gives independent support to the claim of a system behavior that uses repeatable solutions to transfer energy and momentum from the magnetosphere to the ionosphere.

1. Introduction

Only a few studies have attempted to address the spatiotemporal behavior of any electrodynamic parameter of the magnetosphere-ionosphere coupling, such as plasma convection and electrical conductances. The main reason for this shortcoming is the observational challenges. Observations must be made at a fixed point in the ionosphere at different times. This is not possible with a single satellite or rocket for which measurements are separated in both time and space. In stark contrast to the massive amount of single-satellite data, only a very limited number of multipoint satellite observations exist. For example, The Auroral Turbulence II sounding rocket mission [*Lynch et al.*, 1999], the Enstrophy sounding rocket mission [*Zheng et al.*, 2003], the CLUSTER II mission [*Forsyth et al.*, 2012], the Science and Technology 5 (ST5) mission [*Gjerloev et al.*, 2011], and the Swarm mission [*Olsen et al.*, 2013]. The ST5 mission is so far the most comprehensive multipoint data set of magnetic field perturbations collected by low Earth orbit satellites.

We can, however, utilize ground-based observations of auroral emissions since they also provide extended periods of continuous observations at fixed positions in a nonrotating reference system. Ground-based all-sky imagers are most often used for qualitative loose descriptions of the aurora (without any further data processing) in conjunction to other ground-based [e.g., *Dahlgren et al.*, 2012] or satellite observations. For example, the Time History of Events and Macroscale Interactions during Substorms (THEMIS) mission array of all-sky imagers are used to study the morphology of the aurora on a large scale (auroral oval) and in conjunction with the high-altitude THEMIS spacecrafts. Fixed point analyses by all-sky imagers have been used to understand the mechanism of fluctuating/pulsating aurora, such as tracing the characteristics of pulsating auroral patches in order to put constraints on the observed mechanism [e.g., *Humberset et al.*, 2016], or comparing the best correlation of the emission fluctuations to varying plasma properties at the magnetic equator [e.g., *Nishimura et al.*, 2010]. When it comes to spatiotemporal analyses, they are most often applied to narrow field-of-view imagers over small time intervals in order to investigate the small-scale flickering aurora [e.g., *Whiter et al.*, 2010], the very fast fluctuations superposed on the pulsating aurora [e.g., *Kataoka et al.*, 2012], or to reveal the nature and source of fine-scale structures in the aurora, such as by using different emission lines [e.g., *Dahlgren et al.*, 2016]. We will further focus on the lifetimes of the different mesoscale sizes of the nightside auroral display.

AGU Journal of Geophysical Research: Space Physics 10.1002/2016JA023695

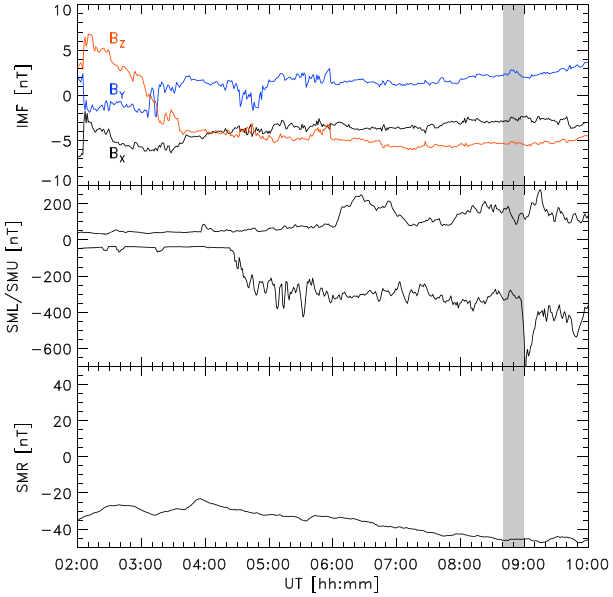

Figure 1. Geomagnetic indices (top) IMF, (middle) SML/SMU maximum westward/eastward auroral electrojet strength, and (bottom) SMR symmetric ring current index. The time of the event is highlighted in grey. We use the SuperMAG data set of indices and ACE IMF data which is propagated to the front of the magnetosphere (courtesy of Dr. James Weygand).

The purpose of this paper is to address the spatiotemporal characteristics of the magnetosphere-ionosphere coupling as observed by an all-sky imager measuring the 557.7 nm auroral emissions. In section 2 we describe the data and event; section 3 outlines the technique and methodology; in section 4 we show a typical example; section 5 shows statistical results; in section 6 we discuss the limitations and results; and finally in section 7 we summarize and draw conclusions.

2. Data and Event

The all-sky imager (ASI) utilized is located at Poker Flat at −147.4° geographic longitude, 65.1° geographic latitude. The ASI uses a 557.7 nm narrow band filter and produces frames with 512 by 512 pixels at a frame rate of 3.31 Hz. Our event was recorded on 2 November 2011 at 08:41:06–08:59:58 UT (~22:15 magnetic local time, ~66° magnetic latitude). Throughout the event the sky is clear, the Moon is down and there are no artifacts such as street lamps.

Figure 1 shows the SuperMAG data set [*Gjerloev*, 2012; *Newell and Gjerloev*, 2011a, 2011b] of indices and propagated interplanetary magnetic field (IMF), which can be obtained through the SuperMAG website. The SuperMAG indices are derived according to the *AL*, *AU* and *SYM-H* indices, but utilize magnetometer observations from 100 or more sites instead of the 12 used in the official auroral electrojet indices and rather than six as is the case for *SYM-H*. Our event (highlighted in grey) occurred during an extended period of moderate activity driven by a southward IMF. The solar wind speed and the dynamic pressure (not shown) were fairly constant at ~370 km/s and ~1 nPa. The *SML* index of the maximum westward auroral electrojet strength shows 4 h of almost continuous activity starting with a substorm onset at 04:27 UT preceding our event, while the *SMR* indicates that there also is some ring current.

Our event is outlined with a keogram and five images in Figure 2. It starts with multiple slightly deformed east-west oriented arcs south in our field of view (FOV) until they fade about 08:46 UT. The entire FOV is then covered by relative dim and uniform arcs with slowly varying structures until a brightening and transition

AGU Journal of Geophysical Research: Space Physics 10.1002/2016JA023695

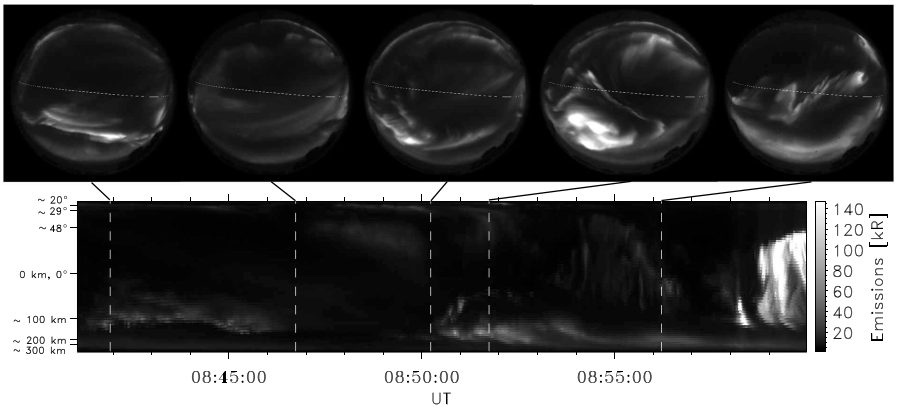

Figure 2. Keogram of the event and five example images. The *y* axis of the keogram shows the approximate distance from zenith and the elevation above the horizon. Note that the ASI images have a scaling of 0–70 kR, while the keogram has a scaling of 0–140 kR. This is done to avoid saturation of the keogram, while ensuring that the emissions are visible in the images. The magnetic east-west orientation is elucidated by the 66° magnetic latitude at 110 km altitude.

to highly structured rapidly changing arcs at about 8:49 UT. At around 8:55 UT highly deformed arcs extend along the magnetic latitudes in the center of the image while diffuse aurora can be found equatorward of the arc and a large part of the northern sky is dark. At about 8:57:30 UT we see that one of the arcs near the eastern horizon brightens and an auroral bulge spreads northwestward and saturates the ASI. This is likely the onset of an auroral substorm, which is also detected by the SuperMAG substorm database [*Newell and Gjerloev*, 2011a] at 08:57 UT.

3. Technique and Methodology

Prior to the actual analysis we transform the ASI frames from the distorted fish-eye lens view to a Cartesian grid with uniform spatial resolution of 1.98 by 1.98 km, as described in *Humberset et al.* [2016]. The Cartesian grid is organized geographically as indicated on Figure 3. To avoid the most distorted limb pixels of the image, we find the characteristics within the center 507 by 507 km FOV (the square box). The spatiotemporal characteristics of the auroral emissions are found by performing a simple, yet robust, analysis that combines a two-dimensional (2-D) spatial Fast Fourier Transform (FFT) with a temporal correlation. This is a four-step process:

1. Perform a 2-D spatial FFT of each image and use a sweeping 2-D narrow Hanning-type band-pass filter to produce 256 filtered images.
2. Correct for Earth's rotation.
3. Calculate the correlation coefficient between two frequency-filtered images, $C = C(f, \Delta T)$, where f is the frequency of the band-pass filter, and ΔT is the time between two images.
4. Convert frequency to auroral scale size, S, to determine $C = C(S, \Delta T)$.

In step 2 we correct for the rotation of the all-sky imager with Earth. In the center of the image (65° geographic latitude) the Earth's rotation is 0.2 km/s eastward, assuming an emission altitude of 110 km [e.g., *Egeland and Burke*, 2013]. An auroral feature fixed in inertial space will therefore get an apparent westward velocity component of 0.2 km/s. To correct for this, we move the band-pass-filtered images 1 pixel (~2 km) every ~10 s eastward relative to the band-pass-filtered images at the start time (T_0) of the analysis. We only use the part of the image that is monitored throughout the time interval. For example, pixels that overlap for the entire event ($\Delta T = 18.9$ min) make up a FOV of 283 km in the east-west direction and 507 km in the north-south direction.

Step 3 calculates the linear Pearson correlation coefficient between two frequency-filtered images:

$$C(f, \Delta T) = \text{Correlate}(\text{Image}(f, T_0), \text{Image}(f, T_0 + \Delta T))$$

AGU Journal of Geophysical Research: Space Physics 10.1002/2016JA023695

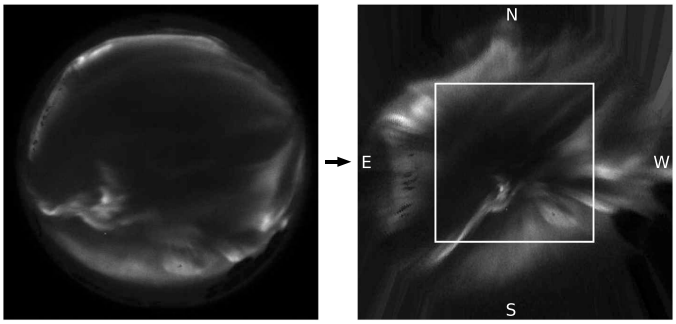

Figure 3. (left) The distorted ASI fish-eye view and (right) the resulting image when projected onto the Cartesian grid of 3.96 km^2 uniform pixel size. To avoid the most distorted limb pixels of the image, we find the characteristics within the center 507 by 507 km FOV (the square box). The Cartesian grid is organized with geographical north on top and west to the right.

Using all possible combinations of images and available frequencies would result in a total of $256 \cdot n \cdot \frac{(n-1)}{2} \simeq 1.8 \cdot 10^9$ correlation coefficients, where n = 3753 is the number of images in the event. To confine this overwhelming number, the statistical analysis is limited in two ways.

1. Because many of the high frequencies are equivalent to small and similar scale sizes, we ignore some of these higher frequencies. We use all lower frequencies (larger scale sizes). In short, we evaluate 35 of the 256 available frequencies inherent in the FFT.
2. We do not correlate all images with all other images. The first image is correlated to all subsequent images. Then we jump 10 images and correlate that to all subsequent images. Jump another 10 images and so on. This jump corresponds to ~3 s.

These limitations reduce the number of calculations and affect the statistics that are used to derive the results without altering our findings. In parts of the event, especially in the last few minutes, the emissions are so bright that >50 pixels are saturated. These images are therefore not included in the analysis. With these limitations in mind we evaluate correlation coefficients for image separations of 1000 s or less, leaving us with a total of $\sim 1.8 \cdot 10^7$ correlation coefficients. We linearly interpolate the resulting median correlation values to find the correlation coefficients for the frequencies that are not covered by the FFT.

In step 4 we determine the auroral scale size, S. The 2-D narrow band-pass filtering (step 1) is done in frequency space passing through frequencies that correspond to the scale size in question. This conversion between frequency and scale size is determined as

$$S = s(f_x) \cdot s(f_y) = \frac{512}{2f_x} \cdot \frac{512}{2f_y} \cdot 3.92 \text{ km}^2 \quad (1)$$

The scale size (S) is an area, where 512 is the number of pixels in the image in the x and y directions and 3.92 km^2 is the pixel size, again assuming an emission altitude of 110 km. The frequencies f_x and f_y in the x and y direction, respectively, are inherent in the FFT. In this way we can determine the scale size-dependent variability of the auroral images, $C = C(S, \Delta T)$. The scale size-dependent amplitude $A = A(S)$ is determined from the complex spectrum as the square root of the power.

4. Typical Example

This section is intended to illustrate the technique outlined in the previous section as well as to show a typical example supporting the statistical results presented in the next section.

Figure 4 shows examples of four image separations ΔT; 0.3 s, 2 s, 10 s, and 60 s. The panels show the respective images as well as their absolute difference and scale size-dependent correlations, $C(S,0.3)$, $C(S,2)$, $C(S,10)$, and $C(S,60)$ calculated from the corresponding sets of band-pass-filtered images. The images are scaled

AGU Journal of Geophysical Research: Space Physics 10.1002/2016JA023695

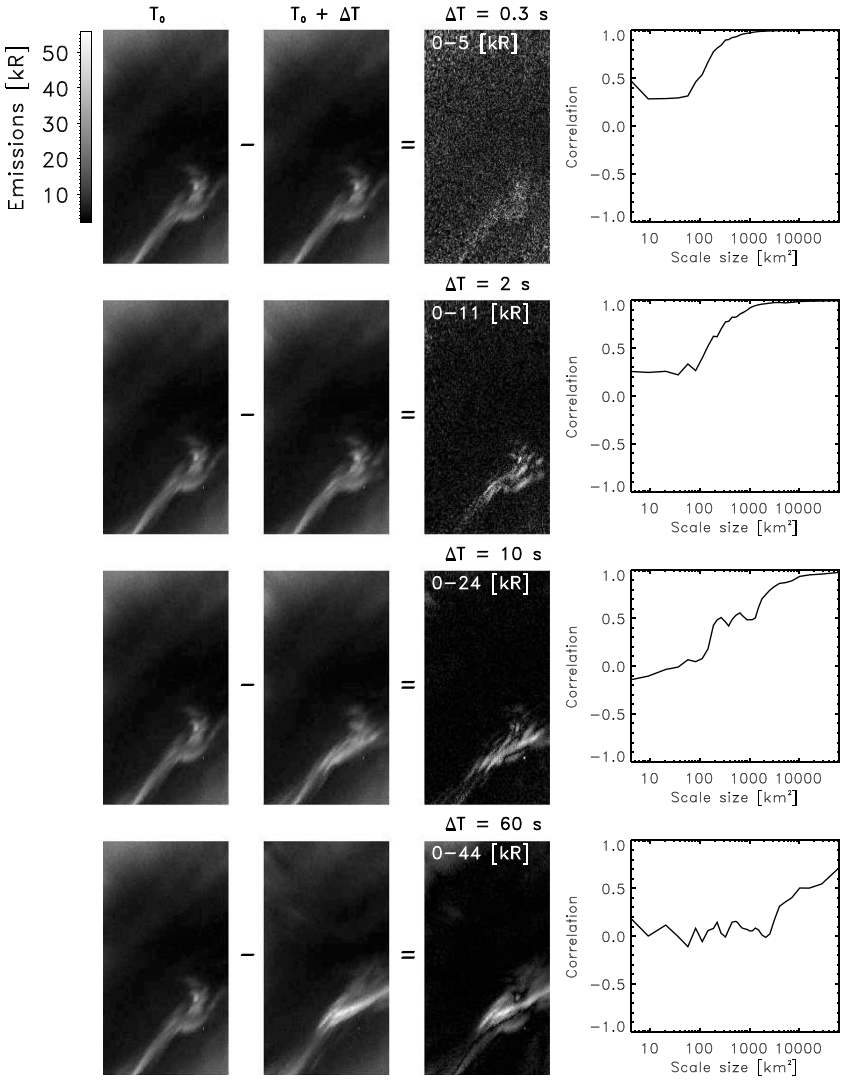

Figure 4. Examples of four-image separations ΔT; 0.3 s, 2 s, 10 s, and 60 s. The panels show the respective images as well as their absolute difference and scale size-dependent correlation. As ΔT increases, note how the correlation drops off for larger scale size as larger auroral forms show up in the difference between the images that are compared.

AGU Journal of Geophysical Research: Space Physics 10.1002/2016JA023695

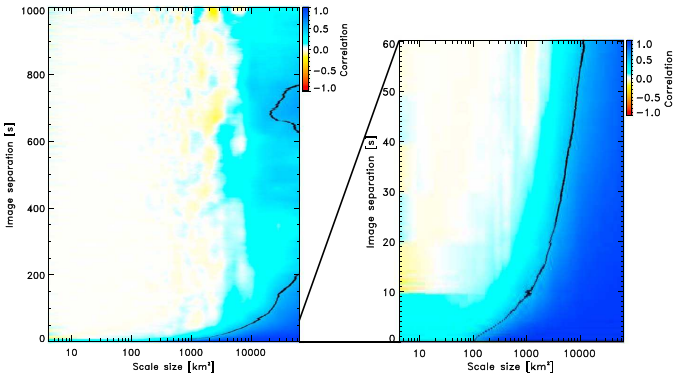

Figure 5. Correlation as a function of scale size (S) and image separation (ΔT). The artifact clearly visible for the small scale sizes is due to the stepwise correction of Earth's rotation for every 10 s image separation. Note the well-organized regions of high and low correlation.

according to a constant color scale, while the difference for visual purposes is scaled according to the maximum difference, which in general are increasing with the image separation. Again, recall that the Earth's rotation has been removed and thus the analysis is performed in an inertial reference frame. The absolute difference is purely for visual inspection, not for actual analysis, but it clearly shows the largest spatial scale sizes that have changed for the respective image separations. Figure 4 (top) shows the smallest possible image separation (0.3 s) in the data set. Even after close inspection, the images look the same. However, their difference shows salt and pepper, meaning small auroral filaments have changed. It can be argued that this is only noise, but the higher intensity in the location of the bright aurora suggests that the structures are real. Moving toward larger image separations, it is easier to see that the images are different and the difference comprises increasingly larger auroral features. The correlation analysis supports this finding; As ΔT increases, the correlation decreases for increasingly larger scale sizes per square kilometer. When the image separation has reached a minute, we clearly see that the large auroral form has started to change and the correlation analysis shows that auroral forms of almost all scale sizes have changed. It is clear that the small scale sizes are more variable.

5. Results

The 2-D correlation distribution $C = C(S, \Delta T)$ is shown in Figure 5. The result is a fairly organized pattern of high correlation and low correlation. For small scale sizes and large image separation the two sets of observations are uncorrelated while short image separation and large scale sizes are highly correlated. We use a correlation of 0.5 to provide a loose separation boundary between regions of "high correlation" and "low correlation" (the black lines in Figure 5). For example, we could assume that correlation values >0.5 means that the auroral forms have not changed much and can be considered relatively stable. This would then imply that auroral forms of 1000 km^2 can be considered as static on timescales of about 10 s or less, while a 10,000 km^2 auroral form can be considered as static on timescales less than a minute. Moving the threshold for what is considered relatively static aurora to correlation values >0.6 or another reasonable number would shift the timescales to lower values, but the overall finding is unaltered. The horizontal lines made by shifts in the correlation values are likely a result of the technique used to correct for Earth's rotation, which is not continuous but moves the images relative to each other 1 pixel every 10 s. Figure 5 also shows that the largest scale sizes are relatively well correlated for an interval of longer image separations. The magnetosphere-ionosphere system (as observed by 557.7 nm emissions) appears to display a scale size-dependent variability where the small scale sizes are more variable and the larger scale sizes more stable.

6. Discussion

We interpret the intriguing coherence pattern shown in Figure 5 as indicative of an underlying magnetosphere-ionosphere (M-I) system behavior. It may sound trivial that small scale sizes change more

AGU Journal of Geophysical Research: Space Physics 10.1002/2016JA023695

rapidly than larger scale sizes, but that implies a systematic behavior of the M-I system. However, before we interpret our results we address the inherent limitations of the data, methodology, and technique.

6.1. Inherent Limitations

The three main assumptions are as follows: (1) The spatiotemporal characteristics of the emissions do not change during the 19 min interval; (2) artifacts due to the 2-D spatial FFT filter are negligible; and (3) conclusions are limited to imager capabilities.

When calculating the correlation coefficient, $C = C(S, \Delta T)$, we assume that this parameter is only a function of S and ΔT. In other words, $C(S, \Delta T, T1) = C(S, \Delta T, T2)$, or the characteristics, are time independent. This is also the case for the amplitude: $A(S, T1) = A(S, T2)$. The validity of this assumption will be investigated in sections 6.3 and 6.4.

The use of a 2-D spatial FFT band pass to analyze scale sizes of course has its limitations and effects that we should be aware of. Equation (1) in step 4 of the technique explains that for each band-pass-filtered image, the band-pass filter all frequency combinations $f = f_x \cdot f_y$ that correspond to the area $S = s(f_x) \cdot s(f_y)$. This is not unambiguous compared to working with one-dimensional band-pass filtering, because we might filter very different shapes. The visual aurora appears in a large variety of forms, such as patches, elongated arcs, and arcs that are deformed by spirals and folds. One scale size and band-pass-filtered image can therefore contain both quadratic shapes ($s(f_x) = s(f_y)$) and very elongated shapes ($s(f_x) \neq s(f_y)$) of the same area, if they are present in the original image. Also the regions of dark skies between the aurora are embedded in the scale sizes. The use of a narrow band pass can of course produce artifacts and uncertainties to the scale sizes. However, these are likely minimized because we in the end are interested in the change between two images filtered with the same band pass. This change is quantified using the linear Pearson correlation coefficient, which has the embedded mathematical property that it is invariant to a dimming or brightening but highly sensitive to distortions in the image. The scale sizes are validated by the typical example (section 4), which shows that the correlation falls off for the same scale sizes that are visible in difference between the images. For instance, in the typical example of a 60 s image separation we clearly see that the correlation of the largest scale sizes falls off and thus responds to the overall change in the auroral arc and not as much by relatively stable large region of dark sky poleward of the arc. Further, the typical example of 60 s image separation shows a scale size-dependent correlation coefficient in excellent agreement with Figure 5. Thus, the artifacts due to the use of a narrow 2-D spatial FFT filter to evaluate the change in auroral images are negligible.

An all-sky imager provides good coverage of the night sky and allows monitoring of rapidly evolving features, but the FOV limits the observations to mesoscale features and the spatial resolution cannot resolve fine-scale features. A more concerning problem, however, is the inherent distortions of an ASI. An ASI is a very wide FOV imager that obtains column-integrated measurements of the auroral emissions. The distortions are due to a variety of different issues which have been discussed in past technical papers. The main issue is that the emissions come from a range of altitudes and are primarily due to precipitating electrons which effectively paint the field lines as they collide with the neutral atmosphere. The ASI obtains column-integrated emissions which typically originate from a range of altitudes and magnetic field lines. Additionally, there are distortions due to optics and elevation (look direction).

The question is whether smearing affects our ability to answer the stated science objective. While there is no robust way to remove smearing, we mediate it by only using the center 507 by 507 km FOV (see Figure 3). The resampled image has a pixel size of 1.98 km and based on the size of the largest pixels in the fish-eye view that are projected onto the resampled grid, we assume that the smearing is about 5 km. The spatiotemporal characteristics of features with scale sizes smaller than 5 km can therefore not be resolved.

6.2. What Is the Source of the Variability?

A velocity component of the auroral arcs will cause a phase shift of the band-pass-filtered images, which will affect the correlation analysis. We have effectively found the scale size-dependent total derivative:

$$\frac{dI}{dt} = \frac{\delta I}{\delta t} + \mathbf{U} \cdot \nabla I$$

where I is the auroral emissions and $\mathbf{U}$ is the velocity of the auroral arcs and forms. This means that the observed variability in the auroral display can be due to changes in the partial derivative with respect to time

AGU Journal of Geophysical Research: Space Physics 10.1002/2016JA023695

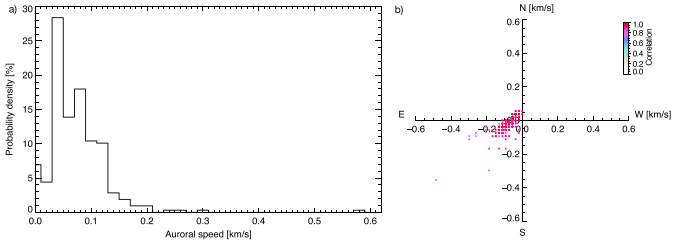

Figure 6. (a) The auroral speed probability from a simple cross correlation between images separated by $\Delta T = 10$ s. (b) The velocity vectors on a geographic grid with the correlation value denoted by the color scale.

as well as any movement of the auroral arcs. Separating these terms in order to determine the cause of the observed dI/dt is not straightforward.

To determine the relative importance of these two source terms (partial derivative and convective term), we performed a simple cross correlation between images separated by $\Delta T = 10$ s. The 2-D spatial shift can be related to a spatial vector, and since we know the time elapsed we straightforwardly calculate the velocity vector (**U**). The weakness of this technique is, of course, that the cross correlation is largely driven by the large scales and thus it is assumed that all scale sizes are moving with the same velocity. This is not necessarily true. Figure 6 shows the resulting velocity vector (**U**) and the speed probability. Using simple estimates, we get the convective term to be on the order of 0.3 kR/s and the total derivative to be on the order of 2.4 kR/s. Thus, the partial derivative must be on the order of 2.1 kR/s leaving us to conclude that we can largely ignore the convective term.

6.3. Controlling Parameters

The single event studied in this paper provides an opportunity to prove the technique and provides a glimpse of the M-I system characteristics, but it does not allow general conclusions. Statistical studies are needed to address how the characteristics of the auroral emissions may be dependent on local time, geomagnetic conditions, seasonal effects, or any other controlling parameters. During our event the solar wind driver is fairly constant but near the end of the interval a substorm onset takes place. This saturates the imager which forces us to terminate the analysis. Thus, we can assume fairly constant geomagnetic conditions, solar wind driver conditions, and since the event is fairly short, the geomagnetic location can be assumed constant.

Figure 5 was derived from the entire interval and thus represents an average result. We may question the assumption that the spatiotemporal characteristics are fairly constant. If we separate the movie into smaller intervals we can test this assumption. We identify two intervals for which we loosely define the aurora as visually (a) "less variable" and (b) "more variable." In interval a (08:46:25 – 08:48:55 UT) the entire FOV is covered by relative dim and uniform arcs with slowly varying structures. Interval a has a median minimum intensity of ~3 kR and maximum of ~35 kR. In interval b (08:55:04 – 08:57:35 UT) highly deformed arcs extend along the magnetic latitudes in the center of the image while diffuse aurora can be found equatorward of the arc and a large part of the northern sky is dark. Interval b has a median minimum intensity of ~2 kR and maximum of ~52 kR.

Figure 7 shows the correlation as a function of scale size and image separation for interval a of less variable aurora (Figure 7a) and interval b of the more variable aurora (Figure 7b). The characteristics from interval a has higher correlations (more blue) for scale sizes of ~2000 km^2 to ~5000 km^2, and perhaps more surprising, lower correlation for scale sizes >9000 km^2 and <800 km^2 compared to interval b. For example, we could assume that correlation values >0.5 means that the auroral forms have not changed much and are relatively stable. This would then imply that auroral forms of ~4000 km^2 are relatively stable for ~30 s during interval a compared to ~20 s for the aurora in interval b. For large auroral forms the situation is turned around with the aurora in interval a having the most variable characteristics. Auroral forms of ~10,000 km^2 are relatively stable for ~50 s during interval a compared to ~100 s for the aurora in interval b. Moving the threshold for what is considered relatively stable aurora to correlation values >0.7 would shift the times to lower values and slightly lower differences between the characteristics, but the overall findings are unaltered. These findings may be

AGU Journal of Geophysical Research: Space Physics 10.1002/2016JA023695

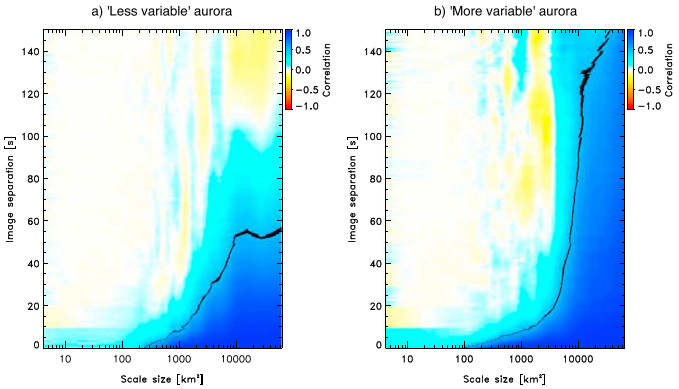

Figure 7. Correlation as a function of scale size and image separation (same format as Figure 5) for the intervals of (a) "less variable" and (b) "more variable" aurora. Correlation values of 0.5 are shown in black to elucidate the location of the correlated/uncorrelated boundary. We get an indication that the spatiotemporal characteristics of the aurora varies.

explained by our visual inspection used to select the time intervals of different auroral displays. It might be that this selection leads to a bias toward structures of a certain size, and we do not notice the larger structures that change on larger timescales. This calls for a more objective quantitative analysis than has been used in most past ASI studies, and it emphasizes the need for the robust technique used in this paper. Finally, it should not be overlooked that although the two intervals show differences they also show similarities.

As we analyze emissions we are indirectly investigating the part of the precipitating electrons that produce the emissions. It thus seems reasonable that the characteristics of the emissions are also the characteristics of the precipitating electrons. For example, it seems reasonable that emissions produced by diffuse precipitation differs from those produced by Alfvénic or Inverted V precipitation. One of the differences between the intervals is that interval b includes diffuse aurora of a higher intensity over a larger part of the FOV and with more structure in the form of fluctuating/pulsating aurora compared to interval a. We note that the characteristics of the aurora in interval b is more variable for scale sizes typical for fluctuating/pulsating features (~1600–3600 km^2) and more stable for large scale sizes covering the relatively stable total area of the diffuse aurora, compared to the characteristics of interval a. We have, however, no objective way to separate the different emissions and their characteristics.

It is in general difficult to distinguish between the Inverted V/monoenergetic and Alfvénic/broadband precipitation by observing the discrete aurora alone. For example, *Colpitts et al.* [2013] observed Alfvénic aurora intermittently and perhaps simultaneously with inverted V aurora during an event of continuous substorm activity. They described the aurora as extremely dynamic changing on timescales of seconds with bright spots and arcs that were not as elongated in the east-west direction as during typical inverted V events. Neither interval a nor b clearly holds such features. Further, *Mende et al.* [2003a] found that in the substorm aurora outside of the surge, the Alfvénic electrons were less clearly separated from the inverted Vs, and *Mende et al.* [2003b] observed intense Alfvénic precipitation in the substorm auroral surge that were likely not present prior to the onset. It is therefore unfortunate that we could not study the substorm auroral bulge in the last minutes of data. If *Mende et al.* [2003b] are right, we could expect to see a difference in the lifetimes of different scale sizes of the distorted arcs before the substorm (monoenergetic) and the substorm auroral bulge (monoenergetic and Alfvénic aurora), which would enable a further discussion on how the characteristics vary in response to the types of electron precipitation that produce the discrete aurora.

We argue that our analysis is analogous to a study of for example field-aligned currents without a separation into underlying magnetospheric processes. As such our analysis could be applied to specific events such as north-south structures, poleward boundary intensifications and discrete arcs.

AGU Journal of Geophysical Research: Space Physics 10.1002/2016JA023695

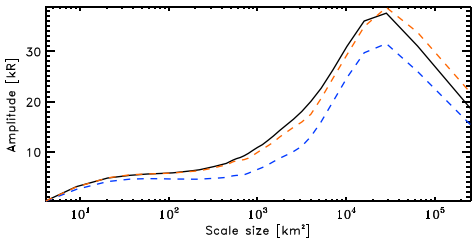

Figure 8. The scale size-dependent amplitude for all available images (black) and for the intervals of "less variable" (blue) and "more variable" (orange) aurora.

6.4. Significance of Different Scale Sizes

To understand the significance of the different auroral scale sizes, we determine the scale size-dependent amplitude $A = A(S)$. It is found from the complex spectrum as the square root of the band-pass power and thus tell us "how much" the band passed frequencies (and thus scale size) are contributing to the emission intensity in the original image. We find the amplitude for each band pass and then calculate the median scale size dependent amplitude over all available images. Figure 8 shows that the scale size of about 30,000 km^2 has the largest amplitude, while the amplitude falls off toward larger and smaller scale sizes. This corresponds to 173 km wide features when $s(f_x) = s(f_y)$. For scale sizes less than about 800 km^2 the amplitudes are less than 10 kR. The scale size-dependent amplitude is also found for the intervals of "less variable" (blue) and "more variable" (orange) aurora. The "more variable" aurora all scale sizes have a higher amplitude than the scale sizes of the "less variable" aurora. We can conclude that the smaller scale sizes both have shorter lifetimes and smaller amplitudes.

6.5. Comparison to the Spatiotemporal Characteristics of Field-Aligned Currents

Comparing our results to past findings is complicated by the observational challenges and resulting lack of statistical studies. However, [*Gjerloev et al.*, 2011], reported a study in which they determined the spatiotemporal characteristics of the magnetic field perturbations (dB) at low Earth orbit altitudes. The comparison is, however, not straightforward since the precipitating electrons producing the emissions are not necessarily the same that carry the current. This is obvious in the downward current region. Several past studies have tested if one can obtain field-aligned current (FAC) density by integrating the measured number flux of particles which is the definition of current density. Such a particle-based approach has been tested examining upward FACs collocated with accelerated auroral precipitation [e.g., *Hoffman et al.*, 1985; *Olsson et al.*, 1998; *Morooka et al.*, 2004]. It was found that FACs tend to be carried by high-energy electrons and an agreement with emissions would therefore be expected. However, the results showed significant disagreement between the current densities estimated from the auroral particle precipitation and from magnetic field measurements. This suggests the existence of missing current carriers, a problem that gets worse when the distance from the accelerated precipitation increases and obviously for downward currents.

Figure 9a shows the correlation as a function of dB (which we here interpret as indicative of FACs) scale size and time between the measurements from >4700 satellite crossings of the nightside auroral oval [*Gjerloev et al.*, 2011]. The time intervals between the measurements are determined by the variable interspacecraft separation of the three ST 5 satellites which were in a pearls-on-a-string formation (coorbital). Correlation coefficients of 0.5 are shown as black dots and used to fit the linear lines which elucidate the location of the correlated/uncorrelated boundary. The correlation value of 0.5 was an arbitrarily chosen value and a change to 0.6 would simply result in a shift in the positive x axis direction without any noteworthy change in the slope [*Gjerloev et al.*, 2011]. The correlations for satellite separations of about 6 s and scale sizes less than about 20 km are due to extrapolation since the dB was determined from spin-averaged measurements. The red line indicates the FAC filament scale size (1-D) of about 250 km, which square is the maximum auroral scale size (2-D).

Figure 9b is the result from Figure 5 for image separations of less than 200 s and average correlation values, as used for the spatiotemporal characteristics of the FACs. For easy comparison, the linear line of the ST 5 study is superposed as a dashed line and the correlation coefficients of about 0.5 are colored black. When comparing

Journal of Geophysical Research: Space Physics 10.1002/2016JA023695

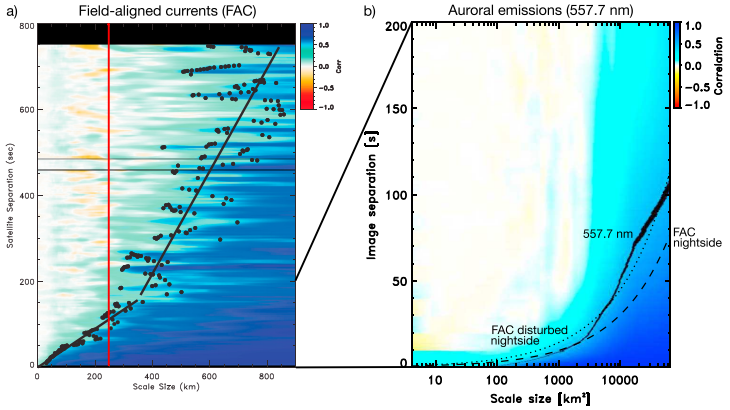

Figure 9. (a) Correlation as a function of FAC scale size and satellite separation for nightside events [*Gjerloev et al.*, 2011]. Correlation values of 0.5 are superposed (black dots) and used to fit the linear lines indicating the location of the correlated/uncorrelated boundary. The red line indicates the FAC filament scale size (1-D) of about 250 km, which square is the maximum auroral scale size (2-D). (b) The same as Figure 5 for image separations of less than 200 s showing the average correlation coefficients. The correlation coefficients of about 0.5 are colored black and the linear line of the ST 5 study is superposed as a dashed line for comparison. A second relationship of the FACs' characteristics during disturbed conditions (AL < −100 nT) is superposed as a dotted line.ăNote the remarkable agreement between the characteristics of the FACs and the auroral emission.

these lines, we find that the variability of the aurora and FACs follow each other closely until about 2000 km^2 (~45 km). For larger scale sizes the aurora is more stable than the FACs. However, the displayed nightside characteristics of the FACs include both quiet and disturbed events, while the characteristics of the auroral emissions are from one moderately disturbed event (SML ≈ −300 nT). Therefore, a second relationship of the FAC characteristics during disturbed conditions (AL < −100 nT) is superposed as a dotted line (valid up to about $\Delta T = 70$ s). When comparing the lines during disturbed conditions (solid and dotted), we find that they follow each other remarkably well. It appears that the disturbed conditions follow our results better than the one for all conditions.

Despite the differences in data set, electromagnetic parameter, and technique, the resulting spatiotemporal characteristics of nightside auroral emissions and the nightside FACs are in remarkable agreement. At first glance, one may argue that the current carriers are also responsible for the emissions but as mentioned above this would be an oversimplification. Rather, we interpret this as indicative that the spatiotemporal characteristics of the emissions are similar to those of dB (or FACs). This seems logical since both are part of the M-I system and in fact it seems difficult to argue that they should differ. We do, however, still emphasize the striking similarity between these two studies despite the differences in technique and electrodynamic parameter.

7. Summary and Conclusion

We have determined objective and quantitative spatiotemporal characteristics of premidnight mesoscale auroral emission (557.7 nm) during a period of fairly constant moderate geomagnetic disturbances. The single event studied in this paper provides an opportunity to prove the technique and provides a glimpse of the M-I system characteristics, but it does not allow general conclusions. Below, we summarize the findings.

1. We find a scale size-dependent variability where the largest scale sizes are stable on timescales of minutes while the small scale sizes are more variable. For example, an auroral form of 1000 km^2 can be considered as static on timescales of about 10 s or less, while a 10,000 km^2 auroral form can be considered as static on timescales less than a minute.
2. We question the assumption that the spatiotemporal characteristics are fairly constant by separating the movie into two smaller intervals of different types of auroral displays. We find that the spatiotemporal characteristics varies during the event. The interval of less variable aurora has more stable auroral forms of

AGU Journal of Geophysical Research: Space Physics 10.1002/2016JA023695

~2000 – 5000 km^2 and less stable large auroral forms (>9000 km^2) compared to the interval of more variable aurora. However, the trend of increasing variability toward the smaller scale sizes is similar.

3. We have effectively found the scale size-dependent total derivative. However, an estimate shows that the source of the variability is mostly due to change in the partial derivative with respect to time and that we largely can ignore the convective term of the auroral arcs.
4. The scale size of about 30,000 km^2 is the most significant, while the amplitude falls off toward larger and smaller scale sizes. For scale sizes less than about 800 km^2 the amplitudes are less than 10 kR.
5. The average spatiotemporal characteristics of the auroral emissions are in remarkable agreement with the spatiotemporal characteristics of the nightside FACs during moderately disturbed times. Thus, two different electrodynamical parameters of the M-I coupling show similar behavior. This result is interpreted as an indication of a system that uses repeatable solutions to transfer energy and momentum from the magnetosphere to the ionosphere.

Acknowledgments
This study was supported by the Research Council of Norway under contract 223252. The authors acknowledge the use of SuperMAG indices and all-sky imager data from the Multi-spectral Observatory of Sensitive EMCCDs (MOOSE). The SuperMAG indices were obtained freely from supermag.uib.no. We greatly acknowledge James Weygand for the ACE solar wind data. MOOSE all-sky imager data were obtained from R.G. Michell and M. Samara. The data analyzed in this study are available upon request from the authors.

References

Colpitts, C. A., S. Hakimi, C. A. Cattell, J. Dombeck, and M. Maas (2013), Simultaneous ground and satellite observations of discrete auroral arcs, substorm aurora, and Alfvénic aurora with FAST and THEMIS GBO, *J. Geophys. Res. Space Physics*, *118*, 6998–7010, doi:10.1002/2013JA018796.

Dahlgren, H., G. W. Perry, J. L. Semeter, J.-P. St.-Maurice, K. Hosokawa, M. J. Nicolls, M. Greffen, K. Shiokawa, and C. Heinselman (2012), Space-time variability of polar cap patches: Direct evidence for internal plasma structuring, *J. Geophys. Res.*, *117*, A09312, doi:10.1029/2012JA017961.

Dahlgren, H., B. S. Lanchester, N. Ivchenko, and D. K. Whiter (2016), Electrodynamics and energy characteristics of aurora at high resolution by optical methods, *J. Geophys. Res. Space Physics*, *121*, 5966–5974, doi:10.1002/2016JA022446.

Egeland, A., and W. J. Burke (2013), *Carl Størmer, Astrophysics and Space Science Library, 393*, Springer, Berlin, doi:10.1007/978-3-642-31457-5_3.

Forsyth, C., et al. (2012), Temporal evolution and electric potential structure of the auroral acceleration region from multispacecraft measurements, *J. Geophys. Res.*, *117*, A12203, doi:10.1029/2012JA017655.

Gjerloev, J. W. (2012), The SuperMAG data processing technique, *J. Geophys. Res.*, *117*, A09213, doi:10.1029/2012JA017683.

Gjerloev, J. W., S. Ohtani, T. Iijima, B. Anderson, J. Slavin, and G. Le (2011), Characteristics of the terrestrial field-aligned current system, *Ann. Geophys.*, *29*(10), 1713–1729, doi:10.5194/angeo-29-1713-2011.

Hoffman, R., M. Sugiura, and N. Maynard (1985), Current carriers for the field-aligned current system, *Adv. Space Res.*, *5*(4), 109–126, doi:10.1016/0273-1177(85)90124-3.

Humberset, B. K., J. W. Gjerloev, M. Samara, R. G. Michell, and I. R. Mann (2016), Temporal characteristics and energy deposition of pulsating auroral patches, *J. Geophys. Res. Space Physics*, *121*, 7087–7107, doi:10.1002/2016JA022921.

Kataoka, R., Y. Miyoshi, D. Hampton, T. Ishii, and H. Kozako (2012), Pulsating aurora beyond the ultra-low-frequency range, *J. Geophys. Res.*, *117*, A08336, doi:10.1029/2012JA017987.

Lynch, K. A., D. Pietrowski, R. B. Torbert, N. Ivchenko, G. Marklund, and F. Primdahl (1999), Multiple-point electron measurements in a nightside auroral arc: Auroral Turbulence II particle observations, *Geophys. Res. Lett.*, *26*(22), 3361–3364, doi:10.1029/1999GL900599.

Mende, S. B. (2016), Observing the magnetosphere through global auroral imaging: 1. Observables, *J. Geophys. Res. Space Physics*, *121*, 10,623–10,637, doi:10.1002/2016JA022558.

Mende, S. B., C. W. Carlson, H. U. Frey, T. J. Immel, and J. Gérard (2003a), IMAGE FUV and in situ FAST particle observations of substorm aurorae, *J. Geophys. Res.*, *108*(A4), 8010, doi:10.1029/2002JA009413.

Mende, S. B., C. W. Carlson, H. U. Frey, L. M. Peticolas, and N. Østgaard (2003b), FAST and IMAGE-FUV observations of a substorm onset, *J. Geophys. Res.*, *108*(A9), 1344, doi:10.1029/2002JA009787.

Morooka, M., T. Mukai, and H. Fukunishi (2004), Current-voltage relationship in the auroral particle acceleration region, *Ann. Geophys.*, *22*(10), 3641–3655, doi:10.5194/angeo-22-3641-2004.

Newell, P. T., and J. W. Gjerloev (2011a), Evaluation of SuperMAG auroral electrojet indices as indicators of substorms and auroral power, *J. Geophys. Res.*, *116*, A12211, doi:10.1029/2011JA016779.

Newell, P. T., and J. W. Gjerloev (2011b), Substorm and magnetosphere characteristic scales inferred from the SuperMAG auroral electrojet indices, *J. Geophys. Res.*, *116*, A12232, doi:10.1029/2011JA016936.

Nishimura, Y., et al. (2010), Identifying the driver of pulsating aurora, *Science*, *330*(6000), 81–84, doi:10.1126/science.1193186.

Olsen, N., et al. (2013), The Swarm Satellite Constellation Application and Research Facility (SCARF) and Swarm data products, *Earth Planets Space*, *65*(11), 1189–1200, doi:10.5047/eps.2013.07.001.

Olsson, A., L. Andersson, A. I. Eriksson, J. Clemmons, R. E. Erlandsson, G. Reeves, T. Hughes, and J. S. Murphee (1998), Freja studies of the current-voltage relation in substorm-related events, *J. Geophys. Res.*, *103*(A3), 4285–4301, doi:10.1029/97JA00560.

Whiter, D. K., B. S. Lanchester, B. Gustavsson, N. Ivchenko, and H. Dahlgren (2010), Using multispectral optical observations to identify the acceleration mechanism responsible for flickering aurora, *J. Geophys. Res.*, *115*, A12315, doi:10.1029/2010JA015805.

Zheng, Y., K. A. Lynch, M. Boehm, R. Goldstein, H. Javadi, P. Schuck, R. L. Arnoldy, and P. M. Kintner (2003), Multipoint measurements of field-aligned current density in the auroral zone, *J. Geophys. Res.*, *108*(A5), 1217, doi:10.1029/2002JA009450.